3.2 SIX-STORY STEEL FRAME BUILDING, SEATTLE, WASHINGTON

In this example, the behavior of a simple, six-story structural steel moment-resisting frame is investigated using a variety of analytical techniques. The structure was initially proportioned using a preliminary analysis, and it is this preliminary design that is investigated. The analysis will show that the structure falls short of several performance expectations. In an attempt to improve performance, viscous fluid dampers are considered for use in the structural system. Analysis associated with the added dampers is performed in a very preliminary manner.

The following analytical techniques are employed:

1. Linear static analysis,
2. Plastic strength analysis (using virtual work),
3. Nonlinear static (pushover) analysis,
4. Linear dynamic analysis, and
5. Nonlinear dynamic analysis.

The primary purpose of this example is to highlight some of the more advanced analytical techniques; hence, more detail is provided on the last three analytical techniques. The *Provisions* provides some guidance and requirements for the advanced analysis techniques. Nonlinear static analysis is covered in the Appendix to Chapter 5, nonlinear dynamic analysis is covered in Sec. 5.7 [5.5], and analysis of structures with added damping is prescribed in the Appendix to Chapter 13 [new Chapter 15].

3.2.1 Description of Structure

The structure analyzed for this example is a 6-story office building in Seattle, Washington. According to the descriptions in *Provisions* Sec. 1.3 [1.2], the building is assigned to Seismic Use Group I. From *Provisions* Table 1.4 [1.3-1], the occupancy importance factor (I) is 1.0. A plan and elevation of the building are shown in Figures 3.2-1 and 3.2-2, respectively. The lateral-load-resisting system consists of steel moment-resisting frames on the perimeter of the building. There are five bays at 28 ft on center in the N-S direction and six bays at 30 ft on center in the E-W direction. The typical story height is 12 ft-6 in. with the exception of the first story, which has a height of 15 ft. There are a 5-ft-tall perimeter parapet at the roof and one basement level that extends 15 ft below grade. For this example, it is assumed that the columns of the moment-resisting frames are embedded into pilasters formed into the basement wall.

For the moment-resisting frames in the N-S direction (Frames A and G), all of the columns bend about their strong axes, and the girders are attached with fully welded moment-resisting connections. It is assumed that these and all other fully welded connections are constructed and inspected according to post-Northridge protocol. Only the demand side of the required behavior of these connections is addressed in this example.

For the frames in the E-W direction (Frames 1 and 6), moment-resisting connections are used only at the interior columns. At the exterior bays, the E-W girders are connected to the weak axis of the exterior (corner) columns using non-moment-resisting connections.

All interior columns are gravity columns and are not intended to resist lateral loads. A few of these columns, however, would be engaged as part of the added damping system described in the last part of this example. With minor exceptions, all of the analyses in this example will be for lateral loads acting in the N-S direction. Analysis for lateral loads acting in the E-W direction would be performed in a similar manner.

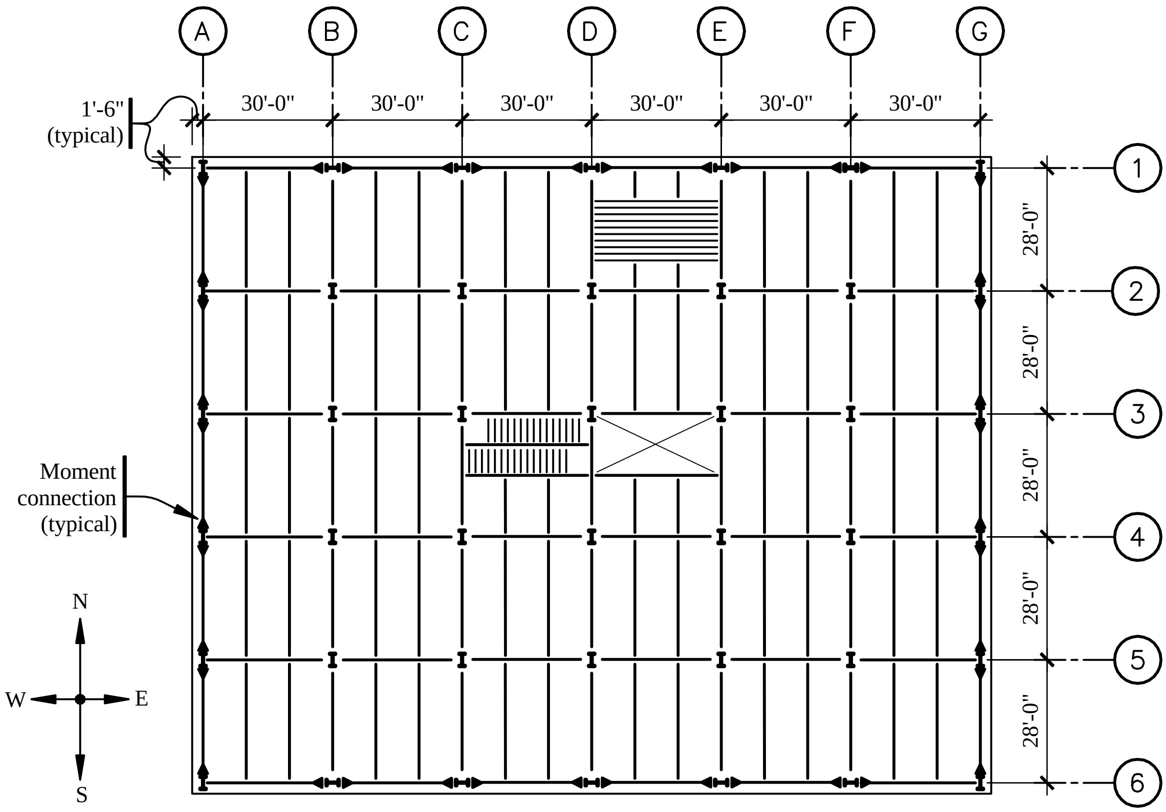

Figure 3.2-1 Plan of structural system.

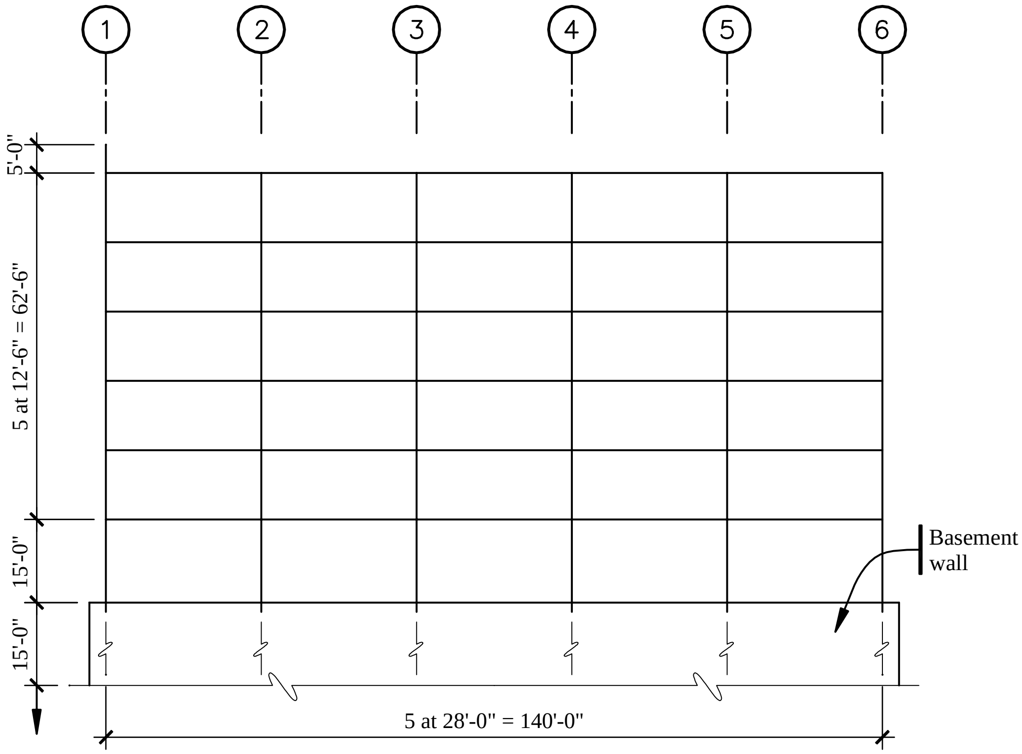

Figure 3.2-2 Elevation of structural system.

Prior to analyzing the structure, a preliminary design was performed in accordance with the AISC Seismic. All members, including miscellaneous plates, were designed using steel with a nominal yield stress of 50 ksi. Detailed calculations for the design are beyond the scope of this example. Table 3.2-1 summarizes the members selected for the preliminary design.[1]

Table 3.2-1 Member Sizes Used in N-S Moment Frames

Member Supporting Level	Column	Girder	Doubler Plate Thickness (in.)
R	W21x122	W24x84	1.00
6	W21x122	W24x84	1.00
5	W21x147	W27x94	1.00
4	W21x147	W27x94	1.00
3	W21x201	W27x94	0.875
2	W21x201	W27x94	0.875

[1]The term *Level* is used in this example to designate a horizontal plane at the same elevation as the centerline of a girder. The top level, Level R, is at the roof elevation; Level 2 is the first level above grade; and Level 1 is at grade. A *Story* represents the distance between adjacent levels. The story designation is the same as the designation of the level at the bottom of the story. Hence, Story 1 is the lowest story (between Levels 2 and 1) and Story 6 is the uppermost story between Levels R and 6.

The sections shown in Table 3.2-1 meet the width-to-thickness requirements for special moment frames, and the size of the column relative to the girders should ensure that plastic hinges will form in the girders. Doubler plates 0.875 in. thick are used at each of the interior columns at Levels 2 and 3, and 1.00 in. thick plates are used at the interior columns at Levels 4, 5, 6, and R. Doubler plates were not used in the exterior columns.

3.2.2 Loads

3.2.2.1 Gravity Loads

It is assumed that the floor system of the building consists of a normal weight composite concrete slab on formed metal deck. The slab is supported by floor beams that span in the N-S direction. These floor beams have a span of 28 ft and are spaced 10 ft on center.

The dead weight of the structural floor system is estimated at 70 psf. Adding 15 psf for ceiling and mechanical, 10 psf for partitions at Levels 2 through 6, and 10 psf for roofing at Level R, the total dead load at each level is 95 psf. The cladding system is assumed to weigh 15 psf. A basic live load of 50 psf is used over the full floor. Twenty-five percent of this load, or 12.5 psf, is assumed to act concurrent with seismic forces. A similar reduced live load is used for the roof.

Based on these loads, the total dead load, live load, and dead plus live load applied to each level are given in Table 3.2-2. The slight difference in loads at Levels R and 2 is due to the parapet and the tall first story, respectively.

Tributary areas for columns and girders as well as individual element gravity loads used in the analysis are illustrated in Figure 3.2-3. These are based on a total dead load of 95 psf, a cladding weight of 15 psf, and a live load of 0.25(50) = 12.5 psf.

Table 3.2-2 Gravity Loads on Seattle Building

	Dead Load (kips)		Reduced Live Load (kips)		Total Load (kips)	
Level	Story	Accumulated	Story	Accumulated	Story	Accumulated
R	2,549	2,549	321	321	2,870	2,870
6	2,561	5,110	321	642	2,882	5,752
5	2,561	7,671	321	963	2,882	8,634
4	2,561	10,232	321	1,284	2,882	11,516
3	2,561	12,792	321	1,605	2,882	14,398
2	2,573	15,366	321	1,926	2,894	17,292

3.2.2.2 Earthquake Loads

Although the main analysis in this example is nonlinear, equivalent static forces are computed in accordance with the *Provisions*. These forces are used in a preliminary static analysis to determine whether the structure, as designed, conforms to the drift requirements of the *Provisions*.

The structure is situated in Seattle, Washington. The short period and the 1-second mapped spectral acceleration parameters for the site are:

$S_S = 1.63$
$S_1 = 0.57$

The structure is situated on Site Class C materials. From *Provisions* Tables 4.1.2.4(a) and 4.1.2.4(b) [Tables 3.3-1 and 3.3-2]:

$F_a = 1.00$
$F_v = 1.30$

From *Provisions* Eq. 4.1.2.4-1 and 4.1.2.4-2 [3.3-1 and 3.3-2], the maximum considered spectral acceleration parameters are:

$$S_{MS} = F_a S_S = 1.00(1.63)$$
$$= 1.63$$

$$S_{M1} = F_v S_1 = 1.30(0.57)$$
$$= 0.741$$

And from *Provisions* Eq. 4.1.2.5-1 and Eq. 4.1.2.5-2 [3.3-3 and 3.3-4], the design acceleration parameters are:

$$S_{DS} = (2/3)S_{M1} = (2/3)1.63$$
$$= 1.09$$

$$S_{D1} = (2/3)S_{M1} = (2/3)0.741$$
$$= 0.494$$

Based on the above coefficients and on *Provisions* Tables 4.2.1a and 4.2.1b [1.4-1 and 1.4-2], the structure is assigned to Seismic Design Category D. For the purpose of analysis, it is assumed that the structure complies with the requirements for a special moment frame, which, according to *Provisions* Table 5.2.2 [4.3-1], has $R = 8$, $C_d = 5.5$, and $\Omega_0 = 3.0$.

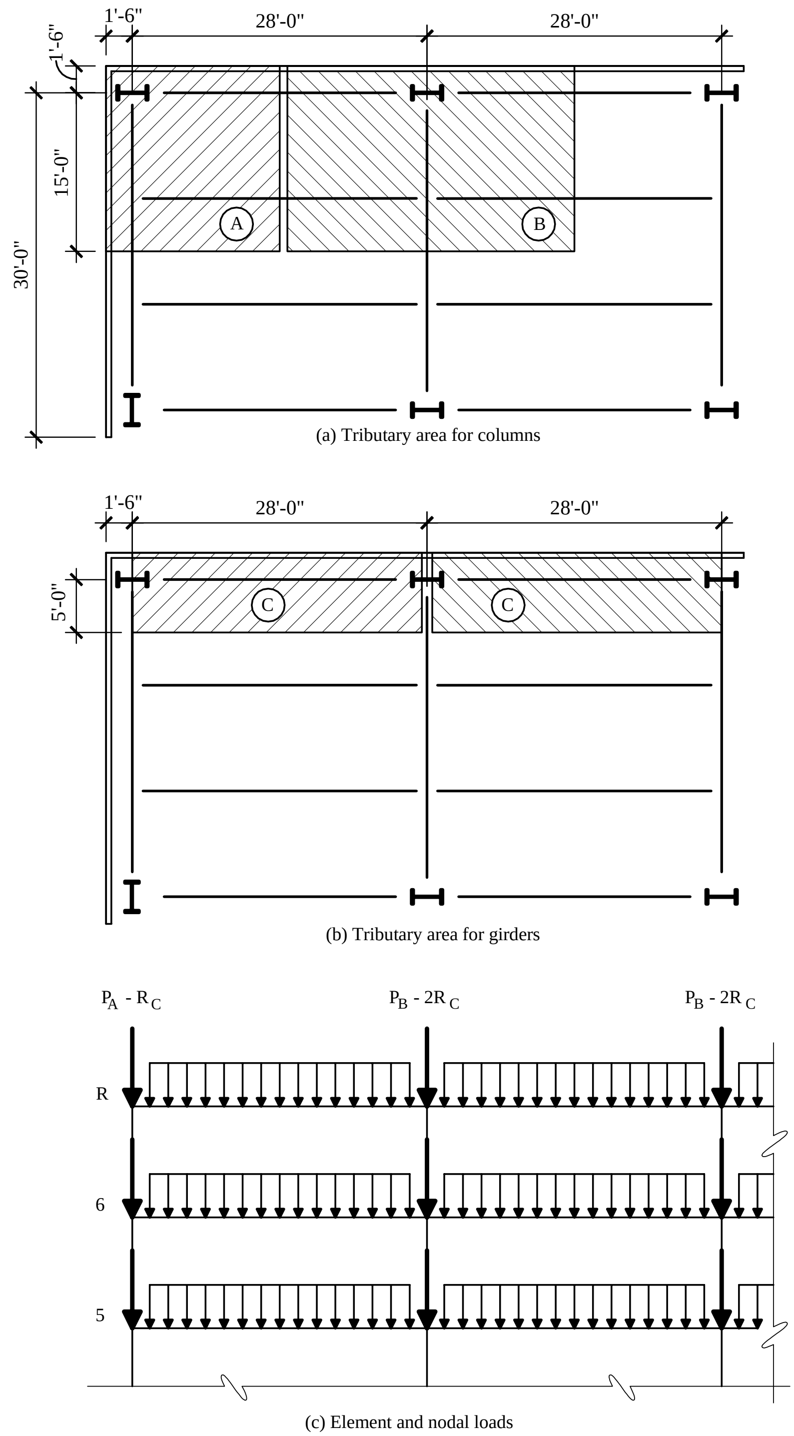

Figure 3.2-3 Element loads used in analysis.

3.2.2.2.1 Approximate Period of Vibration

Provisions Eq. 5.4.2.1-1 [5.2-6] is used to estimate the building period:

$$T_a = C_r h_n^x$$

where, from *Provisions* Table 5.4.2.1 [5.5-2], C_r = 0.028 and x = 0.8 for a steel moment frame. Using h_n (the total building height above grade) = 77.5 ft, $T_a = 0.028(77.5)^{0.8} = 0.91$ sec.

When the period is determined from a properly substantiated analysis, the *Provisions* requires that the period used for computing base shear not exceed C_uT_a where, from *Provisions* Table 5.4.2 [5.2-1] (using S_{D1} = 0.494), C_u = 1.4. For the structure under consideration, C_uT_a = 1.4(0.91) = 1.27 sec.

3.2.2.2.2 Computation of Base Shear

Using *Provisions* Eq. 5.4.1 [5.2-1], the total seismic shear is:

$$V = C_S W$$

where W is the total weight of the structure. From *Provisions* Eq. 5.4.1.1-1 [5.2-2], the maximum (constant acceleration region) seismic response coefficient is:

$$C_{S_{max}} = \frac{S_{DS}}{(R/I)} = \frac{1.09}{(8/1)} = 0.136$$

Provisions Eq. 5.4.1.1-2 [5.2-3] controls in the constant velocity region:

$$C_S = \frac{S_{D1}}{T(R/I)} = \frac{0.494}{1.27(8/1)} = 0.0485$$

The seismic response coefficient, however, must not be less than that given by Eq. 5.4.1.1-3 [revised for the 2003 *Provisions*]:

$$C_{S_{min}} = 0.044 I S_{DS} = 0.044(1)(1.09) = 0.0480\ .$$

[In the 2003 *Provisions*, this equation for minimum base shear coefficient has been revised. The results of this example problem would not be affected by the change.]

Thus, the value from Eq. 5.4.1.1-2 [5.2-3] controls for this building. Using W = 15,366 kips, V = 0.0485(15,366) = 745 kips.

3.2.2.2.3 Vertical Distribution of Forces

The *Provisions* Eq. 5.4.1.1-2 [5.2-3] base shear is distributed along the height of the building using *Provisions* Eq. 5.4.3.1 and 5.4.3.2 [5.2-10 and 5.2-11]:

$$F_x = C_{vx}V$$

and

$$C_{vx} = \frac{w_x h^k}{\sum_{i=1}^{n} w_i h_i^k}$$

where $k = 0.75 + 0.5T = 0.75 + 0.5(1.27) = 1.385$. The lateral forces acting at each level and the story shears and story overturning moments acting at the bottom of the story below the indicated level are summarized in Table 3.2-3. These are the forces acting on the whole building. For analysis of a single frame, one-half of the tabulated values are used.

Table 3.2-3 Equivalent Lateral Forces for Seattle Building Responding in N-S Direction

Level x	w_x (kips)	h_x (ft)	$w_x h_x^k$	C_{vx}	F_x (kips)	V_x (kips)	M_x (ft-kips)
R	2,549	77.5	1,060,663	0.321	239.2	239.2	2,990
6	2,561	65.0	835,094	0.253	188.3	427.5	8,334
5	2,561	52.5	621,077	0.188	140.1	567.6	15,429
4	2,561	40.0	426,009	0.129	96.1	663.7	23,725
3	2,561	27.5	253,408	0.077	57.1	720.8	32,735
2	2,561	15.0	109,882	0.033	24.8	745.6	43,919
Σ	15,366		3,306,133	1.000	745.6		

3.2.3 Preliminaries to Main Structural Analysis

Performing a nonlinear analysis of a structure is an incremental process. The analyst should first perform a linear analysis to obtain some basic information on expected behavior and to serve later as a form of verification for the more advanced analysis. Once the linear behavior is understood (and extrapolated to expected nonlinear behavior), the anticipated nonlinearities are introduced. If more than one type of nonlinear behavior is expected to be of significance, it is advisable to perform a preliminary analysis with each nonlinearity considered separately and then to perform the final analysis with all nonlinearities considered. This is the approach employed in this example.

3.2.3.1 The Computer Program DRAIN-2Dx

The computer program DRAIN-2Dx (henceforth called DRAIN) was used for all of the analyses described in this example. DRAIN allows linear and nonlinear static and dynamic analysis of two-dimensional (planar) structures only.

As with any finite element analysis program, DRAIN models the structure as an assembly of nodes and elements. While a variety of element types is available, only three element types were used:

Type 1, inelastic bar (truss) element
Type 2, beam-column element
Type 4, connection element

Two models of the structure were prepared for DRAIN. The first model, used for preliminary analysis and for verification of the second (more advanced) model, consisted only of Type 2 elements for the main structure and Type 1 elements for modeling P-delta effects. All analyses carried out using this model were linear.

For the second more detailed model, Type 1 elements were used for modeling *P*-delta effects, the braces in the damped system, and the dampers in the damped system. It was assumed that these elements would remain linear elastic throughout the response. Type 2 elements were used to model the beams and columns as well as the rigid links associated with the panel zones. Plastic hinges were allowed to form in all columns. The column hinges form through the mechanism provided in DRAIN's Type 2 element. Plastic behavior in girders and in the panel zone region of the structure was considered through the use of Type 4 connection elements. Girder yielding was forced to occur in the Type 4 elements (in lieu of the main span represented by the Type 2 elements) to provide more control in hinge location and modeling. A complete description of the implementation of these elements is provided later.

3.2.3.2 Description of Preliminary Model and Summary of Preliminary Results

The preliminary DRAIN model is shown in Figure 3.2-4. Important characteristics of the model are as follows:

1. Only a single frame was modeled. Hence one-half of the loads shown in Tables 3.2-2 and 3.2-3 were applied.

2. Columns were fixed at their base.

3. Each beam or column element was modeled using a Type 2 element. For the columns, axial, flexural, and shear deformations were included. For the girders, flexural and shear deformations were included but, because of diaphragm slaving, axial deformation was not included. Composite action in the floor slab was ignored for all analysis.

4. Members were modeled using centerline dimensions without rigid end offsets. This allows, in an approximate but reasonably accurate manner, deformations to occur in the beam-column joint region. Note that this model does not provide any increase in beam-column joint stiffness due to the presence of doubler plates.

5. P-delta effects were modeled using the leaner column shown in Figure 3.2-4 at the right of the main frame. This column was modeled with an axially rigid Type 1 (truss) element. *P*-delta effects were activated for this column only (P-delta effects were turned off for the columns of the main frame). The lateral degree of freedom at each level of the P-delta column was slaved to the floor diaphragm at

the matching elevation. When P-delta effects were included in the analysis, a special initial load case was created and executed. This special load case consisted of a vertical force equal to one-half of the total story weight (dead load plus fully reduced live load) applied to the appropriate node of the P-delta column. P-delta effects were modeled in this manner to avoid the inconsistency of needing true column axial forces for assessing strength and requiring total story forces for assessing stability.

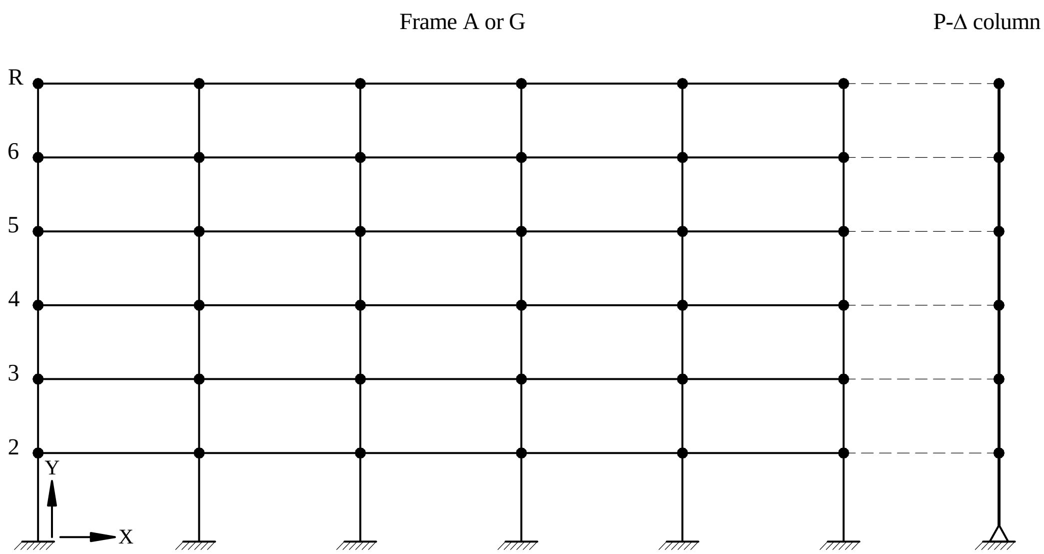

Figure 3.2-4 Simple wire frame model used for preliminary analysis.

3.2.3.2.1 Results of Preliminary Analysis: Drift and Period of Vibration

The results of the preliminary analysis for drift are shown in Tables 3.2-4 and 3.2-5 for the computations excluding and including P-delta effects, respectively. In each table, the deflection amplification factor (C_d) equals 5.5, and the acceptable story drift (story drift limit) is taken as 1.25 times the limit provided by *Provisions* Table 5.2.8. This is in accordance with *Provisions* Sec. 5.7.3.3 [5.5.3.3] which allows such an increase in drift when a nonlinear analysis is performed. This increased limit is used here for consistency with the results from the following nonlinear time-history analysis.

When P-delta effects are not included, the computed story drift is less than the allowable story drift at each level of the structure. The largest magnified story drift, including C_d = 5.5, is 3.45 in. in Story 2. If the 1.25 multiplier were not used, the allowable story drift would reduce to 3.00 in., and the computed story drift at Levels 3 and 4 would exceed the limit.

As a preliminary estimate of the importance of P-delta effects, story stability coefficients (θ) were computed in accordance with *Provisions* Sec. 5.4.6.2 [5.2.6.2]. At Story 2, the stability coefficient is 0.0839. *Provisions* Sec. 5.4.6.2 [5.2.6.2] allows P-delta effects to be ignored when the stability coefficient is less than 0.10. For this example, however, analyses are performed with and without P-delta effects. [In the 2003 *Provisions*, the stability coefficient equation has been revised to include the importance factor in the numerator and the calculated result is used simply to determine whether a special analysis (in accordance with Sec. A5.2.3) is required.]

When P-delta effects are included, the drifts at the lower stories increase by about 10 percent as expected from the previously computed stability ratios. (Hence, the stability ratios provide a useful check.[2]) Recall that this analysis ignored the stiffening effect of doubler plates.

Table 3.2-4 Results of Preliminary Analysis Excluding P-delta Effects

Story	Total Drift (in.)	Story Drift (in.)	Magnified Story Drift (in.)	Drift Limit (in.)	Story Stability Ratio
6	3.14	0.33	1.82	3.75	0.0264
5	2.81	0.50	2.75	3.75	0.0448
4	2.31	0.54	2.97	3.75	0.0548
3	1.77	0.61	3.36	3.75	0.0706
2	1.16	0.63	3.45	3.75	0.0839
1	0.53	0.53	2.91	4.50	0.0683

Table 3.2-5 Results of Preliminary Analysis Including P-delta Effects

Story	Total Drift (in.)	Story Drift (in.)	Magnified Story Drift (in.)	Drift Limit (in.)
6	3.35	0.34	1.87	3.75
5	3.01	0.53	2.91	3.75
4	2.48	0.57	3.15	3.75
3	1.91	0.66	3.63	3.75
2	1.25	0.68	3.74	3.75
1	0.57	0.57	3.14	4.50

The computed periods for the first three natural modes of vibration are shown in Table 3.2-6. As expected, the period including P-delta effects is slightly larger than that produced by the analysis without such effects. More significant is the fact that the first mode period is considerably longer than that predicted from *Provisions* Eq. 5.4.2.1-1 [5.2-6]. Recall from previous calculations that this period (T_a) is 0.91 seconds, and the upper limit on computed period C_uT_a is 1.4(0.91) = 1.27 seconds. When doubler plate effects are included in the analysis, the period will decrease slightly, but it remains obvious that the structure is quite flexible.

[2]The story drifts including P-delta effects can be estimated as the drifts without P-delta times the quantity $1/(1-\theta)$, where θ is the stability coefficient for the story.

Table 3.2-6 Periods of Vibration From Preliminary Analysis (sec)

Mode	P-delta Excluded	P-delta Included
1	1.985	2.055
2	0.664	0.679
3	0.361	0.367

3.2.3.2.2 Results of Preliminary Analysis: Demand-to-Capacity Ratios

To determine the likelihood of and possible order of yielding, demand-to-capacity ratios were computed for each element. The results are shown in Figure 3.2-5. For this analysis, the structure was subjected to full dead load plus 25 percent of live load followed by the equivalent lateral forces of Table 3.2-3. P-delta effects were included.

For girders, the demand-to-capacity ratio is simply the maximum moment in the member divided by the member's plastic moment capacity where the plastic capacity is $Z_{girder}F_y$. For columns, the ratio is similar except that the plastic flexural capacity is estimated to be $Z_{col}(F_y - P_u/A_{col})$ where P_u is the total axial force in the column. The ratios were computed at the end of the member, not at the face of the column or girder. This results in slightly conservative ratios, particularly for the columns, because the columns have a smaller ratio of clear span to total span than do the girders.

Level R	0.176	0.177	0.169	0.172	0.164	
	0.066	0.182	0.177	0.177	0.170	0.135
Level 6	0.282	0.281	0.277	0.282	0.280	
	0.148	0.257	0.255	0.255	0.253	0.189
Level 5	0.344	0.333	0.333	0.333	0.354	
	0.133	0.274	0.269	0.269	0.269	0.175
Level 4	0.407	0.394	0.394	0.394	0.420	
	0.165	0.314	0.308	0.308	0.309	0.211
Level 3	0.452	0.435	0.435	0.434	0.470	
	0.162	0.344	0.333	0.333	0.340	0.223
Level 2	0.451	0.425	0.430	0.424	0.474	
	0.413	0.492	0.485	0.485	0.487	0.492

Figure 3.2-5 Demand-to-capacity ratios for elements from analysis with P-delta effects included.

It is very important to note that the ratios shown in Figure 3.2-5 are based on the inelastic seismic forces (using $R = 8$). Hence, a ratio of 1.0 means that the element is just at yield, a value less than 1.0 means the element is still elastic, and a ratio greater than 1.0 indicates yielding.[3]

Several observations are made regarding the likely inelastic behavior of the frame:

1. The structure has considerable overstrength, particularly at the upper levels.

2. The sequence of yielding will progress from the lower level girders to the upper level girders. Because of the uniform demand-to-capacity ratios in the girders of each level, all the hinges in the girders in a level will form almost simultaneously.

3. With the possible exception of the first level, the girders should yield before the columns. While not shown in the table, it should be noted that the demand-to-capacity ratios for the lower story columns were controlled by the moment at the base of the column. It is usually very difficult to prevent yielding of the base of the first story columns in moment frames, and this frame is no exception. The column on the leeward (right) side of the building will yield first because of the additional axial compressive force arising from the seismic effects.

3.2.3.2.3 Results of Preliminary Analysis: Overall System Strength

The last step in the preliminary analysis was to estimate the total lateral strength (collapse load) of the frame using virtual work. In the analysis, it is assumed that plastic hinges are perfectly plastic. Girders hinge at a value $Z_{girder}F_y$ and the hinges form 5.0 in. from the face of the column. Columns hinge only at the base, and the plastic moment capacity is assumed to be $Z_{col}(F_y - P_u/A_{col})$. The fully plastic mechanism for the system is illustrated in Figure 3.2-6. The inset to the figure shows how the angle modification term σ was computed. The strength (V) for the total structure is computed from the following relationships (see Figure 3.2-6 for nomenclature):

Internal Work = External Work

Internal Work = $2[20\sigma\theta M_{PA} + 40\sigma\theta M_{PB} + \theta(M_{PC} + 4M_{PD} + M_{PE})]$

External Work = $V\theta\left[\sum_{i=1}^{nLevels} F_i H_i\right]$ where $\sum_{i=1}^{nLevels} F_i = 1.0$

Three lateral force patterns were used: uniform, upper triangular, and *Provisions* where the *Provisions* pattern is consistent with the vertical force distribution of Table 3.2-3 in this volume of design examples. The results of the analysis are shown in Table 3.2-7. As expected, the strength under uniform load is significantly greater than under triangular or *Provisions* load. The closeness of the *Provisions* and triangular load strengths is due to the fact that the vertical-load-distributing parameter (k) was 1.385, which is close to 1.0. The difference between the uniform and the triangular or *Provisions* patterns is an

[3]To determine the demand-to-capacity ratio on the basis of an elastic analysis, multiply all the values listed in Table 3.2-6 by $R = 8$. With this modification, the ratios are an approximation of the ductility demand for the individual elements.

indicator that the results of a capacity-spectrum analysis of the system will be quite sensitive to the lateral force pattern applied to the structure when performing the pushover analysis.

The equivalent-lateral-force (ELF) base shear, 746 kips (see Table 3.2-3), when divided by the *Provisions* pattern capacity, 2886 kips, is 0.26. This is reasonably consistent with the demand to capacity ratios shown in Figure 3.2-5.

Before proceeding, three important points should be made:

1. The rigid-plastic analysis did not include strain hardening, which is an additional source of overstrength.

2. The rigid-plastic analysis did not consider the true behavior of the panel zone region of the beam-column joint. Yielding in this area can have a significant effect on system strength.

3. Slightly more than 10 percent of the system strength comes from plastic hinges that form in the columns. If the strength of the column is taken simply as M_p (without the influence of axial force), the "error" in total strength is less than 1 percent.

Table 3.2-7 Lateral Strength on Basis of Rigid-Plastic Mechanism

Lateral Load Pattern	Lateral Strength (kips) Entire Structure	Lateral Strength (kips) Single Frame
Uniform	3,850	1,925
Upper Triangular	3,046	1,523
Provisions	2,886	1,443

3.2.4 Description of Model Used for Detailed Structural Analysis

Nonlinear-static and -dynamic analyses require a much more detailed model than was used in the linear analysis. The primary reason for the difference is the need to explicitly represent yielding in the girders, columns, and panel zone region of the beam-column joints.

The DRAIN model used for the nonlinear analysis is shown in Figure 3.2-7. A detail of a girder and its connection to two interior columns is shown in Figure 3.2-8. The detail illustrates the two main features of the model: an explicit representation of the panel zone region and the use of concentrated (Type 4 element) plastic hinges in the girders.

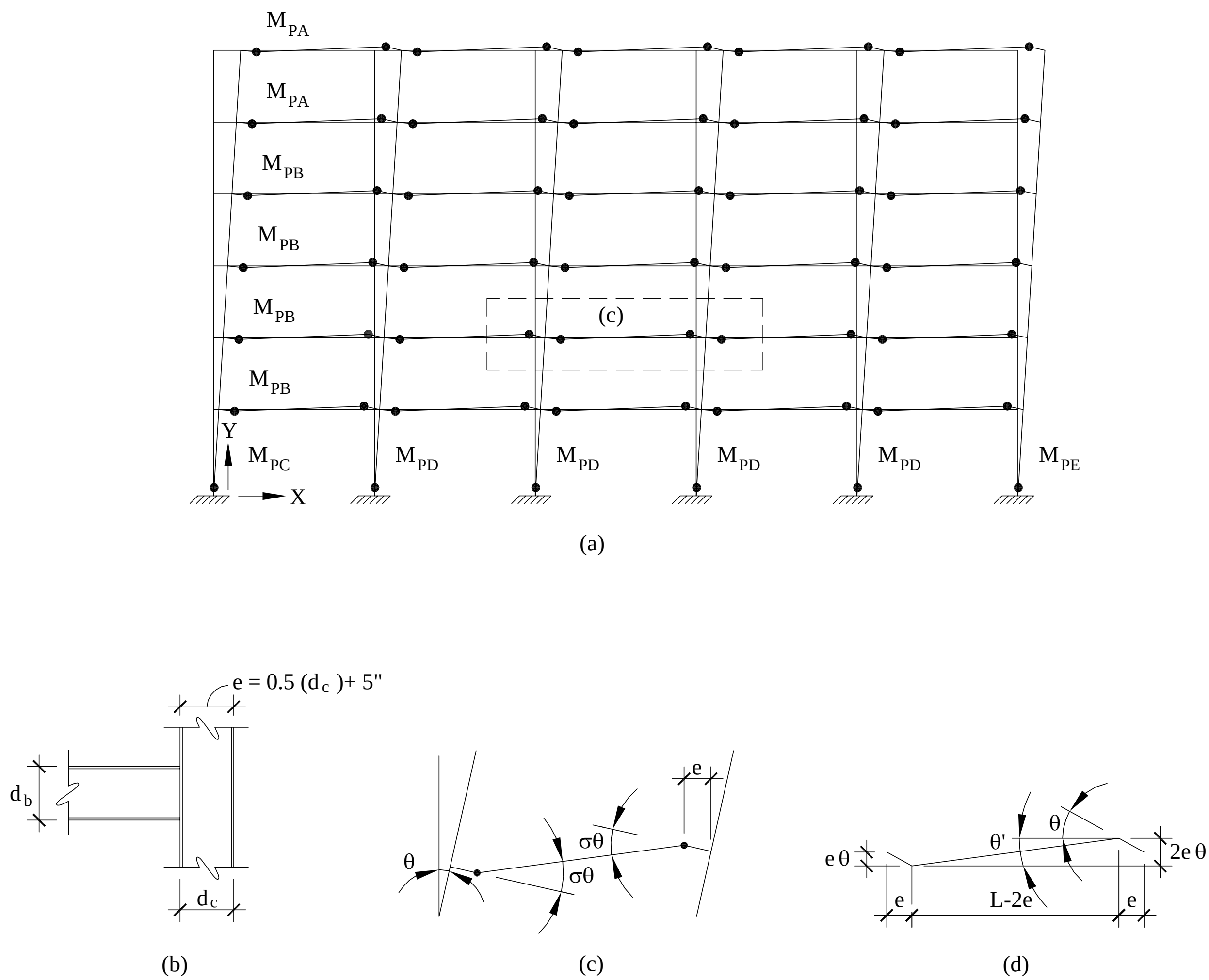

Figure 3.2-6 Plastic mechanism for computing lateral strength.

In Figure 3.2-7, the column shown to the right of the structure is used to represent P-delta effects. See Sec. 3.2.3.2 of this example for details.

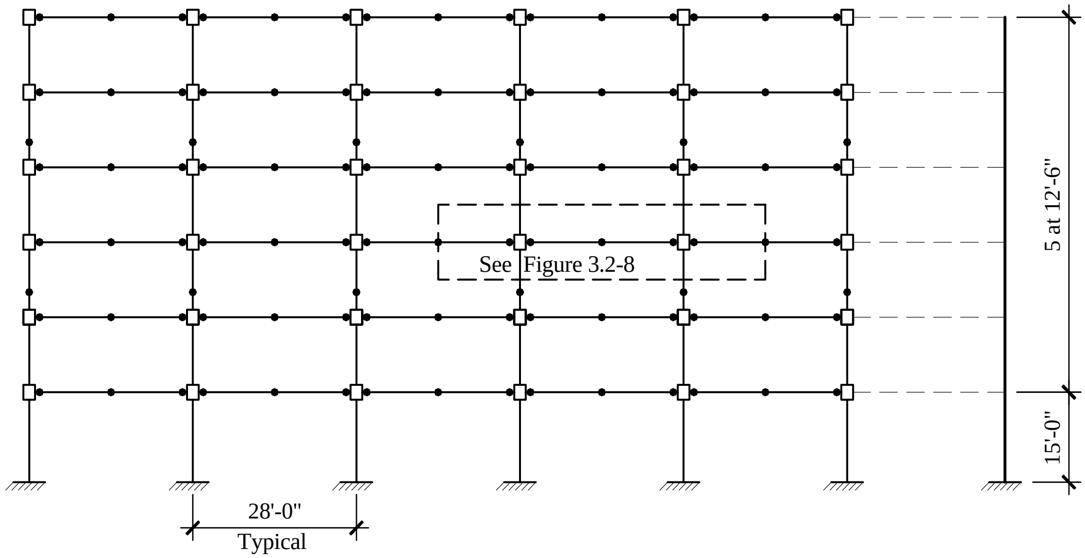

Figure 3.2-7 Detailed analytical model of 6-story frame.

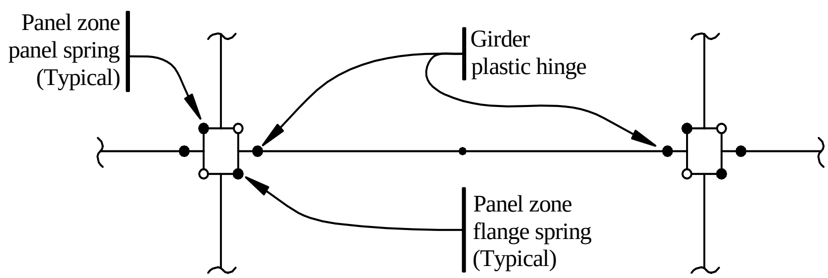

Figure 3.2-8 Model of girder and panel zone region.

The development of the numerical properties used for panel zone and girder hinge modeling is not straightforward. For this reason, the following theoretical development is provided before proceeding with the example.

3.2.4.1 Plastic Hinge Modeling and Compound Nodes

In the analysis described below, much use is made of compound nodes. These nodes are used to model plastic hinges in girders and, through a simple transformation process, deformations in the panel zone region of beam-column joints.

A compound node typically consists of a pair of single nodes with each node sharing the same point in space. The X and Y degrees of freedom of the first node of the pair (the slave node) are constrained to be equal to the X and Y degrees of freedom of the second node of the pair (the master node), respectively. Hence, the compound node has four degrees of freedom: an X displacement, a Y displacement, and two independent rotations.

In most cases, one or more rotational spring connection elements (DRAIN element Type 4) are placed between the two single nodes of the compound node, and these springs develop bending moment in resistance to the relative rotation between the two single nodes. If no spring elements are placed between the two single nodes, the compound node acts as a moment-free hinge. A typical compound node with a single rotational spring is shown in Figure 3.2-9. The figure also shows the assumed bilinear, inelastic moment-rotation behavior for the spring.

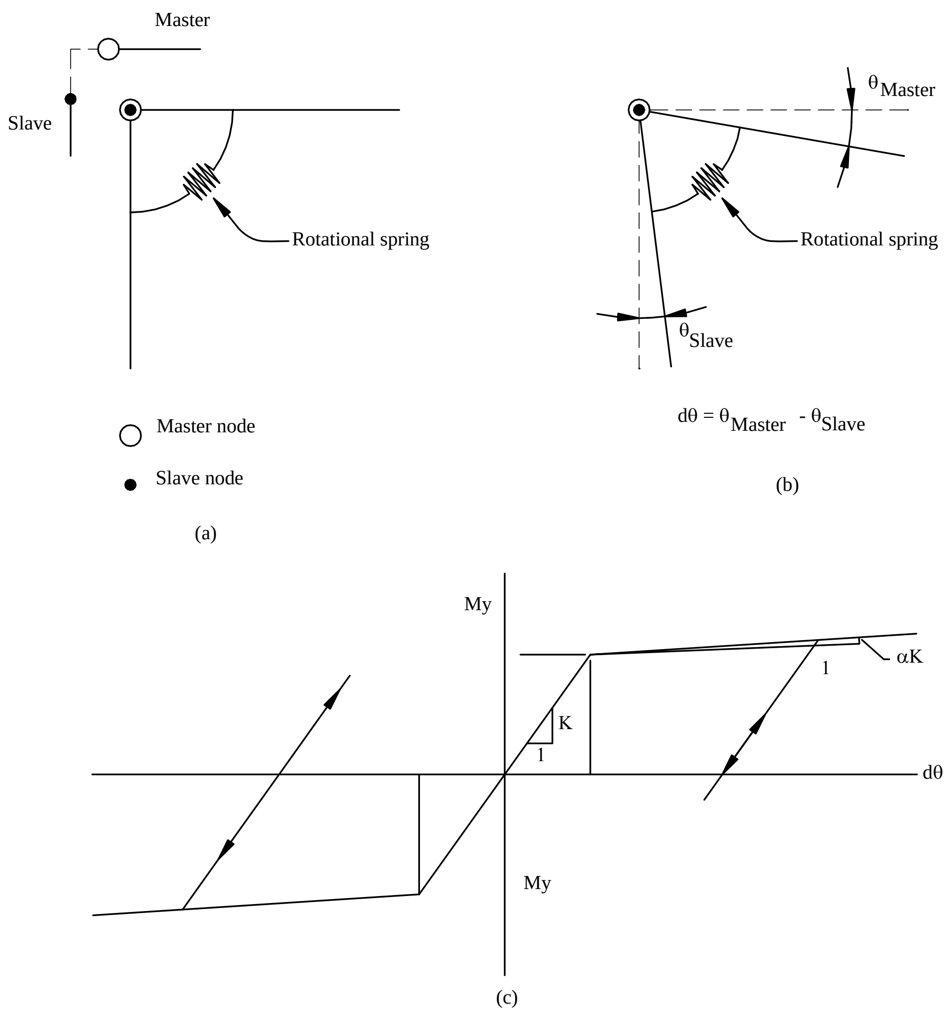

Figure 3.2-9 A compound node and attached spring.

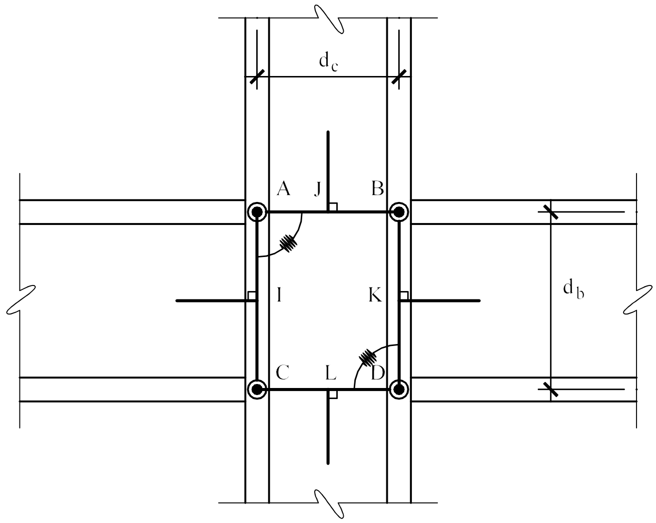

Figure 3.2-10 Krawinkler beam-column joint model.

3.2.4.2 Modeling of Beam-Column Joint Regions

A very significant portion of the total story drift of a moment-resisting frame may be due to deformations that occur in the panel zone region of the beam-column joint. In this example, panel zones are modeled using an approach developed by Krawinkler (1978). This model, illustrated in Figure 3.2-10, has the advantage of being conceptually simple, yet robust. The disadvantage of the approach is that the number of degrees of freedom required to model a structure is significantly increased.

A simpler model, often referred to as the scissors model, also has been developed to represent panel zone behavior. The scissors model has the advantage of using fewer degrees of freedom. However, due to its simplicity, it is generally considered to inadequately represent the kinematics of the problem.[4] For this reason, the scissors model is not used here.

The Krawinkler model assumes that the panel zone area has two resistance mechanisms acting in parallel:

1. Shear resistance of the web of the column, including doubler plates and
2. Flexural resistance of the flanges of the column.

These two resistance mechanisms are apparent in AISC Seismic Eq. (9-1), which is used for determining panel zone shear strength:

[4] The author of this example is completing research at Virginia Tech to determine whether the scissors model is adequate to model steel moment frames. Preliminary results indicate that the kinematics error is not significant and that very good results may be obtained by a properly formulated scissors model.

$$R_v = 0.6F_y d_c t_p \left[1 + \frac{3b_{cf} t_{cf}^2}{d_b d_c t_p} \right].$$

The equation can be rewritten as:

$$R_v = 0.6F_y d_c t_p + 1.8\frac{F_y b_{cf} t_{cf}^2}{d_b} \equiv V_{Panel} + 1.8V_{Flanges}$$

where the first term is the panel shear resistance and the second term is the plastic flexural resistance of the column flange. The terms in the equations are defined as follows:

F_y = yield strength of the column and the doubler plate,
d_c = total depth of column,
t_p = thickness of panel zone region = column web thickness plus doubler plate thickness,
b_{cf} = width of column flange,
t_{cf} = thickness of column flange, and
d_b = total depth of girder.

Additional terms used in the subsequent discussion are:

t_{bf} = girder flange thickness and
G = shear modulus of steel.

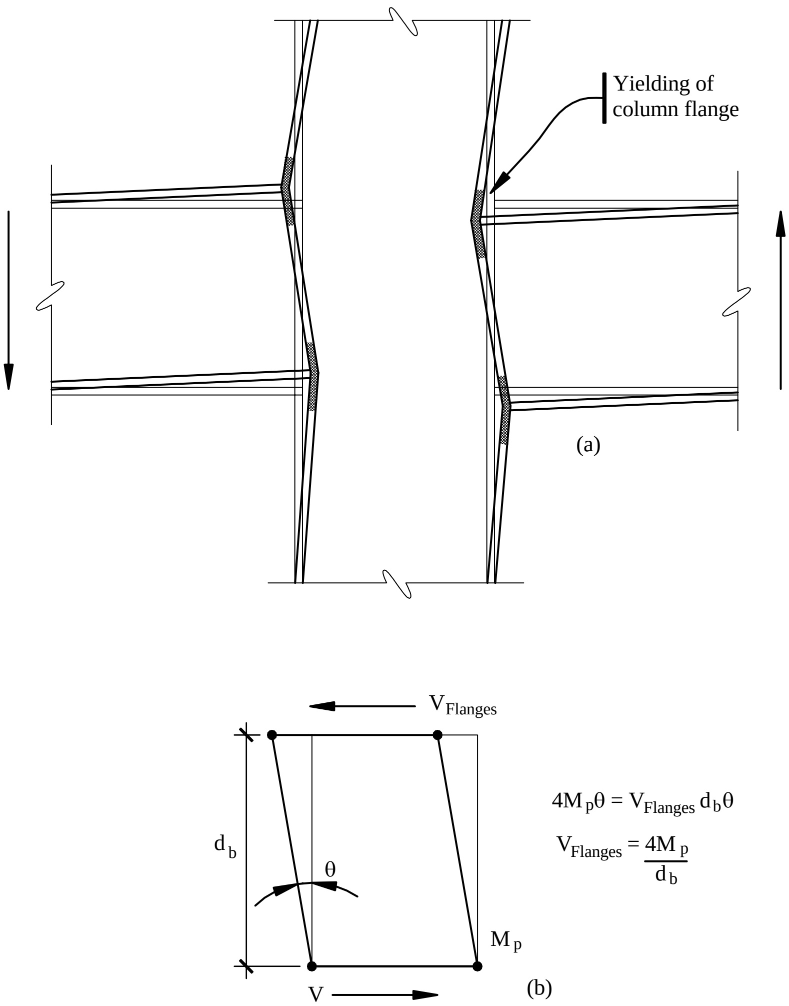

Figure 3.2-11 Column flange component of panel zone resistance.

The panel zone shear resistance (V_{Panel}) is simply the effective shear area of the panel $d_c t_p$ multiplied by the yield stress in shear, assumed as $0.6F_y$. (The 0.6 factor is a simplification of the Von Mises yield criterion that gives the yield stress in shear as $1/\sqrt{3} = 0.577$ times the strength in tension.)

The second term, $1.8V_{Flanges}$, is based on experimental observation. Testing of simple beam-column subassemblies show that a "kink" forms in the column flanges as shown in Figure 3.2-11(a). If it can be assumed that the kink is represented by a plastic hinge with a plastic moment capacity of $M_p = F_y Z = F_y b_{cf} t_{cf}^{\,2}/4$, it follows from virtual work (see Figure 3.2-11b) that the equivalent shear strength of the column flanges is:

$$V_{Flanges} = \frac{4M_p}{d_b}$$

and by simple substitution for M_p:

$$V_{Flanges} = \frac{F_y b_{cf} t_{cf}^2}{d_b}$$

This value does not include the 1.8 multiplier that appears in the AISC equation. This multiplier is based on experimental results. It should be noted that the flange component of strength is small compared to the panel component unless the column has very thick flanges.

The shear stiffness of the panel is derived as shown in Figure 3.2-12:

$$K_{Panel,\gamma} = \frac{V_{Panel}}{\gamma} = \frac{V_{Panel}}{\delta/d_b}$$

noting that the displacement δ can be written as:

$$\delta = \frac{V_{Panel} d_b}{G t_p d_c},$$

$$K_{Panel,\gamma} = \frac{V_{Panel}}{\left(\frac{V_{Panel} d_b}{G t_p d_c}\right)\frac{1}{d_b}} = G t_p d_c$$

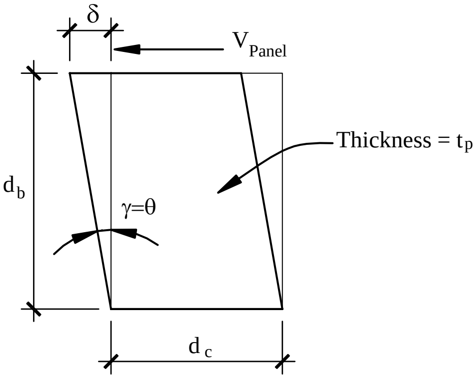

Figure 3.2-12 Column web component of panel zone resistance.

Krawinkler assumes that the column flange component yields at four times the yield deformation of the panel component, where the panel yield deformation is:

$$\gamma_y = \frac{V_{Panel}}{K_{Panel,\gamma}} = \frac{0.6F_y d_c t_p}{G d_c t_p} = \frac{0.6F_y}{G}\ .$$

At this deformation, the panel zone strength is V_{Panel} + 0.25 $_{Vflanges}$; at four times this deformation, the strength is $V_{Panel} + V_{Flanges}$. The inelastic force-deformation behavior of the panel is illustrated in Figure 3.2-13. This figure is applicable also to exterior joints (girder on one side only), roof joints (girders on both sides, column below only), and corner joints (girder on one side only, column below only).

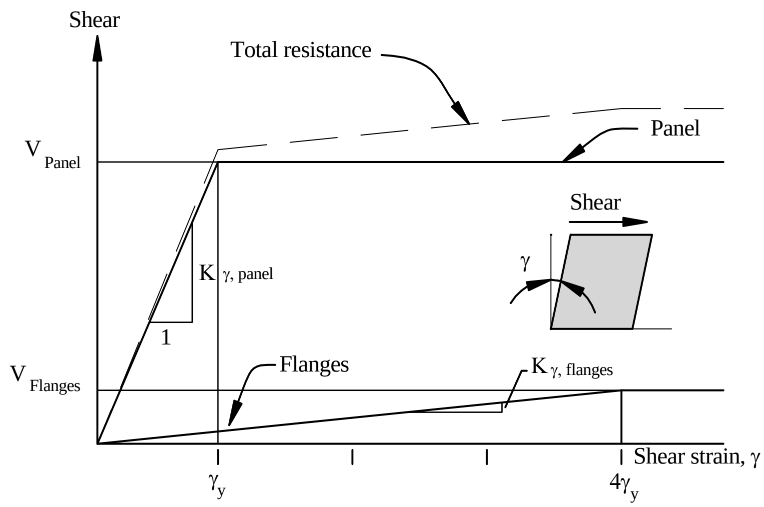

Figure 3.2-13 Force-deformation behavior of panel zone region.

The actual Krawinkler model is shown in Figure 3.2-10. This model consists of four rigid links, connected at the corners by compound nodes. The columns and girders frame into the links at right angles at Points I through L. These are moment-resisting connections. Rotational springs are used at the upper left (point A) and lower right (point D) compound nodes. These springs are used to represent the panel resistance mechanisms described earlier. The upper right and lower left corners (points B and C) do not have rotational springs and thereby act as real hinges.

The finite element model of the joint requires 12 individual nodes: one node each at Points I through L, and two nodes (compound node pairs) at Points A through D. It is left to the reader to verify that the total number of degrees of freedom in the model is 28 (if the only constraints are associated with the corner compound nodes).

The rotational spring properties are related to the panel shear resistance mechanisms by a simple transformation, as shown in Figure 3.2-14. From the figure it may be seen that the moment in the rotational spring is equal to the applied shear times the beam depth. Using this transformation, the properties of the rotational spring representing the panel shear component of resistance are:

$$M_{Panel} = V_{Panel} d_b = 0.6 F_y d_c d_b t_p$$

$$K_{Panel,\theta} = K_{Panel,\gamma} d_b = G d_c d_b t_p$$

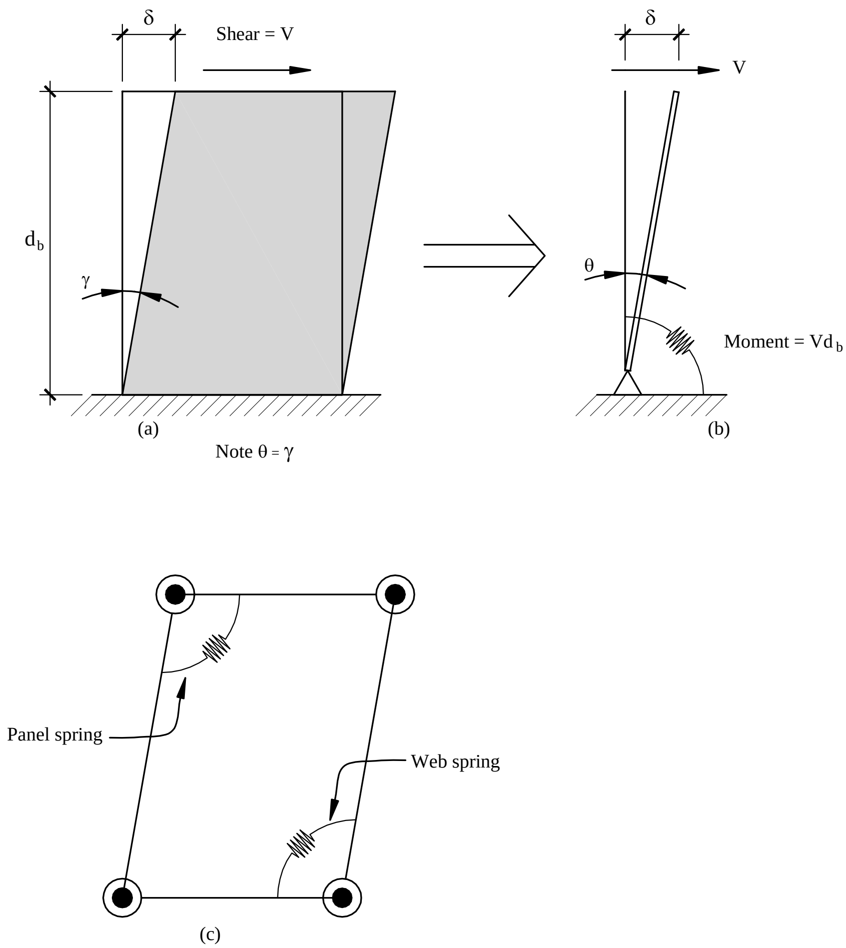

Figure 3.2-14 Transforming shear deformation to rotational deformation in the Krawinkler model.

It is interesting to note that the shear strength in terms of the rotation spring is simply $0.6F_y$ times the volume of the panel, and the shear stiffness in terms of the rotational spring is equal to *G* times the panel volume.

The flange component of strength in terms of the rotational spring is determined in a similar manner:

$$M_{Flanges} = 1.8 V_{Flanges} d_b = 1.8 F_y b_{cf} t_{cf}^2$$

Because of the equivalence of rotation and shear deformation, the yield rotation of the panel is the same as the yield strain in shear:

$$\theta_y = \gamma_y = \frac{M_{Panel}}{K_{Panel,\theta}} = \frac{0.6F_y}{G} \ .$$

To determine the initial stiffness of the flange spring, it is assumed that this spring yields at four times the yield deformation of the panel spring. Hence,

$$K_{Flanges,\theta} = \frac{M_{Flanges}}{4\theta_y} = 0.75Gb_{cf}t_{cf}^2 \ .$$

The complete resistance mechanism, in terms of rotational spring properties, is shown in Figure 3.2-13. This trilinear behavior is represented by two elastic-perfectly plastic springs at the opposing corners of the joint assemblage.

If desired, strain-hardening may be added to the system. Krawinkler suggests using a strain-hardening stiffness equal to 3 percent of the initial stiffness of the joint. In this analysis, the strain- hardening component was simply added to both the panel and the flange components:

$$K_{SH,\theta} = 0.03(K_{Panel,\theta} + K_{Flanges,\theta}) \ .$$

Before continuing, one minor adjustment is made to the above derivations. Instead of using the nominal total beam and girder depths in the calculations, the distance between the center of the flanges was used as the effective depth. Hence:

$$d_c \equiv d_{c,nom} - t_{cf}$$

where the *nom* part of the subscript indicates the property listed as the total depth in the *AISC Manual of Steel Construction*.

The Krawinkler properties are now computed for a typical interior subassembly of the 6-story frame. A summary of the properties used for all connections is shown in Table 3.2-8.

Table 3.2-8 Properties for the Krawinkler Beam-Column Joint Model

Connection	Girder	Column	Doubler Plate (in.)	$M_{panel,\theta}$ (in.-k)	$K_{panel,\theta}$ (in.-k/rad)	$M_{flanges,\theta}$ (in.-k/rad)	$K_{flanges,q}$ (in.-k/rad)
A	W24x84	W21x122	–	8,701	3,480,000	1,028	102,800
B	W24x84	W21x122	1.00	23,203	9,281,000	1,028	102,800
C	W27x94	W21x147	–	11,822	4,729,000	1,489	148,900
D	**W27x94**	**W21x147**	**1.00**	**28,248**	**11,298,000**	**1,489**	**148,900**
E	W27x94	W21x201	–	15,292	6,117,000	3,006	300,600
F	W27x94	W21x201	0.875	29,900	11,998,000	3,006	300,600

Example calculations shown for row in **bold** type.

The sample calculations below are for Connection D in Table 3.2-8.

Material Properties:

F_y = 50.0 ksi (girder, column, and doubler plate)
G = 12,000 ksi

Girder:

W27x94
$d_{b,nom}$ 26.92 in.
t_f 0.745 in.
d_b 26.18 in.

Column:

W21x147
$d_{c,nom}$ 22.06 in.
t_w 0.72 in.
t_{cf} 1.150 in.
d_c 20.91 in.
b_{cf} 12.51 in.

Doubler plate: 1.00 in.

Total panel zone thickness = t_p = 0.72 + 1.00 = 1.72 in.

$$V_{Panel} = 0.6F_y d_c t_p = 0.6(50)(20.91)(1.72) = 1{,}079 \text{ kips}$$

$$V_{Flanges} = 1.8\frac{F_y b_{cf} t_{cf}^2}{d_b} = 1.8\frac{50(12.51)(1.15^2)}{26.18} = 56.9 \text{ kips}$$

$$K_{Panel,\gamma} = Gt_p d_c = 12{,}000(1.72)(20.91) = 431{,}582 \text{ kips/unit shear strain}$$

$$\gamma_y = \theta_y = \frac{0.6F_y}{G} = \frac{0.6(50{,}000)}{12{,}000} = 0.0025$$

$$M_{Panel} = V_{Panel} d_b = 1{,}079(26.18) = 28{,}248 \text{ in.-kips}$$

$$K_{Panel,\theta} = K_{Panel,\gamma} d_b = 431{,}582(26.18) = 11{,}298{,}000 \text{ in.-kips/radian}$$

$$M_{Flanges} = V_{Flanges} d_b = 56.9(26.18) = 1{,}489 \text{ in.-kips}$$

$$K_{Flanges,\theta} = \frac{M_{Flanges}}{4\gamma_y} = \frac{1{,}489}{4(0.0025)} = 148{,}900 \text{ in.-kips/radian}$$

3.2.4.3 Modeling Girders

Because this structure is designed in accordance with the strong-column/weak-beam principle, it is anticipated that the girders will yield in flexure. Although DRAIN provides special yielding beam elements (Type 2 elements), more control over behavior is obtained through the use of the Type 4 connection element.

The modeling of a typical girder is shown in Figure 3.2-8. This figure shows an interior girder, together with the panel zones at the ends. The portion of the girder between the panel zones is modeled as four segments with one simple node at mid span and one compound node near each end. The mid-span node is used to enhance the deflected shape of the structure.[5] The compound nodes are used to represent inelastic behavior in the hinging region.

The following information is required to model each plastic hinge:

1. The initial stiffness (moment per unit rotation),
2. The effective yield moment,
3. The secondary stiffness, and
4. The location of the hinge with respect to the face of the column.

Determination of the above properties, particularly the location of the hinge, is complicated by the fact that the plastic hinge grows in length during increasing story drift. Unfortunately, there is no effective way to represent a changing hinge length in DRAIN, so one must make do with a fixed hinge length and location. Fortunately, the behavior of the structure is relatively insensitive to the location of the hinges.

[5]A graphic post-processor was used to display the deflected shape of the structure. The program represents each element as a straight line. Although the computational results are unaffected, a better graphical representation is obtained by subdividing the member.

To determine the hinge properties, it is necessary to perform a moment-curvature analysis of the cross section, and this, in turn, is a function of the stress-strain curve of the material. In this example, a relatively simple stress-strain curve is used to represent the 50 ksi steel in the girders. This curve does not display a yield plateau, which is consistent with the assumption that the section has yielded in previous cycles, with the Baushinger effect erasing any trace of the yield plateau. The idealized stress-strain curve is shown in Figure 3.2-15.

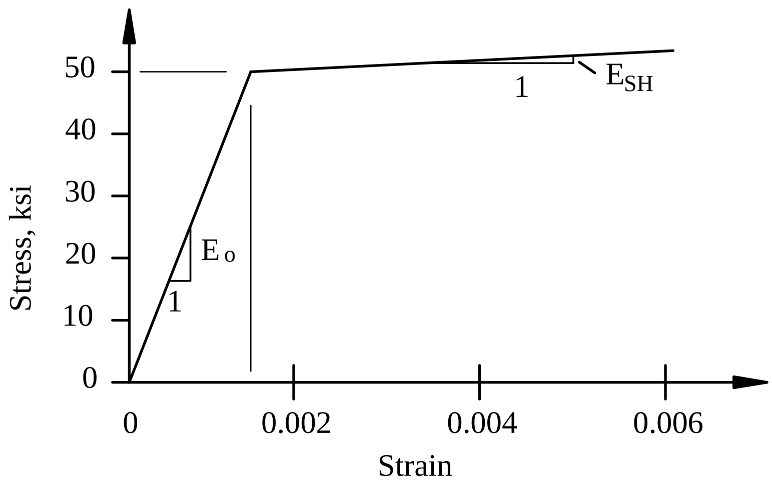

Figure 3.2-15 Assumed stress-strain curve for modeling girders.

To compute the moment-curvature relationship, the girder cross section was divided into 50 horizontal slices, with 10 slices in each flange and 30 slices in the web. The girder cross section was then subjected to gradually increasing rotation. For each value of rotation, strain compatibility (plane sections remain plane) was used to determine fiber strain. Fiber stress was obtained from the stress-strain law and stresses were multiplied by fiber area to determine fiber force. The forces were then multiplied by the distance to the neutral axis to determine that fiber's contribution to the section's resisting moment. The fiber contributions were summed to determine the total resisting moment. Analysis was performed using a Microsoft Excel worksheet. Curves were computed for an assumed strain hardening ratio of 1, 3, and 5 percent of the initial stiffness. The resulting moment-curvature relationship is shown for the W27x94 girder in Figure 3.2-16. Because of the assumed bilinear stress-strain curve, the moment-curvature relationships are essentially bilinear. Residual stresses due to section rolling were ignored, and it was assumed that local buckling of the flanges or the web would not occur.

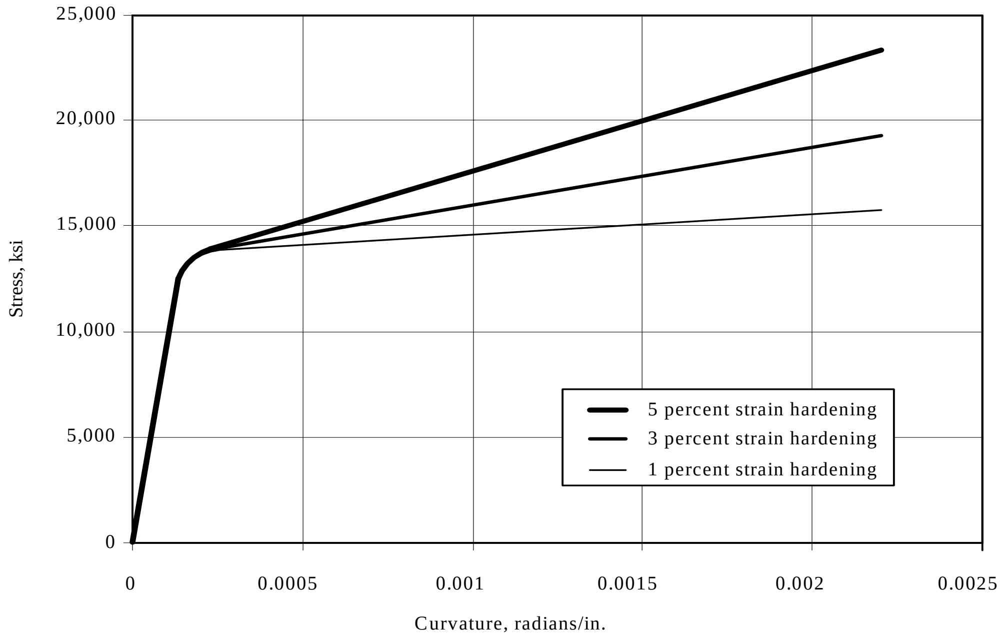

Figure 3.2-16 Moment curvature diagram for W27x94 girder.

To determine the parameters for the plastic hinge in the DRAIN model, a separate analysis was performed on the structure shown in Figure 3.2-17(a). This structure represents half of the clear span of the girder supported as a cantilever. The purpose of the special analysis was to determine a moment-deflection relationship for the cantilever loaded at the tip with a vertical force V. A similar moment-deflection relationship was determined for the structure shown in Figure 3.2-17(b), which consists of a cantilever with a compound node used to represent the inelastic rotation in the plastic hinge. Two Type-4 DRAIN elements were used at each compound node. The first of these is rigid-perfectly plastic and the second is bilinear. The resulting behavior is illustrated in Figure 3.2-17(c).

If the moment-curvature relationship is idealized as bilinear, it is a straightforward matter to compute the deflections of the structure of Figure 3.2-17(a). The method is developed in Figure 3.2-18. Figure 3.2-18(a) is a bilinear moment-curvature diagram. The girder is loaded to some moment M, which is greater than the yield moment. The moment diagram for the member is shown in Figure 3.2-18(b). At some distance x the moment is equal to the yield moment:

$$x = \frac{M_y L}{M}$$

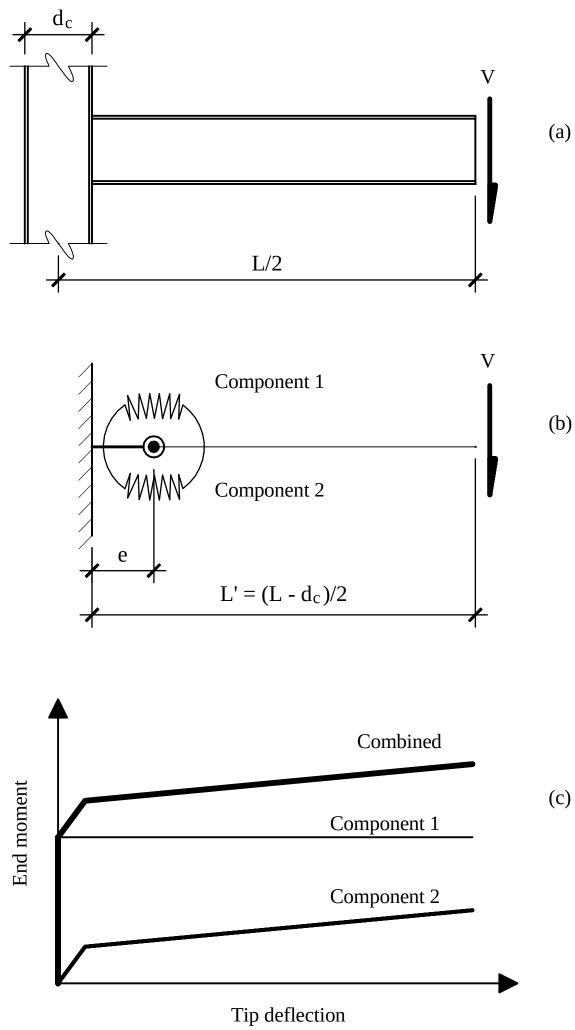

Figure 3.2-17 Developing moment-deflection diagrams for a typical girder.

The curvature along the length of the member is shown in Figure 3.2-18(c). At the distance *x*, the curvature is the yield curvature (ϕ_y), and at the support, the curvature (ϕ_M) is the curvature corresponding to the Point M on the moment-curvature diagram. The deflection is computed using the moment-area method, and consists of three parts:

$$\Delta_1 = \frac{\phi_y x}{2} \cdot \frac{2x}{3} = \frac{\phi_y x^2}{3}$$

$$\Delta_2 = \phi_y \left(L' - x\right) \frac{L' + x}{2} = \frac{\phi_y (L' - x)(L' + x)}{2}$$

$$\Delta_3 = \frac{\left(\phi_M - \phi_y\right)\left(L' - x\right)}{2} \cdot \left[x + \frac{2\left(L' - x\right)}{3}\right]$$
$$= \frac{\left(\phi_M - \phi_y\right)\left(L' - x\right)\left(2L' + x\right)}{6}$$

The first two parts of the deflection are for elastic response and the third is for inelastic response. The elastic part of the deflection is handled by the Type-2 elements in Figure 3.2-17(b). The inelastic part is represented by the two Type-4 elements at the compound node of the structure.

The development of the moment-deflection relationship for the W27x94 girder is illustrated in Figure 3.2-19. Part (a) of the figure is the idealized bilinear moment-curvature relationship for 3 percent strain hardening. Displacements were computed for 11 points on the structure. The resulting moment-deflection diagram is shown in Figure 3.2-19(b), where the total deflection (Δ_1+Δ_2+Δ_3) is indicated. The inelastic part of the deflection (Δ_3 only) is shown separately in Figure 3.2-19(c), where the moment axis has been truncated below 12,000 in.-kips.

Finally, the simple DRAIN cantilever model of Figure 3.2-17(b) is analyzed. The compound node has arbitrarily been placed a distance e = 5 in. from the face of the support. (The analysis is relatively insensitive to the assumed hinge location.)

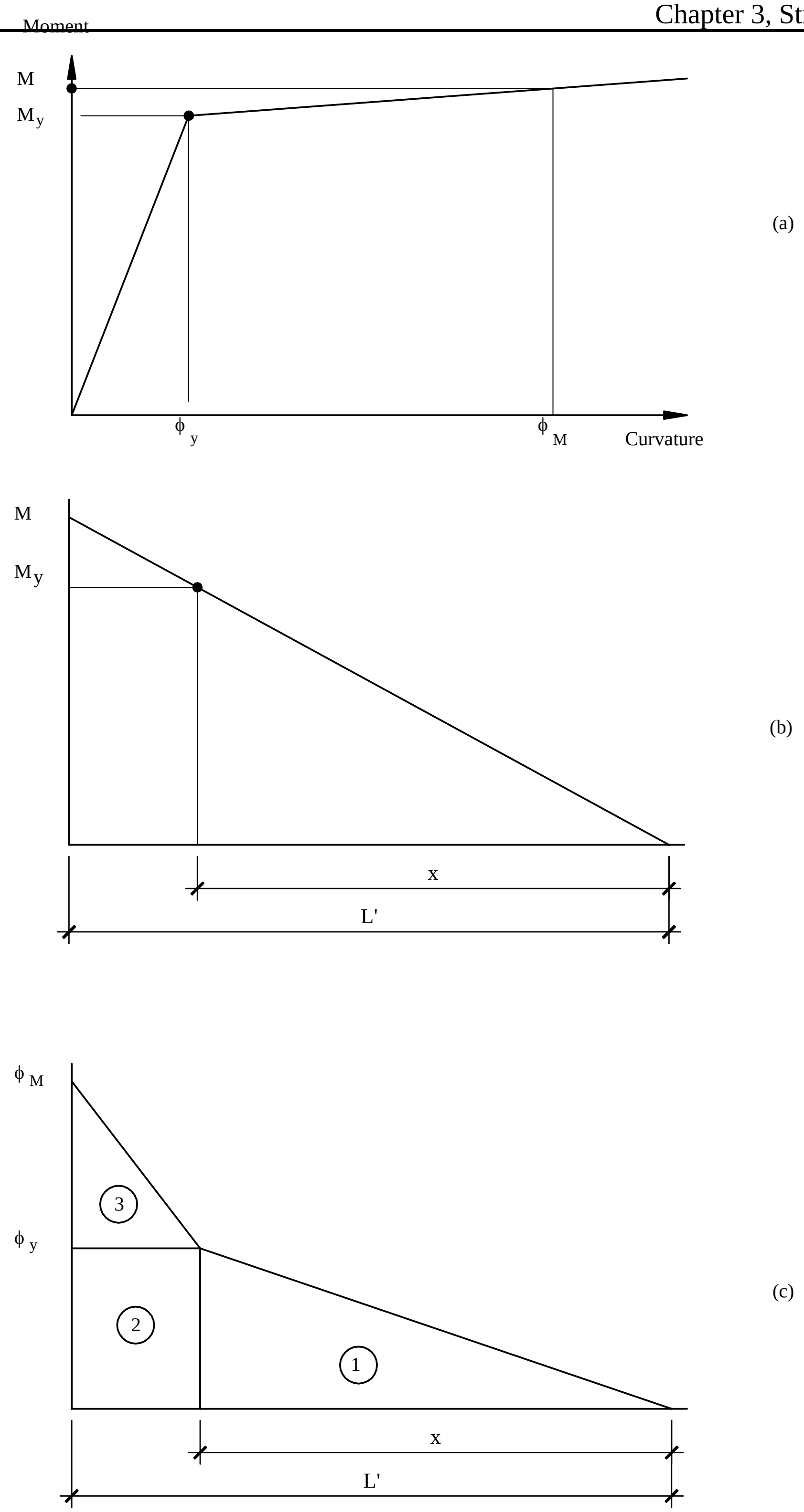

Figure 3.2-18 Development of equations for deflection of moment-deflection curves.

The moment diagram is shown in Figure 3.2-20(a) for the model subjected to a load producing a support moment, M_S, greater than the yield moment. The corresponding curvature diagram is shown in Figure 3.2-20(b). At the location of the plastic hinge, the moment is:

$$M_H = M_S \frac{(L' - e)}{L'}$$

and all inelastic curvature is concentrated into a plastic hinge with rotation θ_H. The tip deflection of the structure of Figure 3.2-20(c) consists of two parts:

$$\Delta_E = \frac{M_{Support} L'^2}{3EI}$$

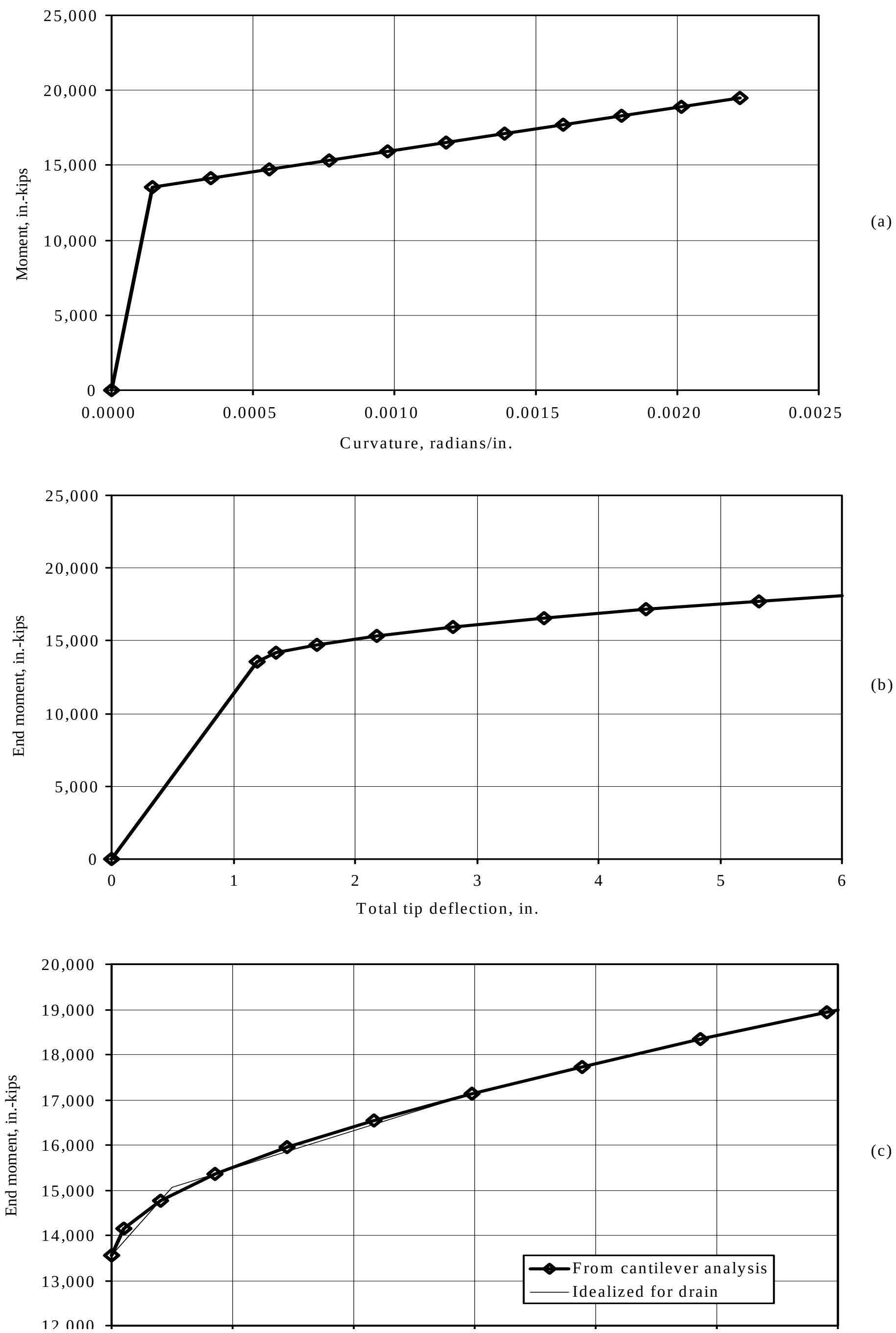

Figure 3.2-19 Moment-deflection curve for W27x94 girder with 3 percent strain hardening.

$$\Delta_I = \theta_H (L' - e) \ .$$

The first part is the elastic deflection and the second part is the inelastic deflection. Note that Δ_E and ($\Delta_1 + \Delta_2$) are not quite equal because the shapes of the curvature diagram used to generate the deflections are not the same. For the small values of strain hardening assumed in this analysis, however, there is little error in assuming that the two deflections are equal. As Δ_E is simply the elastic displacement of a simple cantilever beam, it is possible to model the main portion of the girder using its nominal moment of inertia. The challenge is to determine the properties of the two Type-4 elements such that the deflections predicted using Δ_I are close to those produced using Δ_3. This is a trial-and-error procedure, which is difficult to reproduce in this example. However, the development of the hinge properties is greatly facilitated by the fact that one component of the hinge must be rigid-plastic, with the second component being bilinear. The resulting "fit" for the W27x94 girder is shown in Figure 3.2-19. The resulting properties for the model are shown in Table 3.2-9. The properties for the W24x84 girder are also shown in the table. Note that the first yield of the model will be the yield moment from Component 1, and that this moment is roughly equal to the fully plastic moment of the section.

Table 3.2-9 Girder Properties as Modeled in DRAIN

Property		Section	
		W24x84	W27x94
Elastic Properties	Moment of Inertia (in.^{4})	2,370	3,270
	Shear Area (in.^{2})	11.3	13.2
Inelastic Component 1 (see note below)	Yield Moment (in.-kip)	11,025	13,538
	Initial Stiffness (in.-kip/radian)	10E10	10E10
	S.H. Ratio	0.0	0.0
Inelastic Component 2	Yield Moment (in.-kip)	1,196	1,494
	Initial Stiffness (in.-kip/radian)	326,000	450,192
	S.H. Ratio	0.284	0.295
Comparative Property	Yield Moment = S_xF_y	9,800	12,150
	Plastic Moment = Z_xF_y	11,200	13,900

In some versions of DRAIN the strain hardening stiffness of the Type-4 springs is set to some small value (e.g. 0.001) if a zero value is entered in the appropriate data field. This may cause very large artificial strain hardening moments to develop in the hinge after it yields. It is recommended, therefore, to input a strain hardening value of 10^{-20} to prevent this from happening.

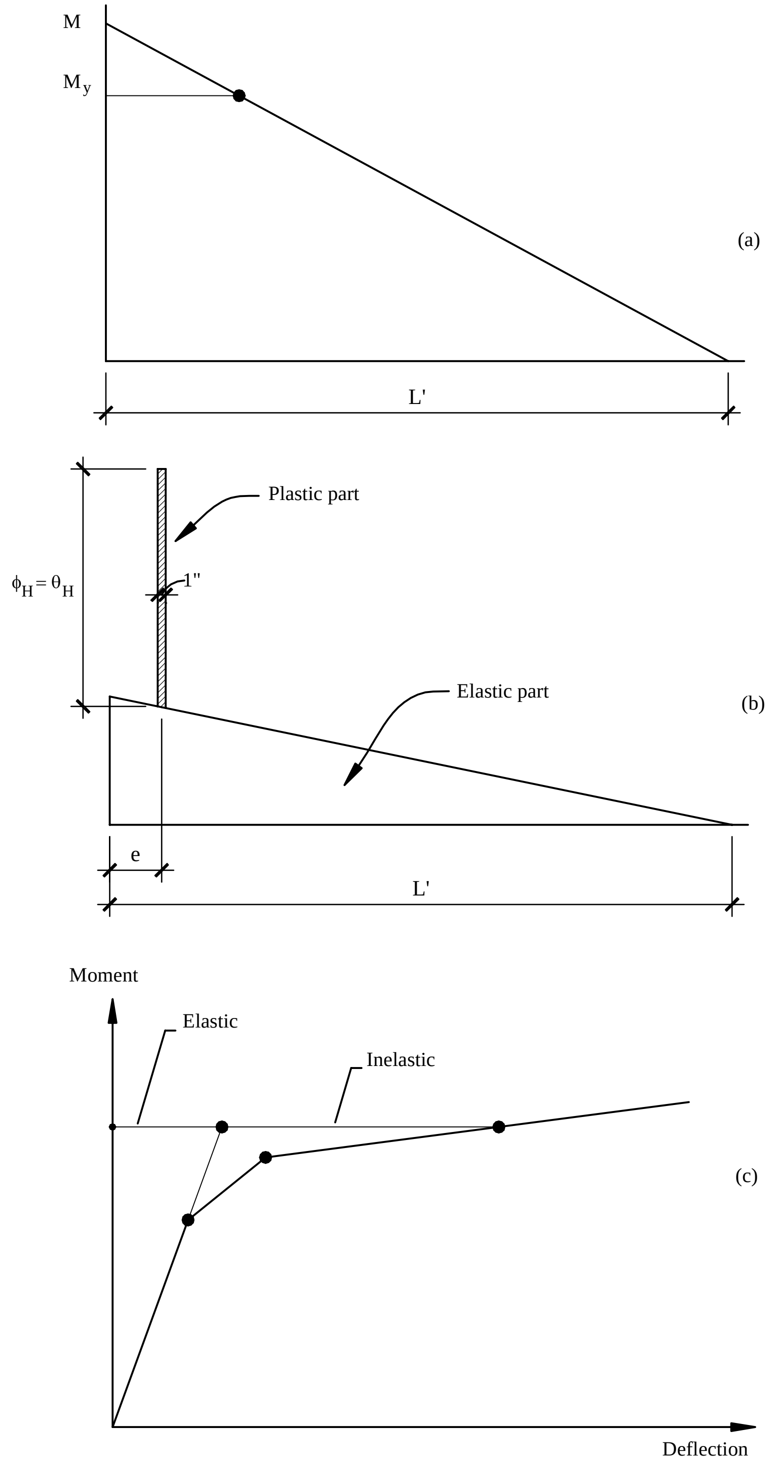

Figure 3.2-20 Development of plastic hinge properties for the W27x97 girder.

3.2.4.4 Modeling Columns

All columns in the analysis were modeled as Type-2 elements. Preliminary analysis indicated that columns should not yield, except at the base of the first story. Subsequent analysis showed that the columns will yield in the upper portion of the structure as well. For this reason, column yielding had to be activated in all of the Type-2 column elements. The columns were modeled using the built-in yielding functionality of the DRAIN program, wherein the yield moment is a function of the axial force in the column. The yield surface used by DRAIN is shown in Figure 3.2-21.

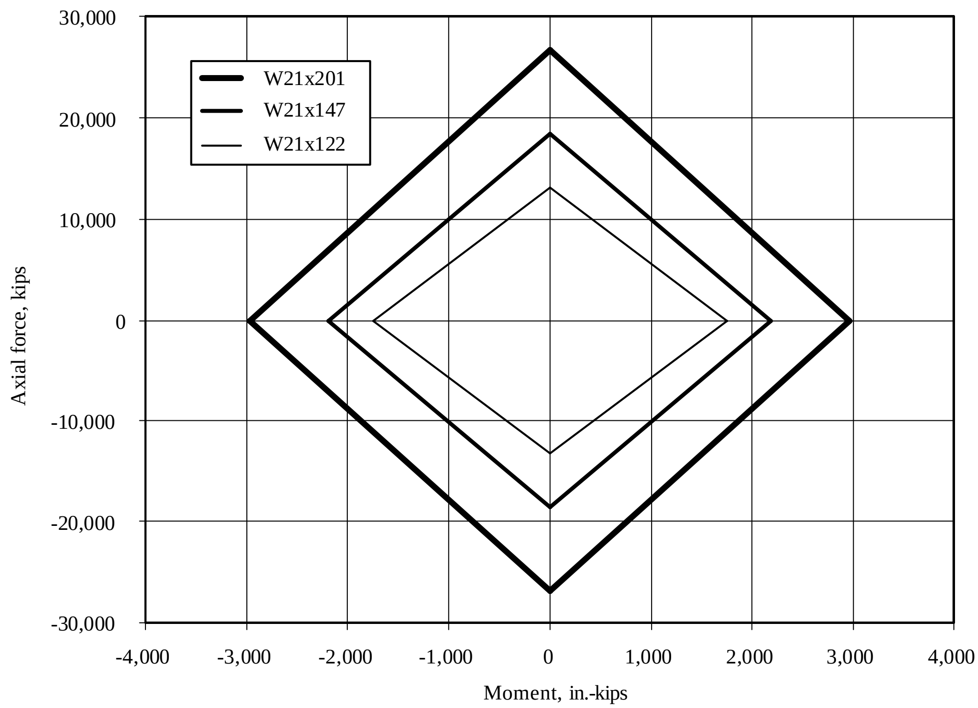

Figure 3.2-21 Yield surface used for modeling columns.

The rules employed by DRAIN to model column yielding are adequate for event-to-event nonlinear static pushover analysis, but leave much to be desired when dynamic analysis is performed. The greatest difficulty in the dynamic analysis is adequate treatment of the column when unloading and reloading. An assessment of the effect of these potential problems is beyond the scope of this example.

3.2.5 Static Pushover Analysis

Nonlinear static analysis is covered for the first time in the Appendix to Chapter 5 of the 2000 *Provisions*. Inclusion of these requirements in an appendix rather than the main body indicates that pushover analysis is in the developmental stage and may not be “ready for prime time.” For this reason, some liberties are taken in this example; however, for the most part, the example follows the appendix. [In the 2003

Provisions, a number of substantive technical changes have been made to the appendix, largely as a result of work performed by the Applied Technology Council in Project 55, Evaluation and Improvement of Inelastic Seismic Analysis Procedures).]

Nonlinear static pushover analysis, in itself, provides the location and sequence of expected yielding in a structure. Additional analysis is required to estimate the amount of inelastic deformation that may occur during an earthquake. These inelastic deformations may then be compared to the deformations that have been deemed acceptable under the ground motion parameters that have been selected. *Provisions* Sec. 5A.1.3 [Appendix to Chapter 5] provides a simple methodology for estimating the inelastic deformations but does not provide specific acceptance criteria.

Another well-known method for determining maximum inelastic displacement is based on the capacity spectrum approach. This method is described in some detail in ATC 40 (Applied Technology Council, 1996). The capacity spectrum method is somewhat controversial and, in some cases may produce unreliable results (Chopra and Goel, 1999). However, as the method is still very popular and is incorporated in several commercial computer programs, it will be utilized here, and the results obtained will be compared to those computed using the simple approach.

Provisions Sec. 5A1.1 [A5.2.1] discusses modeling requirements for the pushover analysis in relatively vague terms, possibly reflecting the newness of the approach. However, it is felt that the model of the structure described earlier in this example is consistent with the spirit of the *Provisions*.[6]

The pushover curve obtained from a nonlinear static analysis is a function of the way the structure is both modeled and loaded. In the analysis reported herein, the structure was first subjected to the full dead load plus reduced live load followed by the lateral loads. The *Provisions* states that the lateral load pattern should follow the shape of the first mode. In this example, four different load patterns were initially considered:

UL = uniform load (equal force at each level)
TL = triangular (loads proportional to height)
ML = modal load (lateral loads proportional to first mode shape)
BL = *Provisions* load distribution (using the forces indicated in Table 3.2-3)

Relative values of these load patterns are summarized in Table 3.2-10. The loads have been normalized to a value of 15 kips at Level 2. Because of the similarity between the TL and ML distributions, the results from the TL distribution are not presented.

DRAIN analyses were run with P-delta effects included and, for comparison purposes, with such effects excluded. The *Provisions* requires “the influence of axial loads” to be considered when the axial load in the column exceeds 15 percent of the buckling load but presents no guidance on exactly how the buckling load is to be determined nor on what is meant by “influence.” In this analysis the influence was taken as inclusion of the story-level P-delta effect. This effect may be easily represented through linearized geometric stiffness, which is the basis of the outrigger column shown in Figure 3.2-4. Consistent

[6] The mathematical model does not represent strength loss due to premature fracture of welded connections. If such fracture is likely, the mathematical model must be adjusted accordingly.

geometric stiffness, which may be used to represent the influence of axial forces on the flexural flexibility of individual columns, may not be used directly in DRAIN. Such effects may be approximated in DRAIN by subdividing columns into several segments and activating the linearized geometric stiffness on a column-by-column basis. That approach was not used here.

Table 3.2-10 Lateral Load Patterns Used in Nonlinear Static Pushover Analysis

Level	Uniform Load UL (kips)	Triangular Load TL (kips)	Modal Load ML (kips)	BSSC Load BL (kips)
R	15.0	77.5	88.4	150.0
6	15.0	65.0	80.4	118.0
5	15.0	52.5	67.8	88.0
4	15.0	40.0	50.3	60.0
3	15.0	27.5	32.0	36.0
2	15.0	15.0	15.0	15.0

As described later, the pushover analysis indicated all yielding in the structure occurred in the clear span of the girders and columns. Panel zone hinging did not occur. For this reason, the ML analysis was repeated for a structure with thinner doubler plates and without doubler plates. Because the behavior of the structure with thin doubler plates was not significantly different from the behavior with the thicker plates, the only comparison made here will be between the structures with and without doubler plates. These structures are referred to as the strong panel (SP) and weak panel (WP) structures, respectively.

The analyses were carried out using the DRAIN-2Dx computer program. Using DRAIN, an analysis may be performed under “load control” or under “displacement control.” Under load control, the structure is subjected to gradually increasing lateral loads. If, at any load step, the tangent stiffness matrix of the structure has a negative on the diagonal, the analysis is terminated. Consequently, loss of strength due to P-delta effects cannot be tracked. Using displacement control, one particular point of the structure (the control point) is forced to undergo a monotonically increasing lateral displacement and the lateral forces are constrained to follow the desired pattern. In this type of analysis, the structure can display loss of strength because the displacement control algorithm adds artificial stiffness along the diagonal to overcome the stability problem. Of course, the computed response of the structure after strength loss is completely fictitious in the context of a static loading environment. Under a dynamic loading, however, structures can display strength loss and be incrementally stable. It is for this reason that the post-strength-loss realm of the pushover response is of interest.

When performing a displacement controlled pushover analysis in DRAIN with *P*-Delta effects included, one must be careful to recover the base-shear forces properly.[7] At any displacement step in the analysis, the true base shear in the system consists of two parts:

[7]If P-delta effects have been included, this procedure needs to be used when recovering base shear from column shear forces. This is true for displacement controlled static analysis, force controlled static analysis, and dynamic time-history analysis.

$$V = \sum_{i=1}^{n} V_{C,i} - \frac{P_1 \Delta_1}{h_1}$$

where the first term represents the sum of all the column shears in the first story and the second term represents the destabilizing P-delta shear in the first story. The P-delta effects for this structure were included through the use of the outrigger column shown at the right of Figure 3.2-4. Figure 3.2-22 plots two base shear components of the pushover response for the SP structure subjected to the ML loading. Also shown is the total response. The kink in the line representing P-delta forces results because these forces are based on first-story displacement, which, for an inelastic system, will not generally be proportional to the roof displacement.

For all of the pushover analyses reported for this example, the maximum displacement at the roof is 42.0 in. This value is slightly greater than 1.5 times the total drift limit for the structure where the total drift limit is taken as 1.25 times 2 percent of the total height. The drift limit is taken from *Provisions* Table 5.2.8 [4.5-1] and the 1.25 factor is taken from *Provisions* Sec. 5A.1.4.3. [In the 2003 *Provisions*, Sec. A5.2.6 requires multiplication by $0.85R/C_d$ rather than by 1.25.] As discussed below in Sec. 3.2.5.3, the Appendix to Chapter 5 of the *Provisions* requires only that the pushover analysis be run to a maximum displacement of 1.5 times the expected inelastic displacement. If this limit were used, the pushover analysis of this structure would only be run to a total displacement of about 13.5 in.

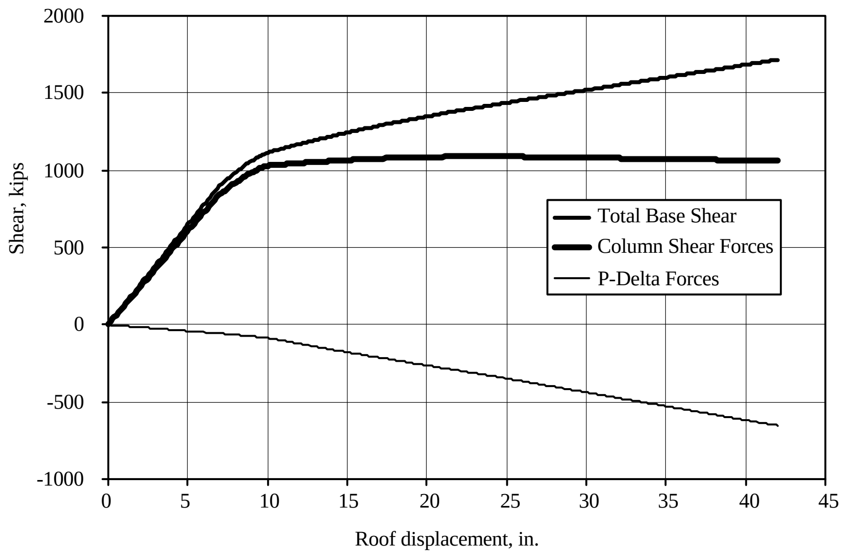

Figure 3.2-22 Two base shear components of pushover response.

3.2.5.1 Pushover Response of Strong Panel Structure

Figure 3.2-23 shows the pushover response of the SP structure to all three lateral load patterns when P-delta effects are excluded. In each case, gravity loads were applied first and then the lateral loads were applied using the displacement control algorithm. Figure 3.2-24 shows the response curves if P-delta effects are included. In Figure 3.2-25, the response of the structure under ML loading with and without

P-delta effects is illustrated. Clearly, P-delta effects are an extremely important aspect of the response of this structure, and the influence grows in significance after yielding. This is particularly interesting in the light of the *Provisions*, which ignore P-delta effects in elastic analysis if the maximum stability ratio is less than 0.10 (see *Provisions* Sec. 5.4.6.2 [5.2.6.2]). For this structure, the maximum computed stability ratio was 0.0839 (see Table 3.2-4), which is less than 0.10 and is also less than the upper limit of 0.0901. The upper limit is computed according to *Provisions* Eq. 5.4.6.2-2 and is based on the very conservative assumption that $\beta = 1.0$. While the *Provisions* allow the analyst to exclude P-delta effects in an elastic analysis, this clearly should not be done in the pushover analysis (or in time-history analysis). [In the 2003 *Provisions*, the upper limit for the stability ratio is eliminated. Where the calculated θ is greater than 0.10 a special analysis must be performed in accordance with Sec. A5.2.3. Sec. A5.2.1 requires that P-delta effects be considered for all pushover analyses.]

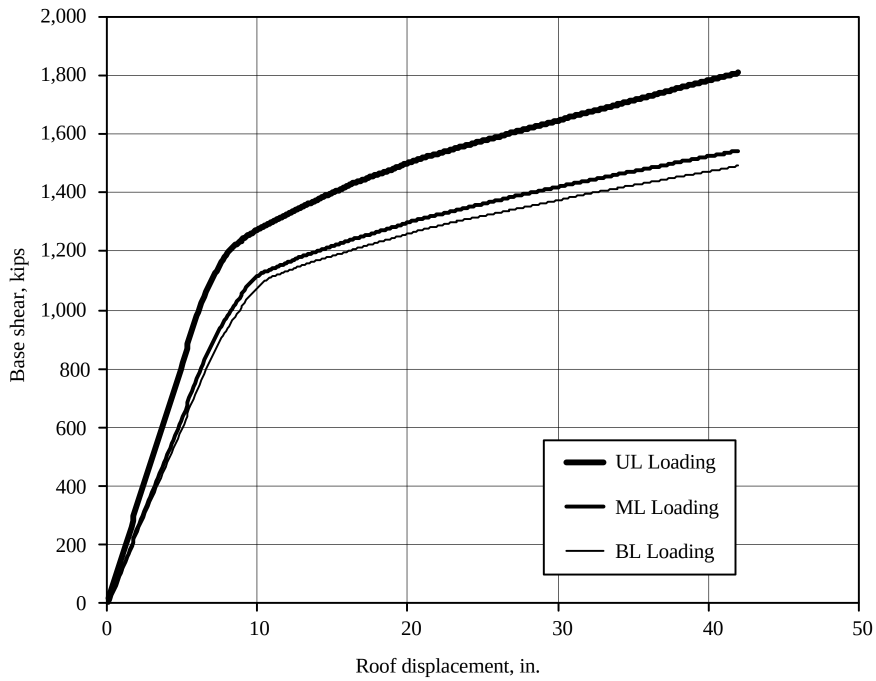

Figure 3.2-23 Response of strong panel model to three load pattern, excluding P-delta effects.

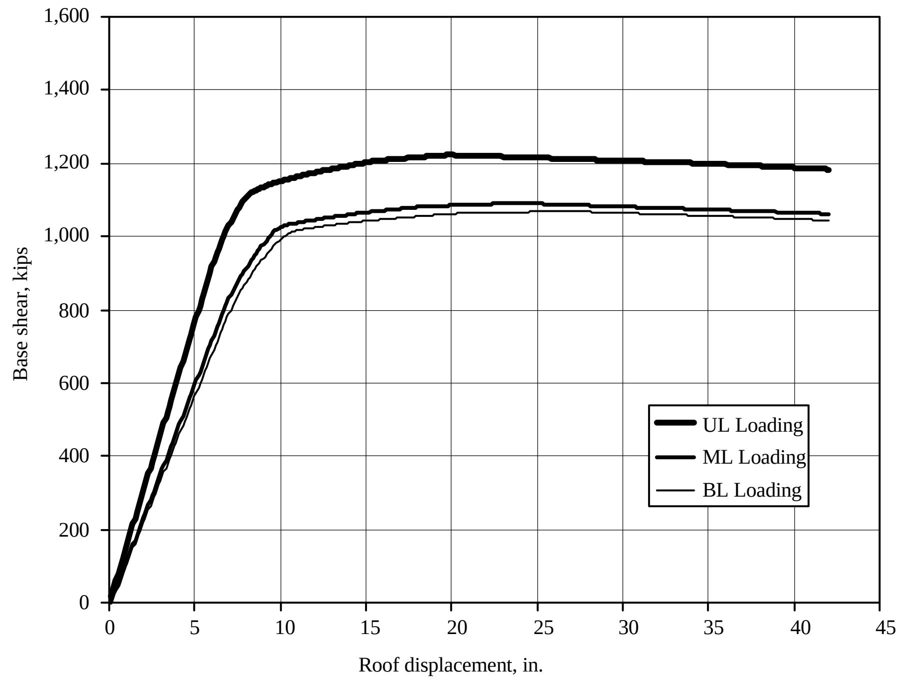

Figure 3.2-24 Response of strong panel model to three load patterns, including P-delta effects.

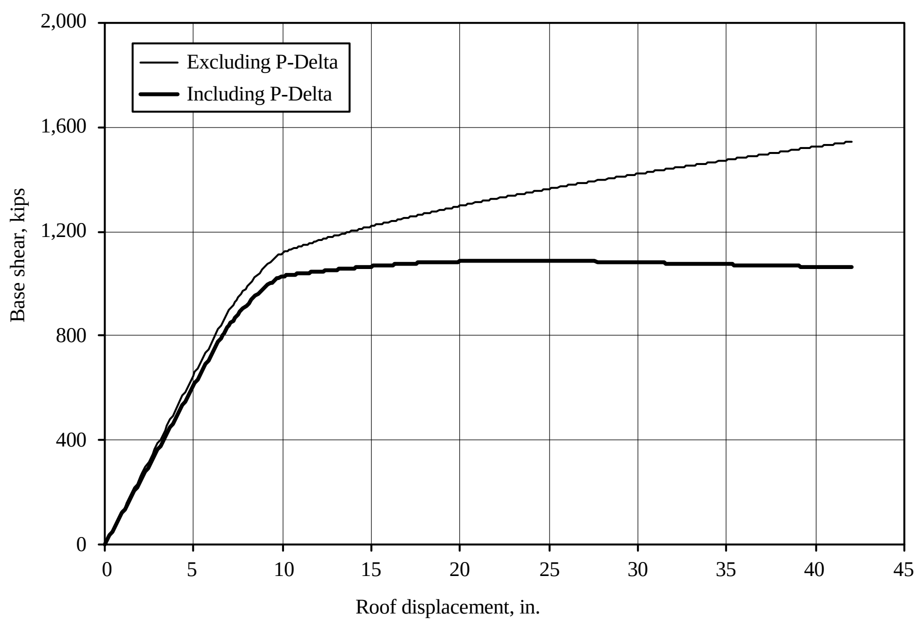

Figure 3.2-25 Response of strong panel model to ML loads, with and wthout P-delta effects.

In Figure 3.2-26, a plot of the tangent stiffness versus roof displacement is shown for the SP structure with ML loading, and with P-delta effects excluded or included. This plot, which represents the slope of the pushover curve at each displacement value, is more effective than the pushover plot in determining when yielding occurs. As Figure 3.2-26 illustrates, the first significant yield occurs at a roof displacement of approximately 6.5 in. and that most of the structure's original stiffness is exhausted by the time the roof drift reaches 10 in.

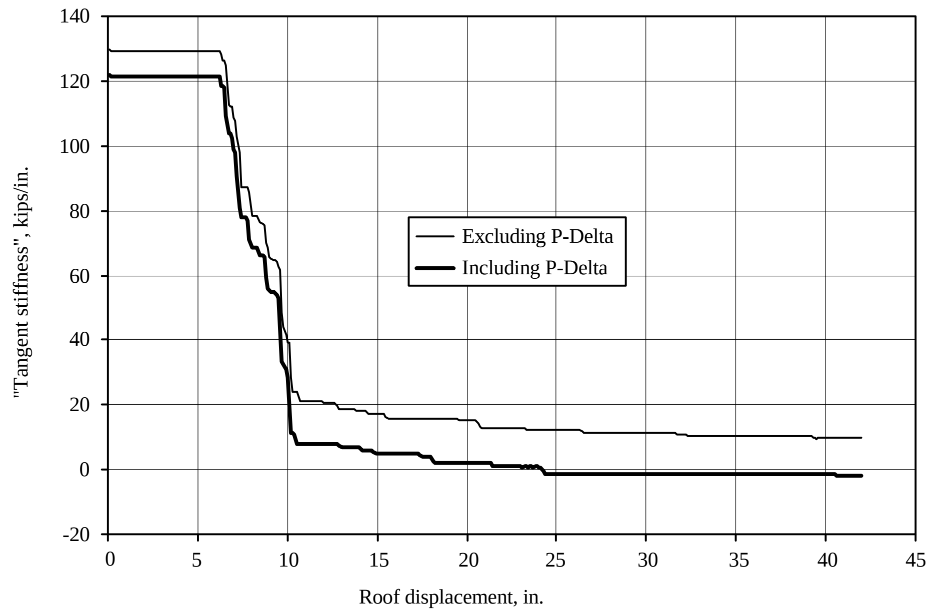

Figure 3.2-26 Tangent stiffness history for structure under ML loads, with and without *P*-delta effects.

For the case with P-delta effects excluded, the final stiffness shown in Figure 3.2-26 is approximately 10 kips/in., compared to an original value of 133 kips/in. Hence, the strain-hardening stiffness of the structure is 0.075 times the initial stiffness. This is somewhat greater than the 0.03 (3.0 percent) strain hardening ratio used in the development of the model because the entire structure does not yield simultaneously.

When P-delta effects are included, the final stiffness is -1.6 kips per in. The structure attains this negative residual stiffness at a displacement of approximately 23 in.

3.2.5.1.1 Sequence and Pattern of Plastic Hinging

The sequence of yielding in the structure with ML loading and with P-delta effects included is shown in Figure 3.2-27. Part (a) of the figure shows an elevation of the structure with numbers that indicate the sequence of plastic hinge formation. For example, the numeral "1" indicates that this was the first hinge to form. Part (b) of the figure shows a pushover curve with several hinge formation events indicated. These events correspond to numbers shown in part (a) of the figure. The pushover curve only shows selected events because an illustration showing all events would be difficult to read.

Several important observations are made from Figure 3.2-27:

1. There was no hinging in Levels 6 and R,
2. There was no hinging in any of the panel zones,
3. Hinges formed at the base of all the first-story columns,
4. All columns on Story 3 and all the interior columns on Story 4 formed plastic hinges, and
5. Both ends of all the girders at Levels 2 through 5 yielded.

It appears the structure is somewhat weak in the middle two stories and is too strong at the upper stories. The doubler plates added to the interior columns prevented panel zone yielding (even at the extreme roof displacement of 42 in.).

The presence of column hinging at Levels 3 and 4 is a bit troublesome because the structure was designed as a strong-column/weak-beam system. This design philosophy, however, is intended to prevent the formation of complete story mechanisms, not to prevent individual column hinging. While hinges did form at the bottom of each column in the third story, hinges did not form at the top of these columns, and a complete story mechanism was avoided.

Even though the pattern of hinging is interesting and useful as an evaluation tool, the performance of the structure in the context of various acceptance criteria cannot be assessed until the expected inelastic displacement can be determined. This is done below in Sec. 3.2.5.3.

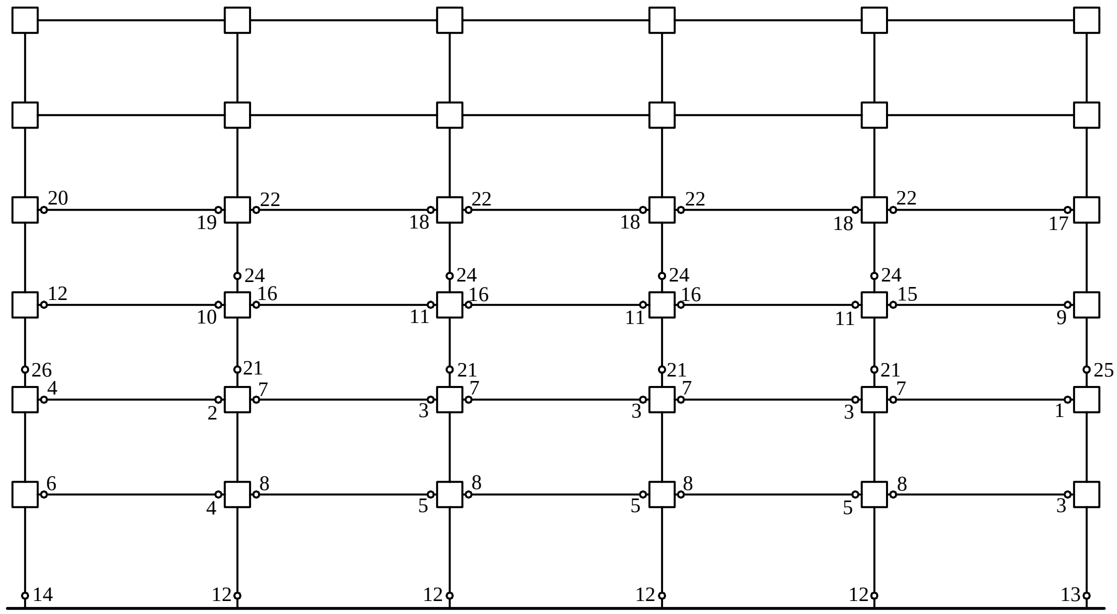

(a)

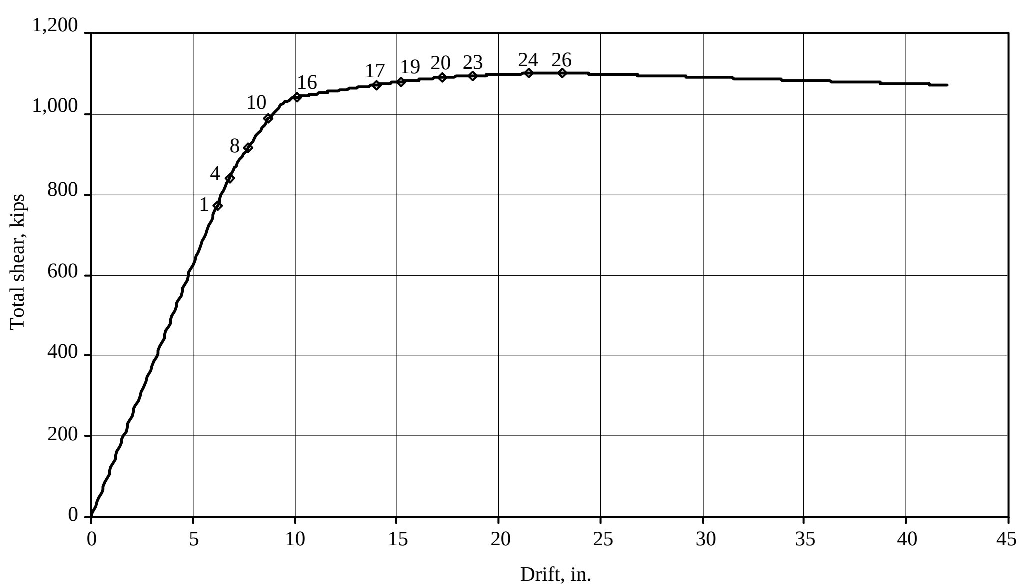

(b)

Figure 3.2-27 Patterns of plastic hinge formation: SP model under ML load, including P-delta effects.

3.2.5.1.2 Comparison with Strength from Plastic Analysis

It is interesting to compare the strength of the structure from pushover analysis with that obtained from the rigid-collapse analysis performed using virtual work. These values are summarized in Table 3.2-11. The strength from the case with P-delta excluded was estimated from the curves shown in Figure 3.2-23 and is taken as the strength at the principal bend in the curve (the estimated yield from a bilinear representation of the pushover curve). Consistent with the upper bound theorem of plastic analysis, the strength from virtual work is significantly greater than that from pushover analysis. The reason for the difference in predicted strengths is related to the pattern of yielding that actually formed in the structure, compared to that assumed in the rigid-plastic analysis.

Table 3.2-11 Strength Comparisons: Pushover vs Rigid Plastic

Pattern	Lateral Strength (kips)		
	P-delta Excluded	P-delta Included	Rigid-Plastic
Uniform	1220	1223	1925
Modal (Triangular)	1137	1101	1523
BSSC	1108	1069	1443

3.2.5.2 Pushover Response of Weak Panel Structure

Before continuing, the structure should be re-analyzed without panel zone reinforcing and the behavior compared with that determined from the analysis described above. For this exercise, only the modal load pattern d is considered but the analysis is performed with and without P-delta effects.

The pushover curves for the structure under modal loading and with weak panels are shown in Figure 3.2-28. Curves for the analyses run with and without P-delta effects are included. Figures 3.2-29 and 3.2-30 are more informative because they compare the response of the structures with and without panel zone reinforcement. Figure 3.2-31 shows the tangent stiffness history comparison for the structures with and without doubler plates. In both cases P-delta effects have been included.

From Figures 3.2-28 through 3.2-31 it may be seen that the doubler plates, which represent approximately 2.0 percent of the volume of the structure, increase the strength by approximately 12 percent and increase the initial stiffness by about 10 percent.

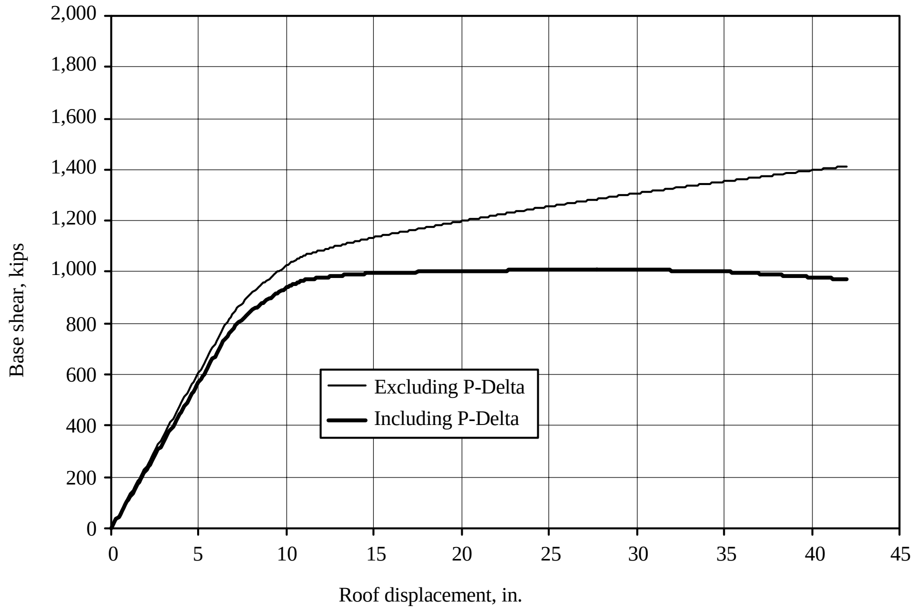

Figure 3.2-28 Weak panel zone model under ML load.

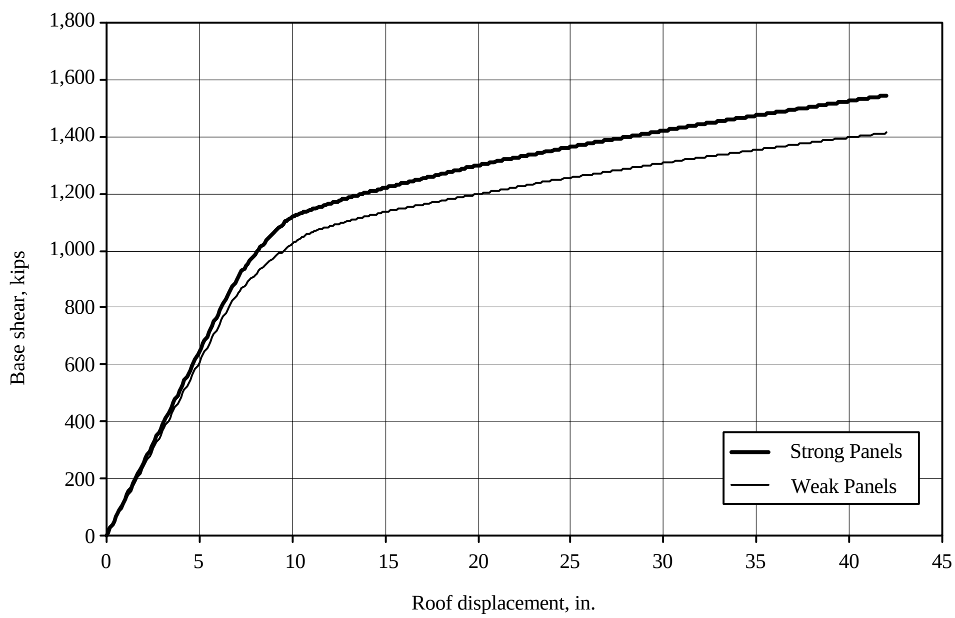

Figure 3.2-29 Comparison of weak panel zone model with strong panel zone model, excluding P-delta effects.

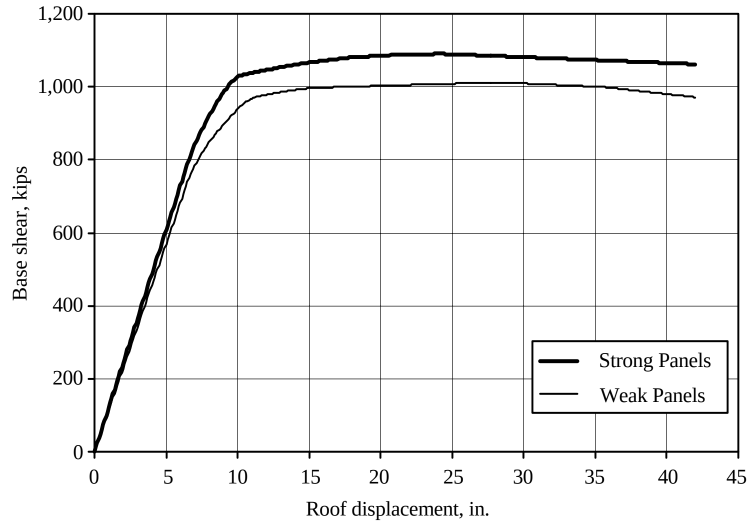

Figure 3.2-30 Comparison of weak panel zone model with strong panel zone model, including P-delta effects.

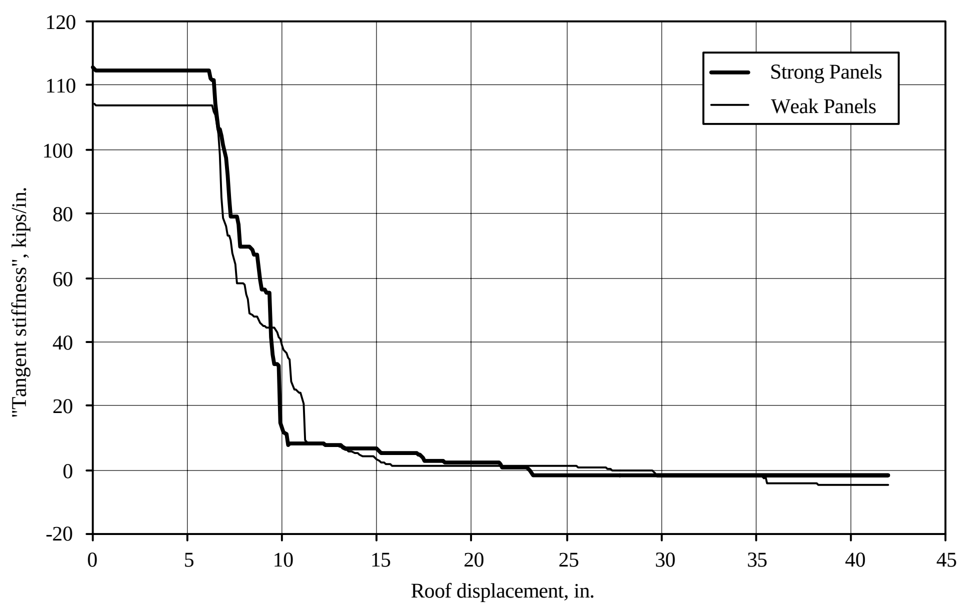

Figure 3.2-31 Tangent stiffness history for structure under ML loads, strong versus weak panels, including P-delta effects.

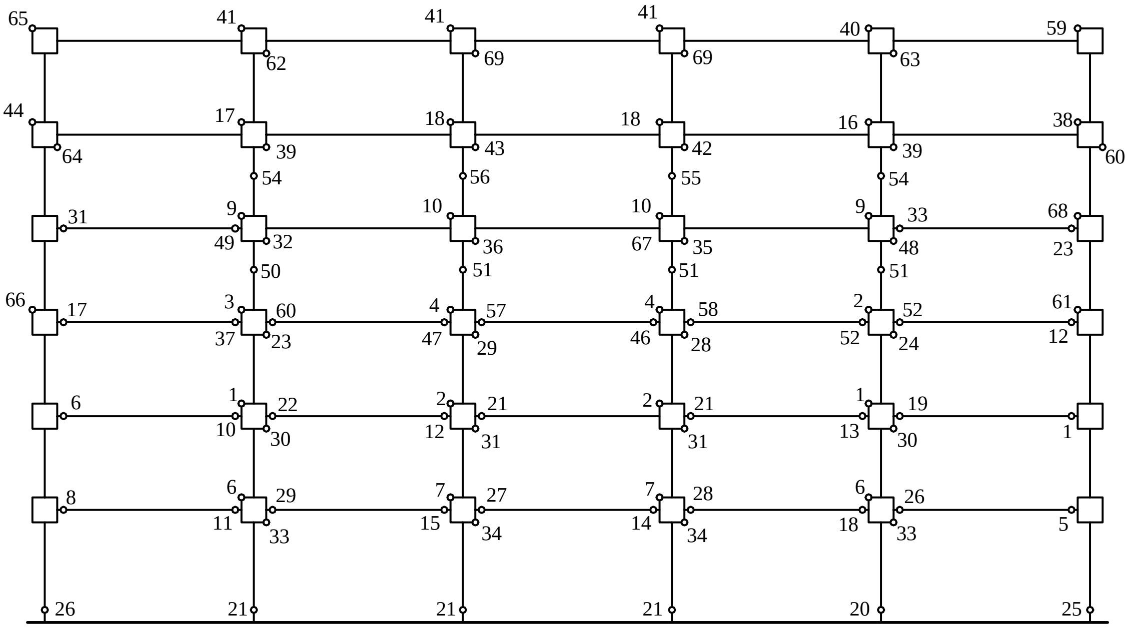

(a)

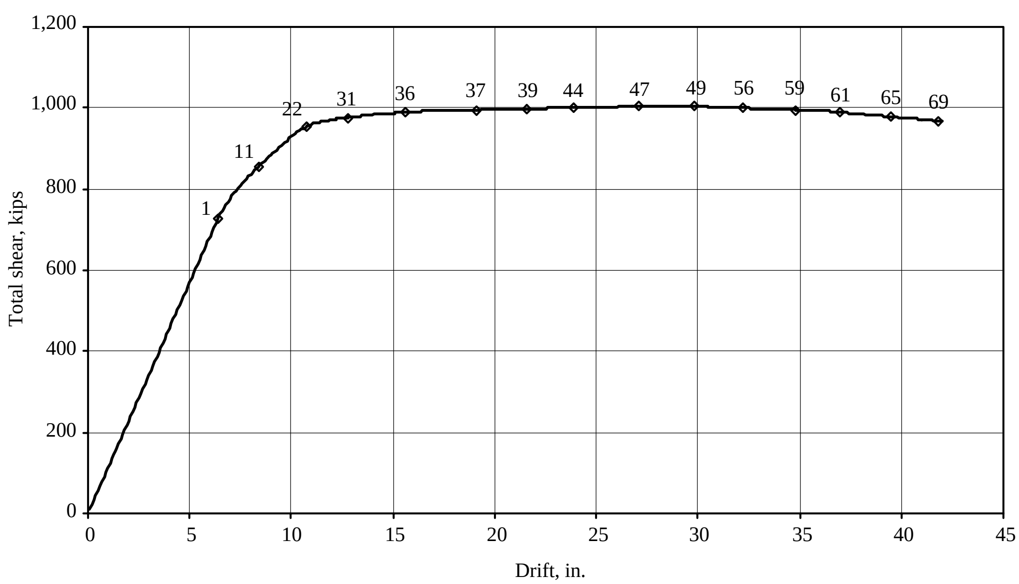

(b)

Figure 3.2-32 Patterns of plastic hinge formation: weak panel zone model under ML load, including P-delta effects.

The difference between the behavior of the structures with and without doubler plates is attributed to the yielding of the panel zones in the structure without panel zone reinforcement. The sequence of hinging is illustrated in Figure 3.2-32. Part (a) of this figure indicates that panel zone yielding occurs early. (Panel zone yielding is indicated by a numeric sequence label in the corner of the panel zone.) In fact, the first yielding in the structure is due to yielding of a panel zone at the second level of the structure.

It should be noted that under very large displacements, the flange component of the panel zone yields. Girder and column hinging also occurs, but the column hinging appears relatively late in the response. It is also significant that the upper two levels of the structure display yielding in several of the panel zones.

Aside from the relatively marginal loss in stiffness and strength due to removal of the doubler plates, it appears that the structure without panel zone reinforcement is behaving adequately. Of course, actual performance cannot be evaluated without predicting the maximum inelastic panel shear strain and assessing the stability of the panel zones under these strains.

3.2.5.3 Predictions of Total Displacement and Story Drift from Pushover Analysis

In the following discussion, the only loading pattern considered is the modal load pattern discussed earlier. This is consistent with the requirements of *Provisions* Sec. 5A.1.2 [A5.2.2]. The structure with both strong and weak panel zones is analyzed, and separate analyses are performed including and excluding P-delta effects.

3.2.5.3.1 Expected Inelastic Displacements Computed According to the Provisions

The expected inelastic displacement was computed using the procedures of *Provisions* Sec. 5.5 [5.3]. In the *Provisions*, the displacement is computed using response-spectrum analysis with only the first mode included. The expected roof displacement will be equal to the displacement computed from the 5-percent-damped response spectrum multiplied by the modal participation factor which is multiplied by the first mode displacement at the roof level of the structure. In the present analysis, the roof level first mode displacement is 1.0.

Details of the calculations are not provided herein. The relevant modal quantities and the expected inelastic displacements are provided in Table 3.2-12. Note that only those values associated with the ML lateral load pattern were used.

Table 3.2-12 Modal Properties and Expected Inelastic Displacements for the Strong and Weak Panel Models Subjected to the Modal Load Pattern

Computed Quantity	Strong Panel w/o P-Delta	Strong Panel with P-Delta	Weak Panel w/o P-Delta	Weak Panel with P-Delta
Period (seconds)	1.950	2.015	2.028	2.102
Modal Participation Factor	1.308	1.305	1.315	1.311
Effective Modal Mass (%)	82.6	82.8	82.1	82.2
Expected Inelastic Disp. (in.)	12.31	12.70	12.78	13.33
Base Shear Demand (kips)	1168	1051	1099	987
6^{th} Story Drift (in.)	1.09	1.02	1.12	1.11
5^{th} Story Drift (in.)	1.74	1.77	1.84	1.88
4^{th} Story Drift (in.)	2.28	2.34	2.44	2.53
3^{rd} Story Drift (in.)	2.10	2.73	2.74	2.90
2^{nd} Story Drift (in.)	2.54	2.73	2.56	2.71
1^{st} Story Drift (in.)	2.18	2.23	2.09	2.18

As the table indicates, the modal quantities are only slightly influenced by P-delta effects and the inclusion or exclusion of doubler plates. The maximum inelastic displacements are in the range of 12.2 to 13.3 in. The information provided in Figures 3.2-23 through 3.2-32 indicates that at a target displacement of, for example, 13.0 in., some yielding has occurred but the displacements are not of such a magnitude that the slope of the pushover curve is negative when P-delta effects are included.

It should be noted that FEMA 356, *Prestandard and Commentary for the Seismic Rehabilitation of Buildings*, provides a simplified methodology for computing the target displacement that is similar to but somewhat more detailed than the approach illustrated above. See Sec. 3.3.3.3.2 of FEMA 356 for details.

3.2.5.3.2 Inelastic Displacements Computed According to the Capacity Spectrum Method

In the capacity spectrum method, the pushover curve is transformed to a capacity curve that represents the first mode inelastic response of the full structure. Figure 3.2-33 shows a bilinear capacity curve. The horizontal axis of the capacity curve measures the first mode displacement of the simplified system. The vertical axis is a measure of simplified system strength to system weight. When multiplied by the acceleration due to gravity (g), the vertical axis represents the acceleration of the mass of the simple system.

Point E on the horizontal axis is the value of interest, the expected inelastic displacement of the simplified system. This displacement is often called the target displacement. The point on the capacity curve directly above Point E is marked with a small circle, and the line passing from the origin through this point represents the secant stiffness of the simplified system. If the values on the vertical axis are multiplied by the acceleration due to gravity, the slope of the line passing through the small circle is equal to the acceleration divided by the displacement. This value is the same as the square of the circular frequency of the simplified system. Thus, the sloped line is also a measure of the secant period of the simplified structure. As will be shown later, an equivalent viscous damping value (ξ_E) can be computed for the simple structure deformed to Point E.

Figure 3.2-34 shows a response spectrum with the vertical axis representing spectral acceleration as a ratio of the acceleration due to gravity and the horizontal axis representing displacement. This spectrum, called a demand spectrum, is somewhat different from the traditional spectrum that uses period of vibration as the horizontal axis. The demand spectrum is drawn for a particular damping value (ξ). Using the demand spectrum, the displacement of a SDOF system may be determined if its period of vibration is known and the system's damping matches the damping used in the development of the demand spectrum. If the system's damping is equal to ξ_E, and its stiffness is the same as that represented by the sloped line in Figure 3.2-33, the displacement computed from the demand spectrum will be the same as the expected inelastic displacement shown in Figure 3.2-33.

The capacity spectrum and demand spectrum are shown together in Figure 3.2-35. The demand spectrum is drawn for a damping value exactly equal to ξ_E, but ξ_E is not known *a priori* and must be determined by the analyst. There are several ways to determine ξ_E. In this example, two different methods will be demonstrated: an iterative approach and a semigraphical approach.

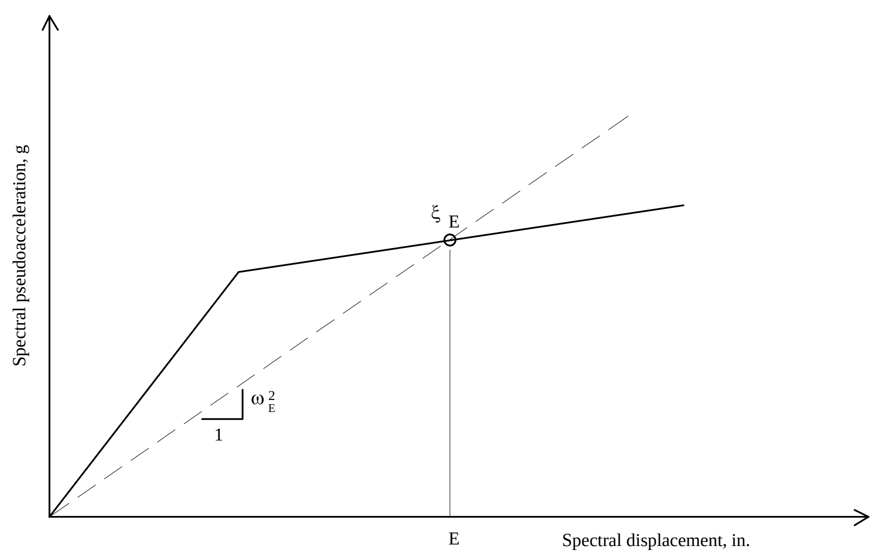

Figure 3.2-33 A simple capacity spectrum.

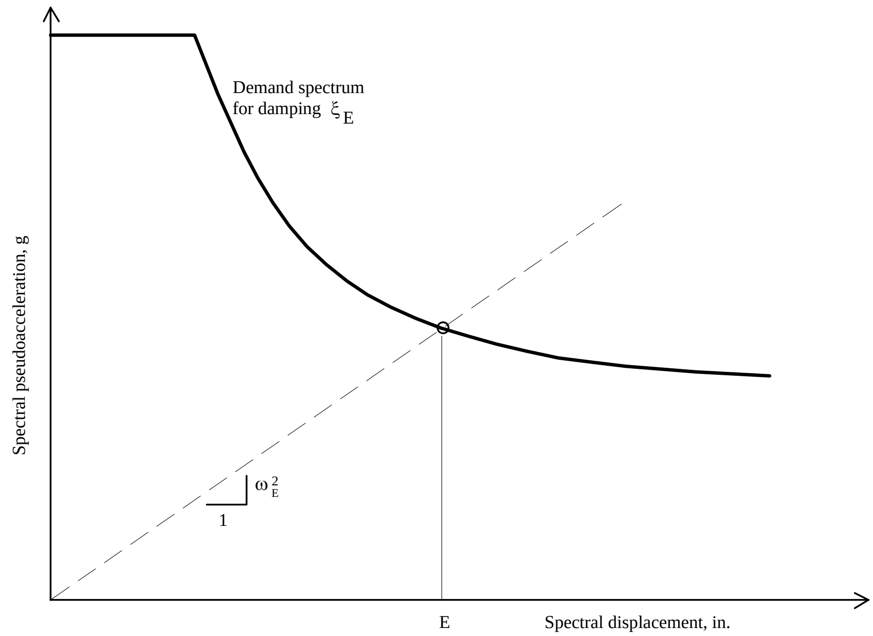

Figure 3.2-34 A simple demand spectrum.

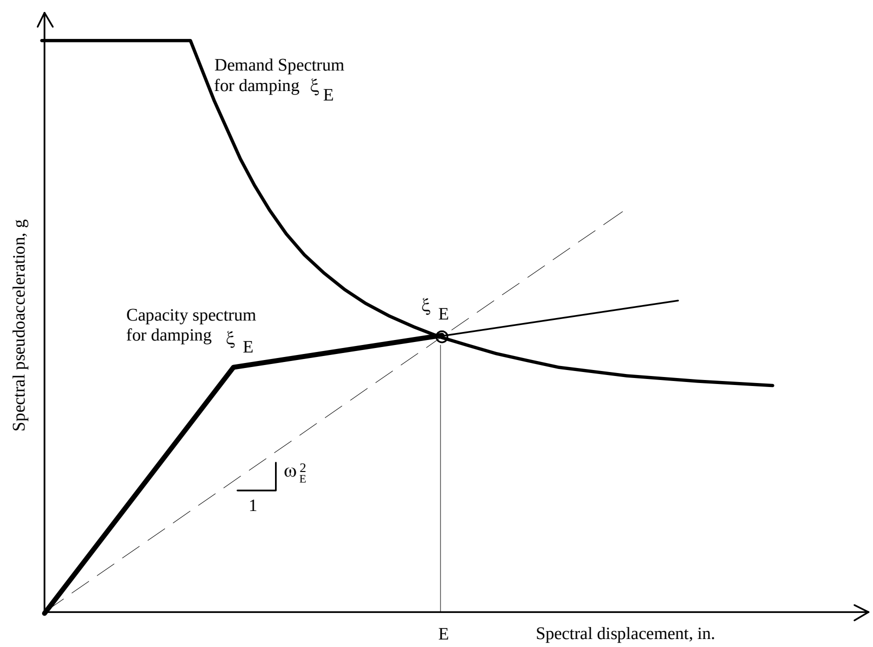

Figure 3.2-35 Capacity and demand spectra plotted together.

The first step in either approach is to convert the pushover curve into a capacity spectrum curve. This is done using the following two transformations:[8]

1. To obtain spectral displacement, multiply each displacement value in the original pushover curve by the quantity:

$$\frac{1}{PF_1 \phi_{Roof,1}}$$

   where PF_1 is the modal participation factor for the fundamental mode and $\phi_{Roof,1}$ is the value of the first mode shape at the top level of the structure. The modal participation factor and the modal displacement must be computed using a consistent normalization of the mode shapes. One must be particularly careful when using DRAIN because the printed mode shapes and the printed modal participation factors use inconsistent normalizations – the mode shapes are normalized to a maximum value of 1.0 and the modal participation factors are based on a normalization that produces a unit generalized mass matrix. For most frame-type structures, the first mode participation factor will be in the range of 1.3 to 1.4 if the mode shapes are normalized for a maximum value of 1.0.

2. To obtain spectral pseudoacceleration, divide each force value in the pushover curve by the total weight of the structure, and then multiply by the quantity:

$$\frac{1}{\alpha_1}$$

   where α_1 is the ratio of the effective mass in the first mode to the total mass in the structure. For frame structures, α_1 will be in the range of 0.8 to 0.85. Note that α_1 is not a function of mode shape normalization.

After performing the transformation, convert the smooth capacity curve into a simple bilinear capacity curve. This step is somewhat subjective in terms of defining the effective yield point, but the results are typically insensitive to different values that could be assumed for the yield point. Figure 3.2-36 shows a typical capacity spectrum in which the yield point is represented by points a_Y and d_Y. The displacement and acceleration at the expected inelastic displacement are d_E and a_E, respectively. The two slopes of the demand spectrum are K_I and K_2, and the intercept on the vertical axis is a_I.

[8]Expressions in this section are taken from ATC40 but have been modified to conform to the nomenclature used herein.

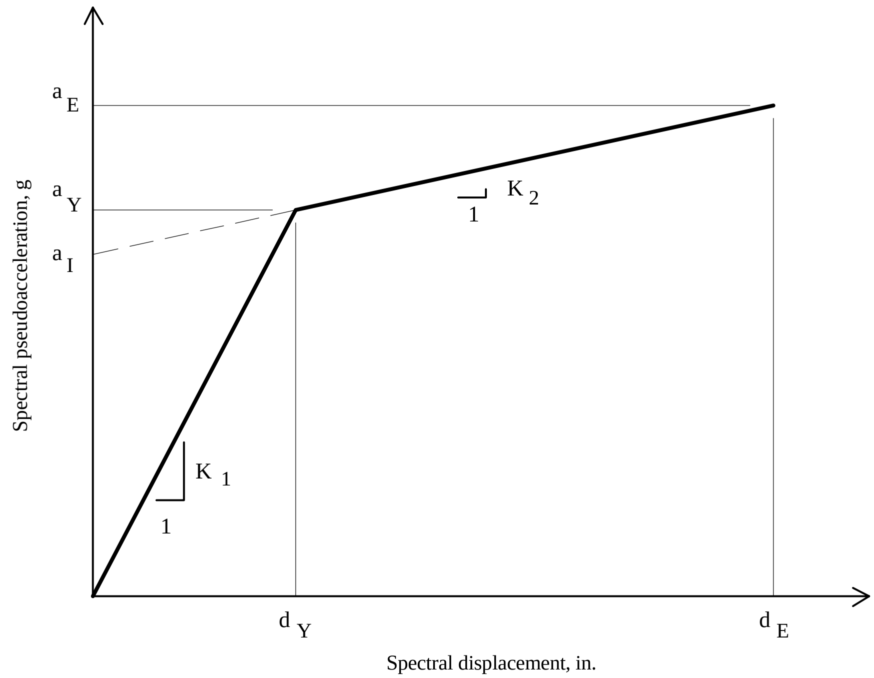

Figure 3.2-36 Capacity spectrum showing control points.

At this point the iterative method and the direct method diverge somewhat. The iterative method will be presented first, followed by the direct method.

Given the capacity spectrum, the iterative approach is as follows:

I-1. Guess the expected inelastic displacement d_E. The displacement computed from the simplified procedure of the *Provisions* is a good starting point.

I-2. Compute the equivalent viscous damping value at the above displacement. This damping value, in terms of percent critical, may be estimated as:

$$\xi_E = 5 + \frac{63.7(a_Y d_E - d_Y a_E)}{a_E d_E}$$

I-3. Compute the secant period of vibration:

$$T_E = \frac{2\pi}{\sqrt{\dfrac{g \times a_E}{d_E}}}$$

where g is the acceleration due to gravity.

I-4. An estimated displacement must now be determined from the demand spectrum. A damping value of ξ_E will be assumed in the development of the spectrum. The demand spectrum at this damping value is adapted from the response spectrum given by *Provisions* Sec. 4.1.2.6 [3.3.4]. This spectrum is based on 5 percent of critical damping; therefore, it must be modified for the higher equivalent damping represented by ξ_E. For the example presented here, the modification factors for systems with higher damping values are obtained from *Provisions* Table 13.3.3.1 [13.3-1], which is reproduced in a somewhat different form as Table 3.2-13 below. In Table 3.2-13, the modification factors are shown as multiplying factors instead of dividing factors as is done in the *Provisions*. The use of the table can be explained by a simple example: the spectral ordinate for a system with 10 percent of critical damping is obtained by multiplying the 5-percent-damped value by 0.833.

The values in Table 3.2-13 are intended for use only for ductile systems without significant strength loss. They are also to be used only in the longer period constant velocity region of the response spectrum. This will be adequate for our needs because the initial period of vibration of our structure is in the neighborhood of 2.0 seconds. See ATC 40 for conditions where the structure does have strength loss or where the period of vibration is such that the constant acceleration region of the spectrum controls. During iteration it may be more convenient to use the information from Table 3.2-13 in graphic form as shown in Figure 3.2-37.

Table 3.2-13 Damping Modification Factors

Effective Damping (% critical)	Damping Modification Factor
5	1.000
10	0.833
20	0.667
30	0.588
40	0.526
50 or greater	0.500

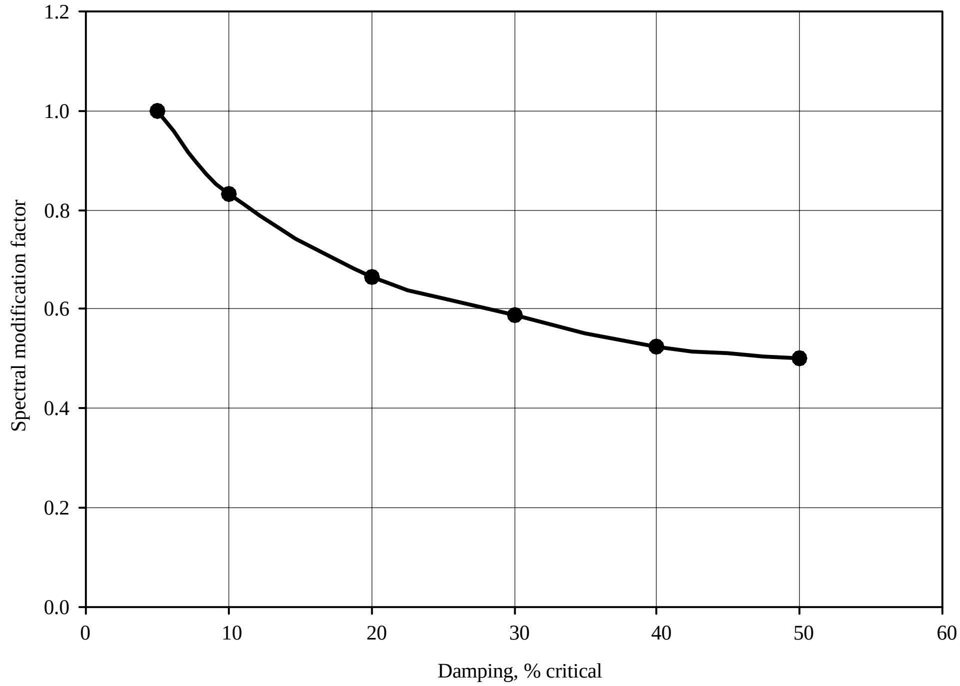

Figure 3.2-37 Damping modification factors.

I-5. Using the period of vibration computed in Step 3 and the damping computed in Step 4, compute the updated estimate of spectral acceleration a_E^{new} and convert to displacement using the following expression:

$$d_E^{new} = \frac{g \times a_E^{new}}{\left[2\pi / T_E\right]^2}$$

If this displacement is the same as that estimated in Step 1, the iteration is complete. If not, set the displacement in Step 1 to d_E^{new} and perform another cycle. Continue iterating until the desired level of accuracy is achieved.

I-6. Convert the displacement for the simple system to the expected inelastic displacement for the complete structure by multiplying by the product of the modal participation factor and the first mode roof displacement.

The procedure will now be demonstrated for the strong panel structure subjected to the ML load pattern. P-delta effects are *excluded*.

For this structure, the modal participation factor and effective modal mass factor for the first mode are:

$\phi_1 = 1.308$ and $\alpha_1 = 0.826$

The original pushover curve is shown in Figure 3.2-23. The capacity spectrum version of the curve is shown in Figure 3.2-38 as is a bilinear representation of the capacity curve.

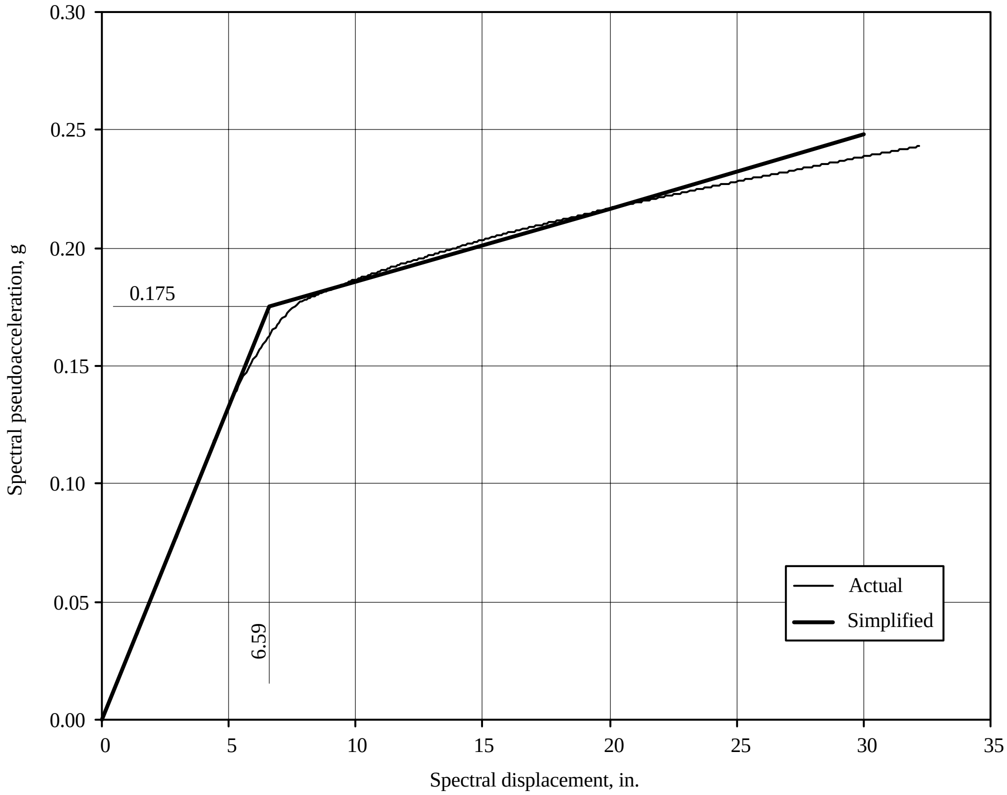

Figure 3.2-38 Capacity spectrum used in iterative solution.

The control values for the bilinear curve are:

$d_Y = 6.592$ in.
$a_Y = 0.1750$ g
$a_1 = 0.1544$ g
$K_1 = 0.0265$ g/in.
$K_2 = 0.00311$ g/in.

The initial period of the structure (from DRAIN) is 1.95 sec. The same period may be recovered from the demand curve as follows:

$$T = \frac{2\pi}{\sqrt{\dfrac{g \times a_Y}{d_Y}}} = \frac{2\pi}{\sqrt{\dfrac{386.1 \times 0.175}{6.659}}} \cong 1.95 \text{ sec.}$$

The 5-percent-damped demand spectrum for this example is based on *Provisions* Figure 4.1.2.6 [3.3-15]. Since the initial period is nearly 2.0 seconds, the only pertinent part of the spectrum is the part that is inversely proportional to period. Using a value of S_{D1} of 0.494 (see Sec. 3.2.2.2), the spectral acceleration as a function of period T is $a = 0.494/T$ where a is in terms of the acceleration due to gravity. For higher damping values, the acceleration will be multiplied by the appropriate value from Table 3.2-13 of this example.

At this point the iteration may commence. Assume an initial displacement d_E of 8.5 in. This is the value computed earlier (see Table 3.2-12) from the simplified procedure in the *Provisions*. At this displacement, the acceleration a_E is:

$$a_E = a_I + K_2 d_E = 0.1544 + 0.00311(8.5) = 0.1808 \text{ g} .$$

At this acceleration and displacement, the equivalent damping is:

$$\xi_E = 5 + \frac{63.7(a_Y d_E - d_Y a_E)}{a_E d_E} = 5 + \frac{63.7(0.175 \times 8.5 - 6.592 \times 0.1808)}{0.1808 \times 8.5} = 17.2\% \text{ critical} .$$

The updated secant period of vibration is:

$$T = \frac{2\pi}{\sqrt{\dfrac{g \times a_E}{d_E}}} = \frac{2\pi}{\sqrt{\dfrac{386.4 \times 0.1808}{8.5}}} = 2.19 \text{ sec} .$$

From Table 3.2-13 (or Figure 3.2-37), the damping modification factor for ξ_E = 17.2 percent is 0.71. Therefore, the updated acceleration is:

$$a_E^{new} = 0.71(0.494)/2.19 = 0.160 \text{ g} .$$

Using this acceleration, the updated displacement for the next iteration is:

$$d_E^{new} = \frac{g \times a_E^{new}}{\left[2\pi / T_E\right]^2} = \frac{386.4 \times 0.160}{\left[2\pi / 2.19\right]^2} = 7.52 \text{ in.}$$

The complete iteration is summarized in Table 3.2-14, where the final displacement from the iteration is 7.82 in. This must be multiplied by the modal participation factor, 1.308, to obtain the actual roof displacement. This value is 7.82(1.308) = 10.2 in. and is somewhat greater than the value of 8.5 in. predicted from the simplified method of the *Provisions*.

This example converged even though some of the accelerations from the demand spectrum were less than the yield value in the development of the capacity spectrum (e.g., 0.161 in iteration 1 is less than 0.175). This particular example predicts displacements very close to the yield displacement d_Y; consequently, there may be some influence of the choice of a_Y and d_Y on the computed displacement.

Table 3.2-14 Results of Iteration for Maximum Expected Displacement

Iteration	a^* (g)	d_E (in.)	a_E (g)	Damping (%)	Damping Mod. Factor	T_E (sec.)
		8.50	0.181	17.2	0.71	2.19
1	0.161	7.52	0.178	11.8	0.80	2.08
2	0.189	8.01	0.179	14.7	0.75	2.14
3	0.173	7.70	0.179	12.9	0.78	2.10
4	0.183	7.88	0.179	14.0	0.76	2.12
5	0.176	7.77	0.179	13.4	0.77	2.12
6	0.180	7.84	0.179	13.7	0.76	2.12
7	0.178	7.80	0.179	13.5	0.77	2.11
8	0.179	7.82	0.179	13.6	0.76	2.11
9	0.178	7.81	0.179	13.6	0.76	2.11
10	0.179	7.82	0.179	13.6	0.76	2.11

Note: a* is from demand spectrum at period T_E.

In the direct approach, a family of demand spectra are plotted together with the capacity spectrum and the desired displacement is found graphically. The steps in the procedure are as follows:

D-1. Develop a bilinear capacity spectrum for the structure.

D-2. Find the points on the capacity spectrum that represent 5, 10, 15, 20, 25, and 30 percent damping.

D-3. Draw a series of secant stiffness lines, one for each damping value listed above.

D-4. Develop demand spectra for damping values of 5, 10, 15, 20, 25, and 30 percent of critical.

D-5. Draw the demand spectra on the same plot as the capacity spectrum.

D-6. Find the points where the secant stiffness lines (from Step 3) for each damping value cross the demand spectrum line for the same damping value.

D-7. Draw a curve connecting the points found in Step 6.

D-8. Find the point where the curve from Step 7 intersects the capacity spectrum. This is the target displacement, but it is still in SDOF spectrum space.

D-9. Convert the target displacement to structural space.

This procedure is now illustrated for the strong panel structure subjected to the modal load pattern. For this example, P-delta effects are excluded.

1. The original pushover curve for this structure is shown in Figure 3.2-23. The effective mass in the first mode is 0.826 times the total mass, and the first mode participation factor is 1.308. The first mode displacement at the roof of the building is 1.0. Half of the dead weight of the structure was used in the conversion because the pushover curve represents the response of one of the two frames. The resulting capacity curve and its bilinear equivalent are shown in Figure 3.2-38. For this example, the yield displacement (d_y) is taken as 6.59 in. and the corresponding yield strength (a_y) is 0.175g. The secant stiffness through the yield point is 0.0263g/in. or 10.2 (rad/sec)^2. Note that the secant stiffness through this point is mathematically equivalent to the circular frequency squared of the structure; therefore, the frequency is 3.19 rad/sec and the period is 1.96 seconds. This period, as required, is the same as that obtained from DRAIN. (The main purpose of computing the period from the initial stiffness of the capacity spectrum is to perform an intermediate check on the analysis.)

2-3. The points on the capacity curve representing β_{eff} values of 5, 10, 15, 20, 25, and 30 percent critical damping are shown in Table 3.2-15. The points are also shown as small diamonds on the capacity spectrum of Figure 3.2-39. The secant lines through the points are also shown.

Table 3.2-15 Points on Capacity Spectrum Corresponding to Chosen Damping Values

Effective Damping (% critical)	Displacement d_{pi} (in.)	Spectral Acceleration a_{pi} (g)
5	6.59	0.175
10	7.25	0.177
15	8.07	0.180
20	9.15	0.183
25	10.7	0.188
30	13.1	0.195

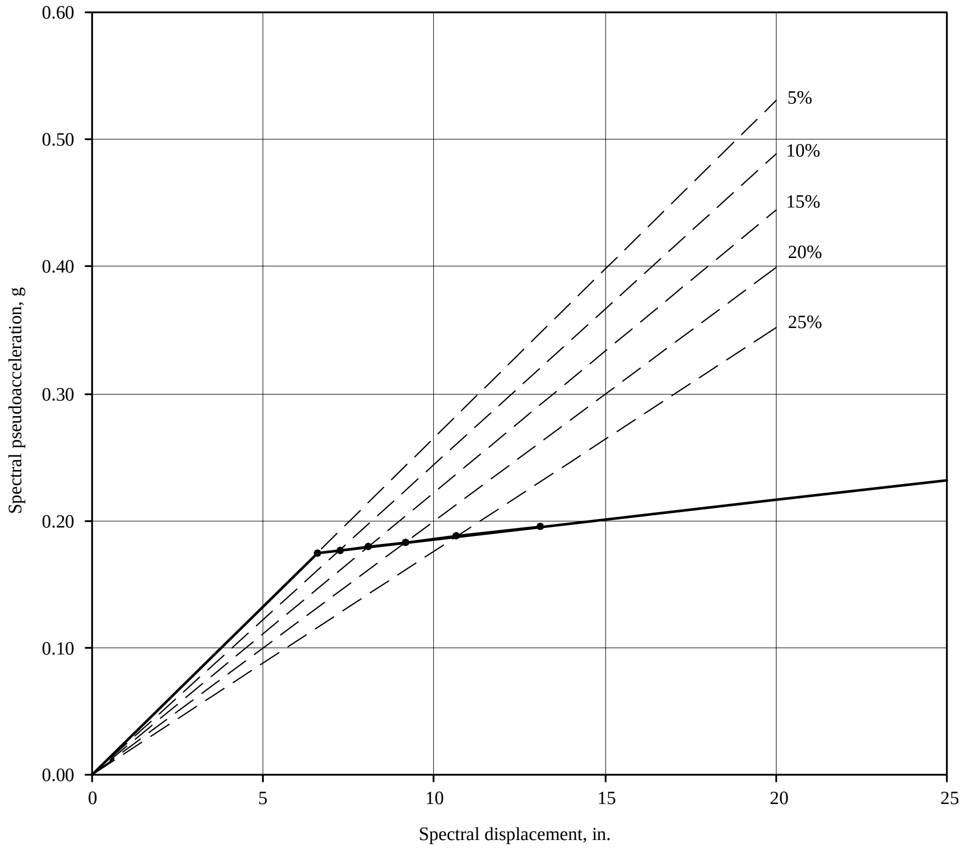

Figure 3.2-39 Capacity spectrum with equivalent viscous damping points and secant stiffnesses.

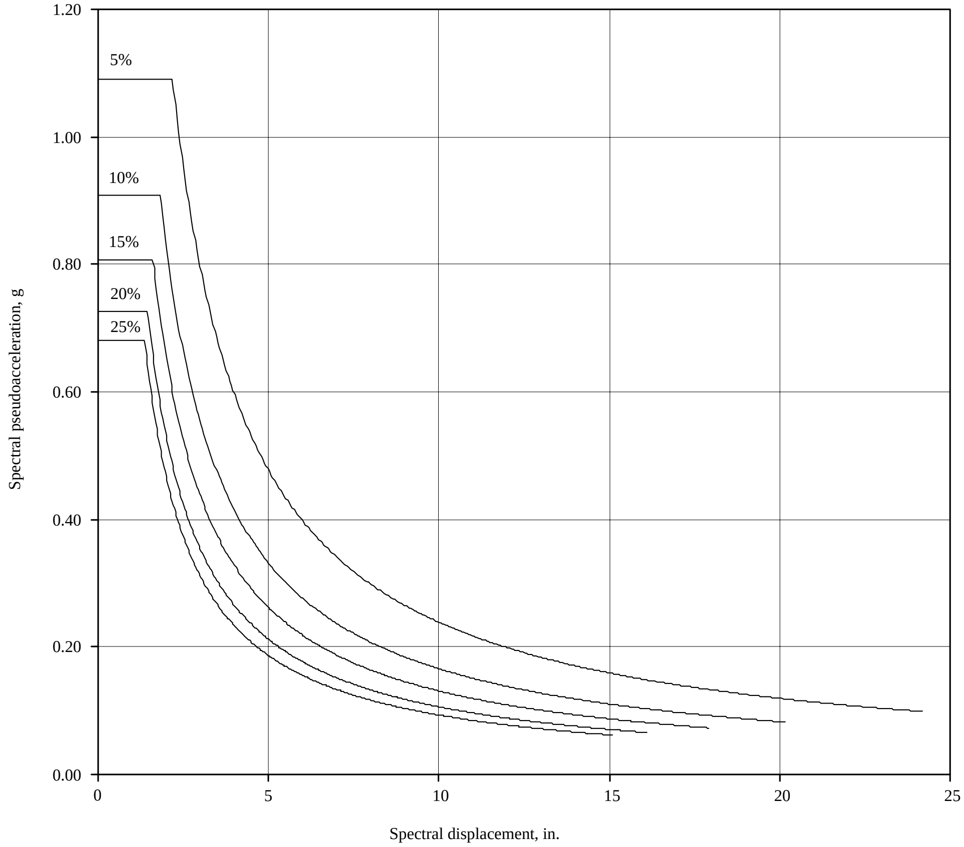

Figure 3.2-40 Demand spectra for several equivalent viscous damping values.

4-5. The demand spectra are based on the short period and 1-second period accelerations obtained in Sec. 3.2.2.2e. These values are S_{DS} = 1.09 and S_{D1} = 0.494. Plots for these spectra are shown individually in Figure 3.2-37. The damping modification factors used to obtain the curves were taken directly or by interpolation from Table 3.2-13. The demand spectra are shown on the same plot as the capacity spectrum in Figure 3.2-41.

6-8. The final steps of the analysis are facilitated by Figure 3.2-42, which is a close-up of the relevant portion of Figure 3.2-41. The expected inelastic roof displacement, still in spectral space, is approximately 7.8 in. This is the same as that found from the iterative solution.

9. The expected inelastic roof displacement for the actual structure is 1.308(7.8) or 10.2 in. This is 20 percent greater than the value of 8.5 in. obtained from the first mode elastic response-spectrum analysis.

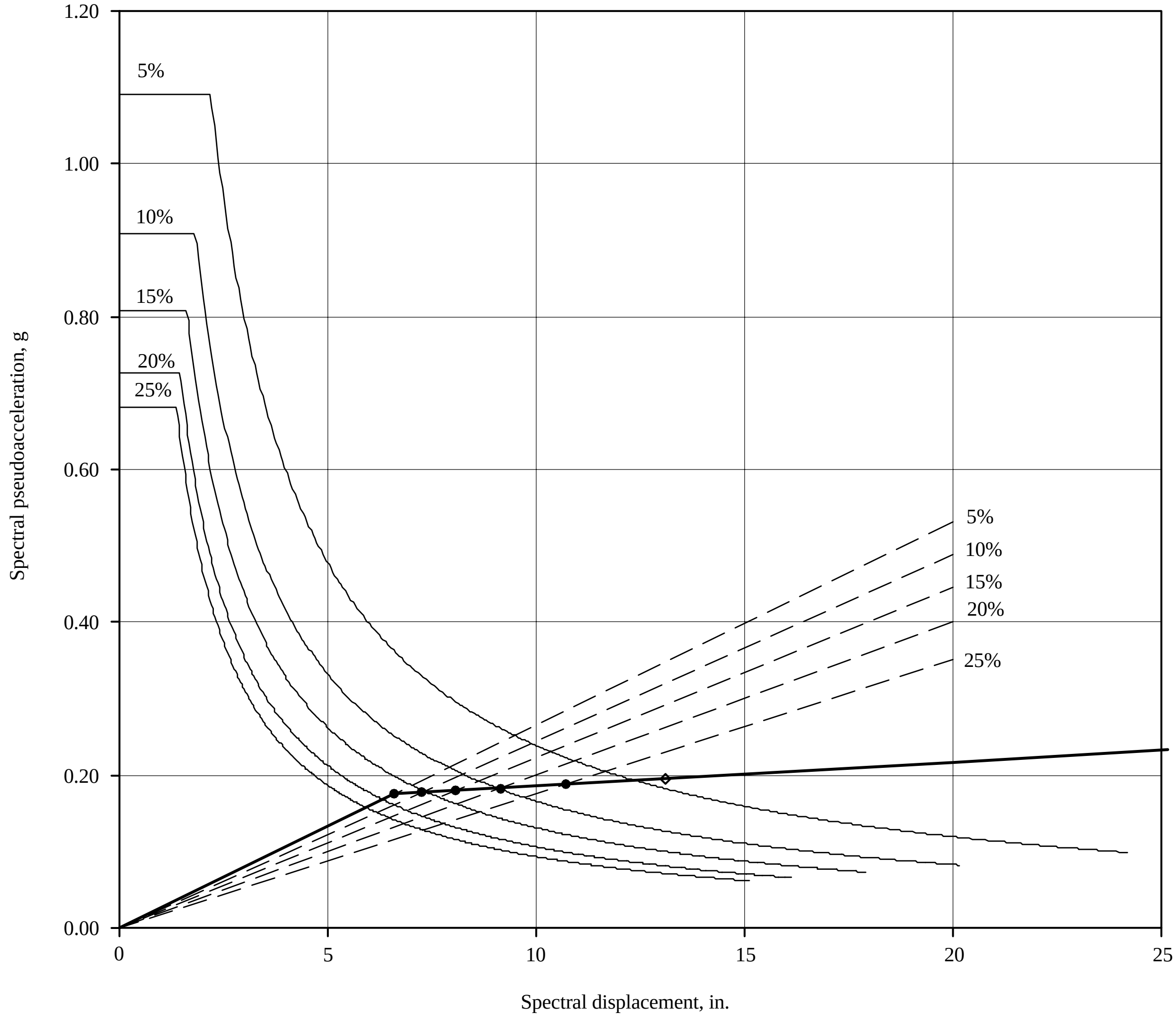

Figure 3.2-41 Capacity and demand spectra on single plot.

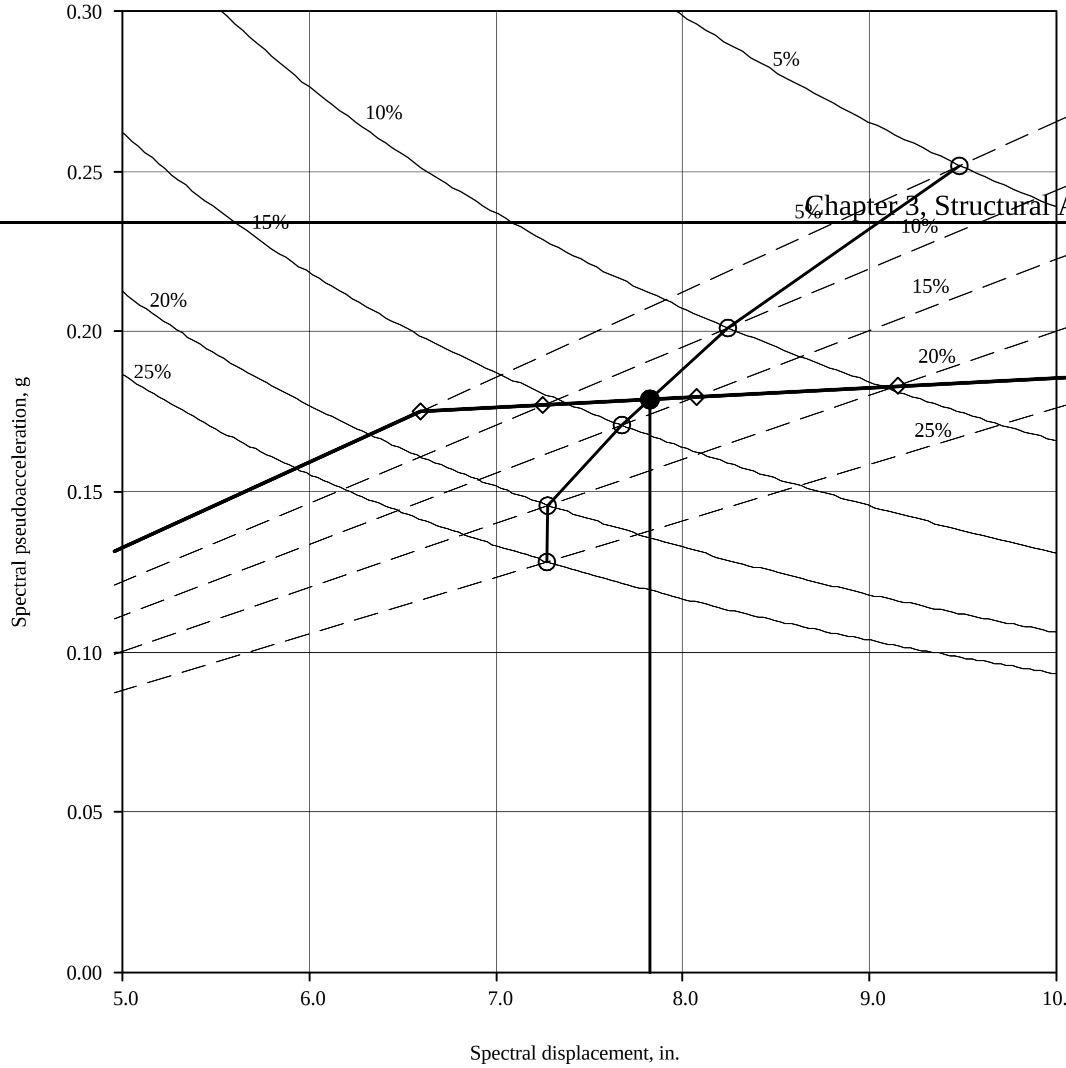

Figure 3.2-42 Close-up view of portion of capacity and demand spectra.

Results for all the strong and weak panel structures under modal load are summarized in Table 3.2-16. All drifts and rotations are consistent with the expected inelastic roof displacement shown at the top of the table.

Table 3.2-16 Summary of Results from Pushover Analysis

Computed Quantity	Strong Panel w/o P-Delta	Strong Panel with P-Delta	Weak Panel w/o P-Delta	Weak Panel with P-Delta
Expected Inelastic Disp. (in.)	10.2	10.3	10.2	10.4
Base Shear Demand (kips)	1125	1031	1033	953
6th Story Drift (in.)	0.81	0.78	0.87	0.84
5th Story Drift (in.)	1.35	1.31	1.55	1.45
4th Story Drift (in.)	1.82	1.81	1.96	2.00
3rd Story Drift (in.)	2.19	2.23	2.21	2.29
2nd Story Drift (in.)	2.20	2.27	2.06	2.14
1st Story Drift (in.)	1.83	1.90	1.64	1.68
Max beam plastic hinge rot. (rad)	0.00522	0.00564	0.00511	0.00524
Max column plastic hinge rot. (rad)	0.0	0.0	0.0	0.0
Max panel zone hinge rot. (rad)	0.0	0.0	0.00421	0.00437

3.2.5.4 Summary and Observations from Pushover Analysis

1. The simplified approach from the *Provisions* predicts maximum expected displacements about 8 to 10 percent lower than the much more complicated capacity spectrum method. Conclusions cannot be drawn from this comparison, however, as only one structure has been analyzed.

2. P-delta effects had a small but significant effect on the response of the system. In particular, base shears for the structure with P-delta effects included were about 8 percent lower than for the structure without P-delta effects. If the maximum expected displacement was larger, the differences between response with and without P-delta effects would have been much more significant.

3. The inelastic deformation demands in the hinging regions of the beams and in the panel zones of the beam-column joints were small and are certainly within acceptable limits. The small inelastic deformations are attributed to the considerable overstrength provided when preliminary member sizes were adjusted to satisfy story drift limits.

4. The structure without panel zone reinforcement appears to perform as well as the structure with such reinforcement. This is again attributed to the overstrength provided.

3.2.6 Time-History Analysis

Because of the many assumptions and uncertainties inherent in the capacity spectrum method, it is reasonable to consider the use of time-history analysis for the computation of global and local deformation demands. A time-history analysis, while by no means perfect, does eliminate two of the main problems with static pushover analysis: selection of the appropriate lateral load pattern and use of equivalent linear viscous damping in the demand spectrum to represent inelastic hysteretic energy dissipation. However, time-history analysis does introduce its own problems, most particularly selection and scaling of ground motions, choice of hysteretic model, and inclusion of inherent (viscous) damping.

The time-history analysis of Example 2 is used to estimate the deformation demands for the structure shown in Figures 3.2-1 and 3.2-2. The analysis, conducted only for the structure with panel zone reinforcement, is carried out for a suite of three ground motions specifically prepared for the site. Analyses included and excluded P-delta effects.

3.2.6.1 Modeling and Analysis Procedure

The DRAIN-2Dx program was used for each of the time-history analyses. The structural model was identical to that used in the static pushover analysis. Second order effects were included through the use of the outrigger element shown to the right of the actual frame in Figure 3.2-4.

Inelastic hysteretic behavior was represented through the use of a bilinear model. This model exhibits neither a loss of stiffness nor a loss of strength and, for this reason, it will generally have the effect of overestimating the hysteretic energy dissipation in the yielding elements. Fortunately, the error produced by such a model will not be of great concern for this structure because the hysteretic behavior of panel zones and flexural plastic hinges should be very robust for this structure when inelastic rotations are less than about 0.02 radians. (Previous analysis has indicated a low likelihood of rotations significantly greater than 0.02 radians.) At inelastic rotations greater than 0.02 radians it is possible for local inelastic buckling to reduce the apparent strength and stiffness.

Rayleigh proportional damping was used to represent viscous energy dissipation in the structure. The mass and stiffness proportional damping factors were set to produce 5 percent damping in the first and third modes. This was done primarily for consistency with the pushover analysis, which use a baseline damping of 5 percent of critical. Some analysts would use a lower damping, say 2.5 percent, to compensate for the fact that bilinear hysteretic models tend to overestimate energy dissipation in plastic hinges.

In Rayleigh proportional damping, the damping matrix (D) is a linear combination of the mass matrix M and the initial stiffness matrix K:

$$D = \alpha M + \beta K$$

where α and β are mass and stiffness proportionality factors, respectively. If the first and third mode frequencies, ω_1 and ω_3, are known, the proportionality factors may be computed from the following expression:[9]

$$\begin{Bmatrix} \alpha \\ \beta \end{Bmatrix} = \frac{2\xi}{\omega_1 + \omega_3} \begin{Bmatrix} \omega_1 \omega_3 \\ 1 \end{Bmatrix}$$

[9]See Ray W. Clough and Joseph Penzien, *Dynamics of Structures*, 2nd Edition.

Note that α and β are directly proportional to ξ. To increase ξ from 5 percent to 10 percent of critical requires only that α and β be increased by a factor of 2.0. The structural frequencies and damping proportionality factors are shown in Table 3.2-17 for the models analyzed by the time-history method.

Table 3.2-17 Structural Frequencies and Damping Factors Used in Time-History Analysis. (Damping Factors that Produce 5 Percent Damping in Modes 1 and 3)

Model/Damping Parameters	ω_1 (Hz.)	ω_3 (Hz.)	α	β
Strong Panel with P-Delta	3.118	18.65	0.267	0.00459
Strong Panel without P-Delta	3.223	18.92	0.275	0.00451

It is very important to note that the stiffness proportional damping factor must *not* be included in the Type-4 elements used to represent rotational plastic hinges in the structure. These hinges, particularly those in the girders, have a very high initial stiffness. Before the hinge yields there is virtually no rotational velocity in the hinge. After yielding, the rotational velocity is significant. If a stiffness proportional damping factor is used for the hinge, a viscous moment will develop in the hinge. This artificial viscous moment – the product of the rotational velocity, the initial rotational stiffness of the hinge, and the stiffness proportional damping factor – can be quite large. In fact, the viscous moment may even exceed the intended plastic capacity of the hinge. These viscous moments occur in phase with the plastic rotation; hence, the plastic moment and the viscous moments are additive. These large moments transfer to the rest of the structure, effecting the sequence of hinging in the rest of the structure, and produce artificially high base shears. The use of stiffness proportional damping in discrete plastic hinges can produce a totally inaccurate analysis result.

The structure was subjected to dead load and full reduced live load, followed by ground acceleration. The incremental differential equations of motion were solved in a step-by-step manner using the Newmark constant average acceleration approach. Time steps and other integration parameters were carefully controlled to minimize errors. The minium time step used for analysis was 0.00025 seconds. Later analyses used time steps as large as 0.001 seconds.

3.2.6.2 Development of Ground Motion Records

The ground motion time histories used in the analysis were developed specifically for the site. Basic information for the records was shown previously in Table 3.1-20 and is repeated as Table 3.2-18.

Table 3.2-18 Seattle Ground Motion Parameters (Unscaled)

Record Name	Orientation	Number of Points and Time Increment	Peak Ground Acceleration (g)	Source Motion
Record A00	N-S	8192 @ 0.005 seconds	0.443	Lucern (Landers)
Record A90	E-W	8192 @ 0.005 seconds	0.454	Lucern (Landers)
Record B00	N-S	4096 @ 0.005 seconds	0.460	USC Lick (Loma Prieta)
Record B90	E-W	4096 @ 0.005 seconds	0.435	USC Lick (Loma Prieta)
Record C00	N-S	1024 @ 0.02 seconds	0.460	Dayhook (Tabas, Iran)
Record C90	E-W	1024 @ 0.02 seconds	0.407	Dayhook (Tabas, Iran)

Time histories and 5-percent-damped response spectra for each of the motions are shown in Figures 3.2-43 through 3.2-45.

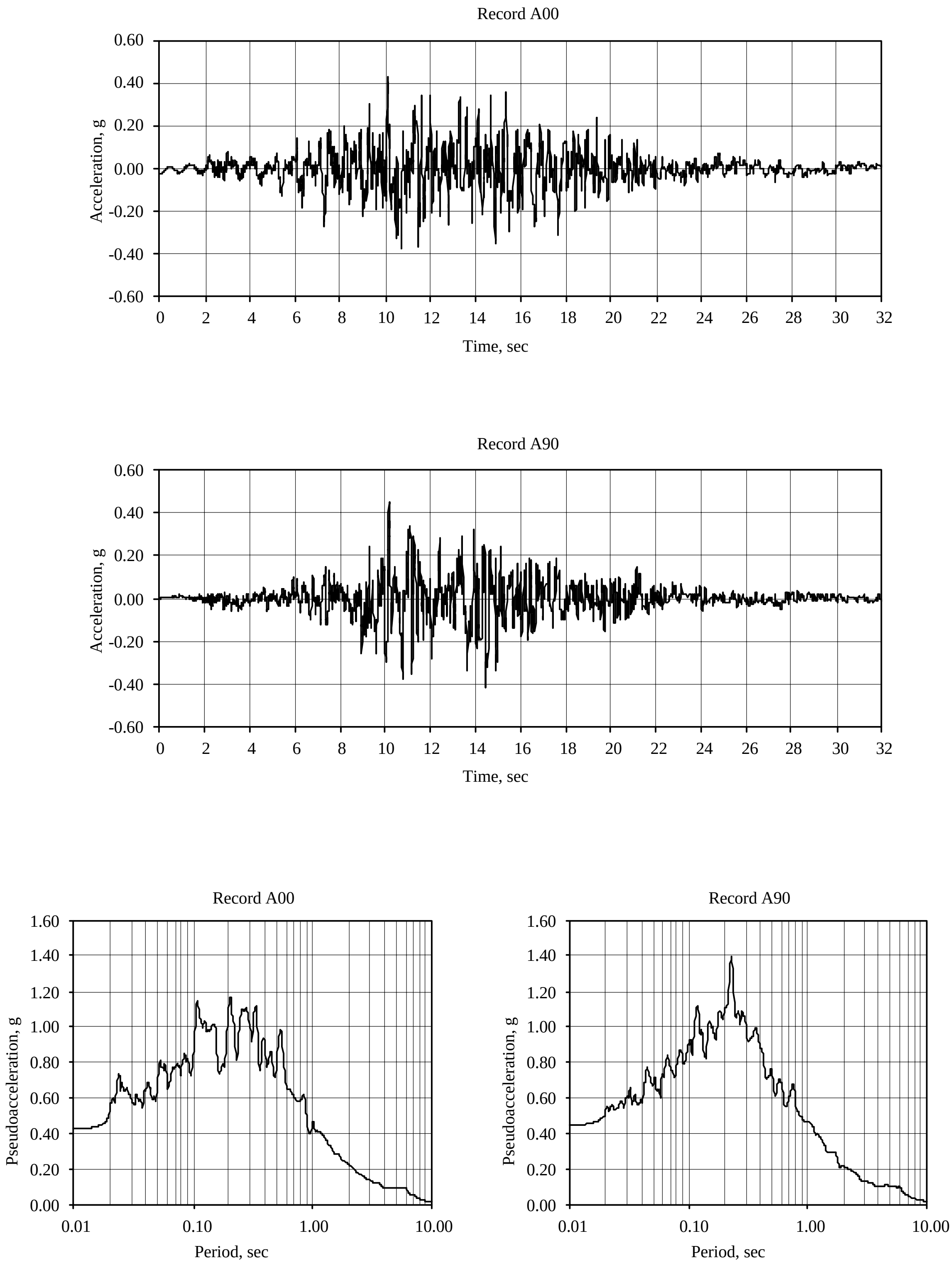

Figure 3.2-43 Time histories and response spectra for Record A.

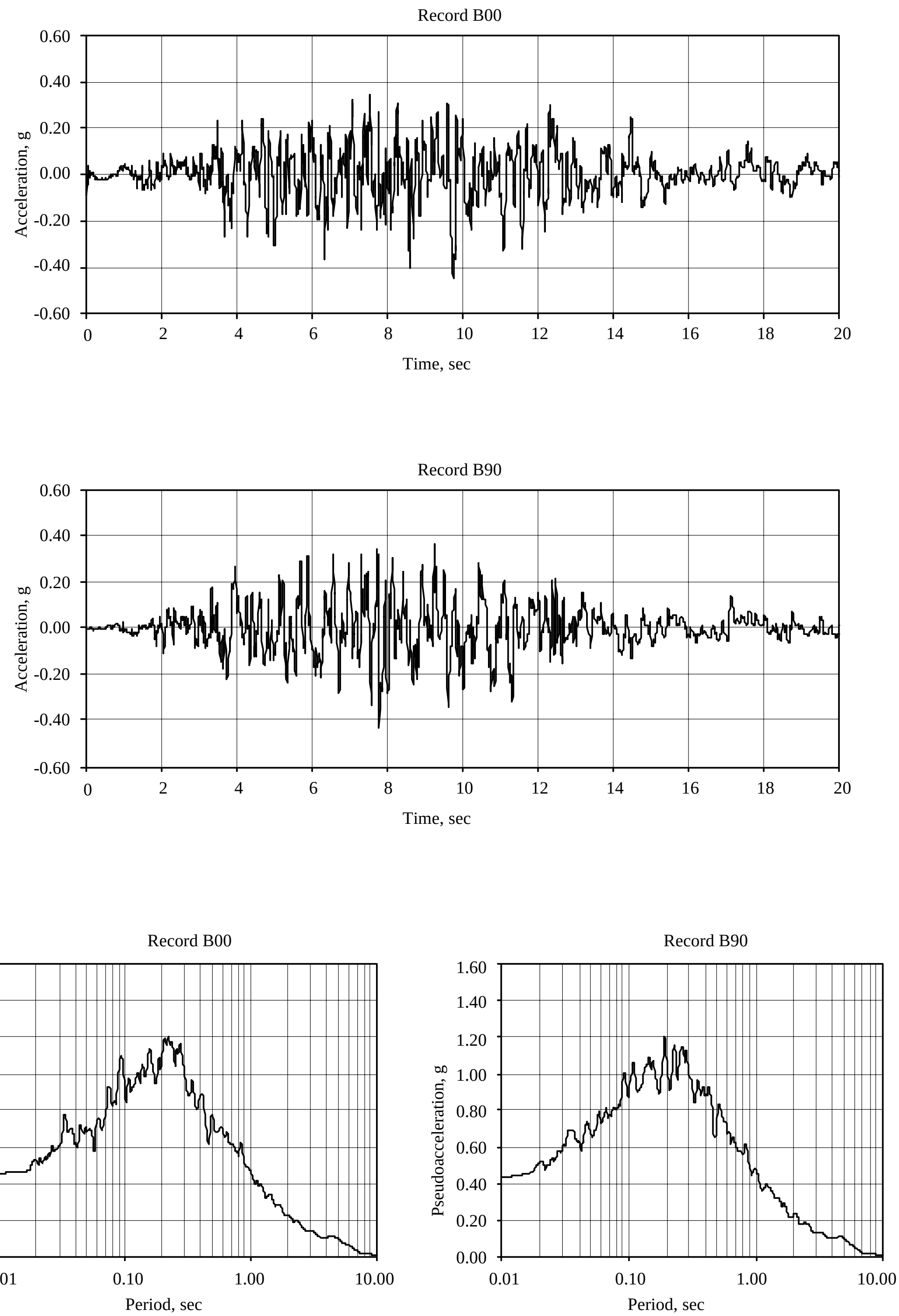

Figure 3.2-44 Time histories and response spectra for Record B.

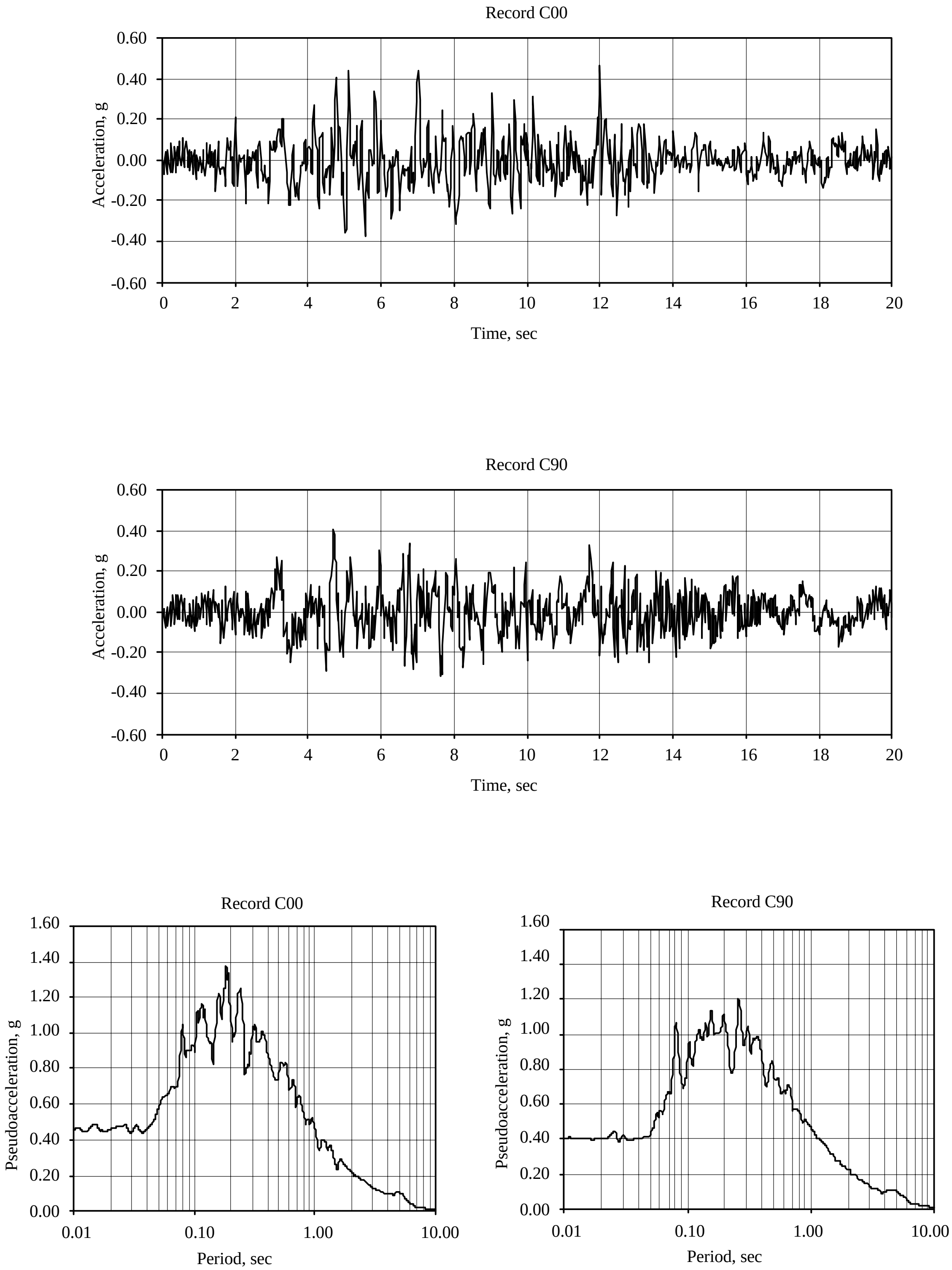

Figure 3.2-45 Time histories and response spectra for Record C.

Because only a two-dimensional analysis of the structure is performed using DRAIN, only a single component of ground motion is applied at one time. For the analyses reported herein, only the N-S (00) records of each ground motion were utilized. A complete analysis would require consideration of both sets of ground motions.

When analyzing structures in two dimensions, *Provisions* Sec. 5.6.2.1 [5.4.2.1] gives the following instructions for scaling:

1. For each pair of motions:
   a. Assume an initial scale factor for each motion pair (for example, S_A for ground motion A00).
   b. Compute the 5-percent-damped elastic response spectrum for each component in the pair.

2. Adjust scale factors S_A, S_B, and S_C such that the average of the scaled response spectra over the period range $0.2T_1$ to 1.5 T_1 is not less than the 5-percent-damped spectrum determined in accordance with *Provisions* Sec. 4.1.3. T_1 is the fundamental mode period of vibration of the structure.

As with the three-dimensional time-history analysis for the first example in this chapter, it will be assumed that the scale factors for the three earthquakes are to be the same. If a scale factor of 1.51 is used, Figure 3.2-46 indicates that the criteria specified by the *Provisions* have been met for all periods in the range 0.2(2.00) = 0.40 sec to 1.5(2.00) = 3.0 seconds.[10] The scale factor of 1.51 is probably conservative because it is controlled by the period at 0.47 seconds, which will clearly be in the higher modes of response of the structure. If the *Provisions* had called for a cutoff of $0.25T$ instead of the (somewhat arbitrary) value of $0.2T$, the required scale factor would be reduced to 1.26.

3.2.6.3 Results of Time-History Analysis

Time-history analyses were performed for the structure subjected to the first 20 seconds of the three different ground motions described earlier. The 20-second cutoff was based on a series of preliminary analyses that used the full duration.

The following parameters were varied to determine the sensitivity of the response to the particular variation:

1. Analysis was run with and without P-delta effects for all three ground motions.

2. Analysis was run with 2.5, 5, 10, and 20 percent damping (Ground Motion A00, including P-delta effects). These analyses were performed to assess the potential benefit of added viscous fluid damping devices.

3.2.6.3.1 Response of Structure with 5 Percent of Critical Damping

[10] 2.00 seconds is approximately the average of the period of the strong panel model with and without P-delta effects. See Table 3.2-12.

The results from the first series of analyses, all run with 5 percent of critical damping, are summarized in Tables 3.2-19 through 3.2-22. Selected time-history traces are shown in Figures 3.2-47 through 3.2-64. Energy time histories are included for each analysis.

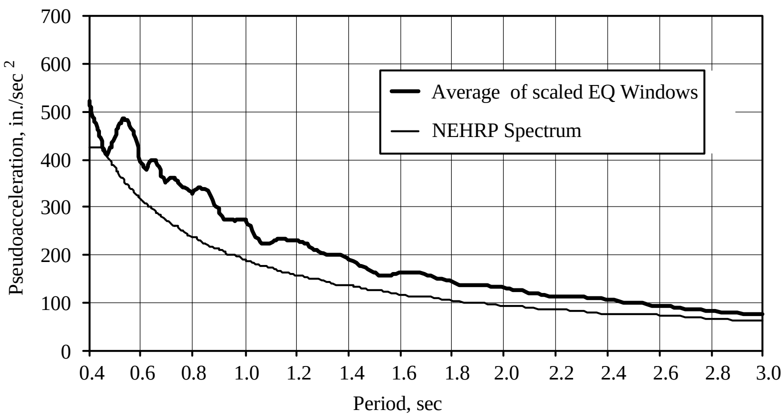

(a) Comparison of Average of Scaled Spectra and NEHRP Spectrum (S.F.=1.51)

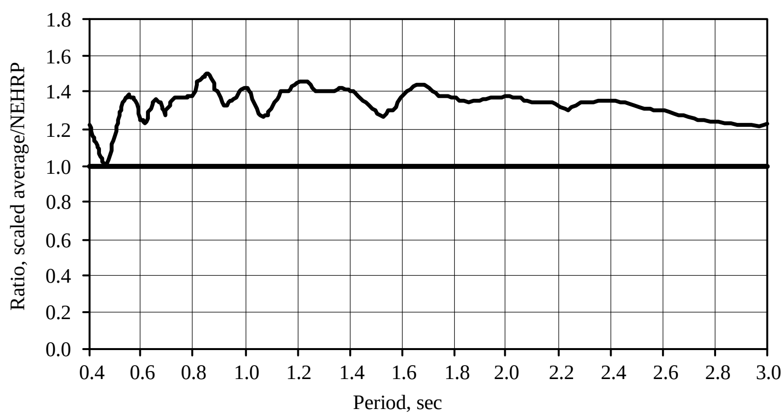

(b) Ratio of Average of Scaled Spectra to NEHRP Spectrum (S.F.=1.51)

Figure 3.2-46 Ground motion scaling parameters.

The tabulated shears in Tables 3.2-19 and 3.2-21 are for the single frame analyzed and should be doubled to obtain the total shear in the structure. The tables of story shear also provide two values for each ground motion. The first value is the maximum total elastic column story shear, including P-delta effects if applicable. The second value represents the maximum total inertial force for the structure. The inertial base shear, which is not necessarily concurrent with the column shears, was obtained as sum of the products of the total horizontal accelerations and nodal mass of each joint. For a system with no damping, the story shears obtained from the two methods should be identical. For a system with damping, the base shear obtained from column forces generally will be less than the shear from inertial forces because the viscous component of column shear is not included. Additionally, the force absorbed by the mass proportional component of damping will be lost (as this is not directly recoverable in DRAIN).

The total roof drift and the peak story drifts listed in Tables 3.2-20 and 3.2-22 are peak (envelope) values at each story and are not necessarily concurrent.

Tables 3.2-19 and 3.2-20 summarize the global response of the structure with *excluding* P-delta effects. Time-history traces are shown in Figures 3.2-47 through 3.2-55. Significant yielding occurred in the girders, columns, and panel zone regions for each of the ground motions. Local quantification of such effects is provided later for the structure responding to Ground Motion A00.

Table 3.2-19 Maximum Base Shear (kips) in Frame Analyzed with 5 Percent Damping, Strong Panels, Excluding P-Delta Effects

Level	Motion A00	Motion B00	Motion C00
Column Forces	1559	1567	1636
Inertial Forces	1307	1370	1464

Table 3.2-20 Maximum Story Drifts (in.) from Time-History Analysis with 5 percent Damping, Strong Panels, Excluding P-Delta Effects

Level	Motion A00	Motion B00	Motion C00	Limit
Total Roof	16.7	13.0	11.4	NA
R-6	1.78	1.60	1.82	3.75
6-5	3.15	2.52	2.63	3.75
5-4	3.41	2.67	2.65	3.75
4-3	3.37	2.75	2.33	3.75
3-2	3.98	2.88	2.51	3.75
2-G	**4.81**	3.04	3.13	4.50

Table 3.2-21 Maximum Base Shear (kips) in Frame Analyzed with 5 Percent Damping, Strong Panels, Including P-Delta Effects

Level	Motion A00	Motion B00	Motion C00
Column Forces	1426	1449	1474
Inertial Forces	1282	1354	1441

Table 3.2-22 Maximum Story Drifts (in.) from Time-History Analysis with 5 Percent Damping, Strong Panels, Including P-Delta Effects

Level	Motion A00	Motion B00	Motion C00	Limit
Total Roof	17.4	14.2	10.9	NA
R-6	1.90	1.59	1.78	3.75
6-5	3.31	2.48	2.61	3.75
5-4	3.48	2.66	2.47	3.75
4-3	3.60	2.89	2.31	3.75
3-2	4.08	3.08	2.78	3.75
2-G	**4.84**	3.11	3.75	4.50

The peak base shears (for a single frame), taken from the sum of column forces, are very similar for each of the ground motions and range from 1307 kips to 1464 kips. There is, however, a pronounced difference in the recorded peak displacements. For Ground Motion A00 the roof displacement reached a maximum value of 16.7 in., while the peak roof displacement from Ground Motion C00 was only 11.4 in. Similar differences occurred for the first-story displacement. For Ground Motion A00, the maximum story drift was 4.81 in. for Level 1 and 3.98 in. for Levels 2 through 6. The first-story drift of 4.81 in. exceeds the allowable drift of 4.50 in. Recall that the allowable drift includes a factor of 1.25 that is permitted when nonlinear analysis is performed.

As shown in Figure 3.2-47, the larger displacements observed in Ground Motion A00 are due to a permanent inelastic displacement offset that occurs at about 10.5 seconds into the earthquake. The sharp increase in energy at this time is evident in Figure 3.2-49. Responses for the other two ground motions shown in Figures 3.2-50 and 3.2-53 do not have a significant residual displacement. The reason for the differences in response to the three ground motions is not evident from their ground acceleration time-history traces (see Figures 3.2-43 through 3.2-45).

The response of the structure *including* P-delta effects is summarized in Tables 3.2-21 and 3.2-22. Time-history traces are shown in Figures 3.2-56 through 3.2-64. P-delta effects have a significant influence on the response of the structure to each of the ground motions. This is illustrated in Figures 3.2-65 and 3.2-66, which are history traces of roof displacement and base shear, respectively, in response to Ground Motion A00. Responses for analysis with and without P-delta effects are shown in the same figure. The P-delta effect is most evident after the structure has yielded.

Table 3.2-21 summarizes the base shear response and indicates that the maximum base shear from the column forces, 1441 kips, occurs during Ground Motion C00. This shear is somewhat less than the shear of 1464 kips which occurs under the same ground motion when P-delta effects are excluded. A reduction in base shear is to be expected for yielding structures when P-delta effects are included.

Table 3.2-22 shows that inclusion of P-delta effects led to a general increase in displacements with the peak roof displacement of 17.4 in. occurring during ground motion A00. The story drift at the lower level of the structure is 4.84 in. when P-delta effects are included and this exceeds the limit of 4.5 in. The larger drifts recorded during Ground Motion A00 are again associated with residual inelastic deformations. This may be seen clearly in the time-history trace of roof and first-story displacement shown in Figure 3.2-56.

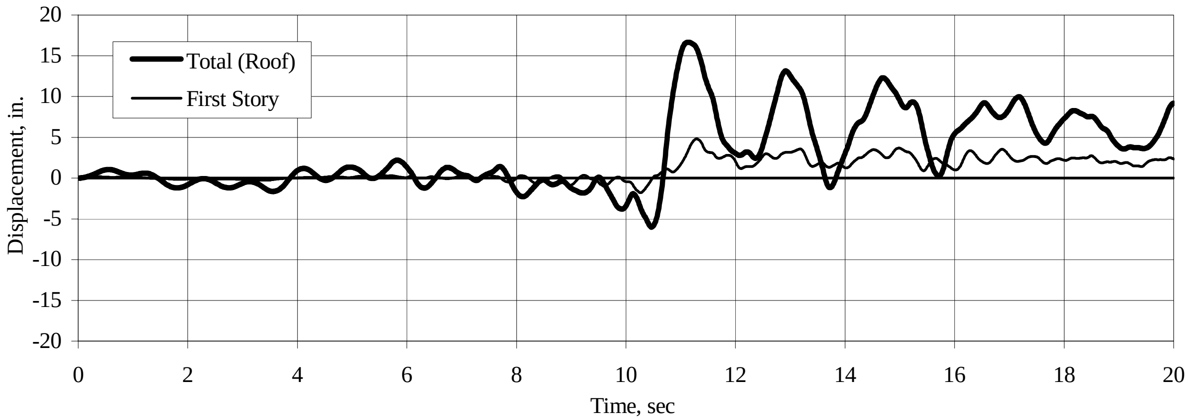

Figure 3.2-47 Time history of roof and first-story displacement, Ground Motion A00, excluding P-delta effects.

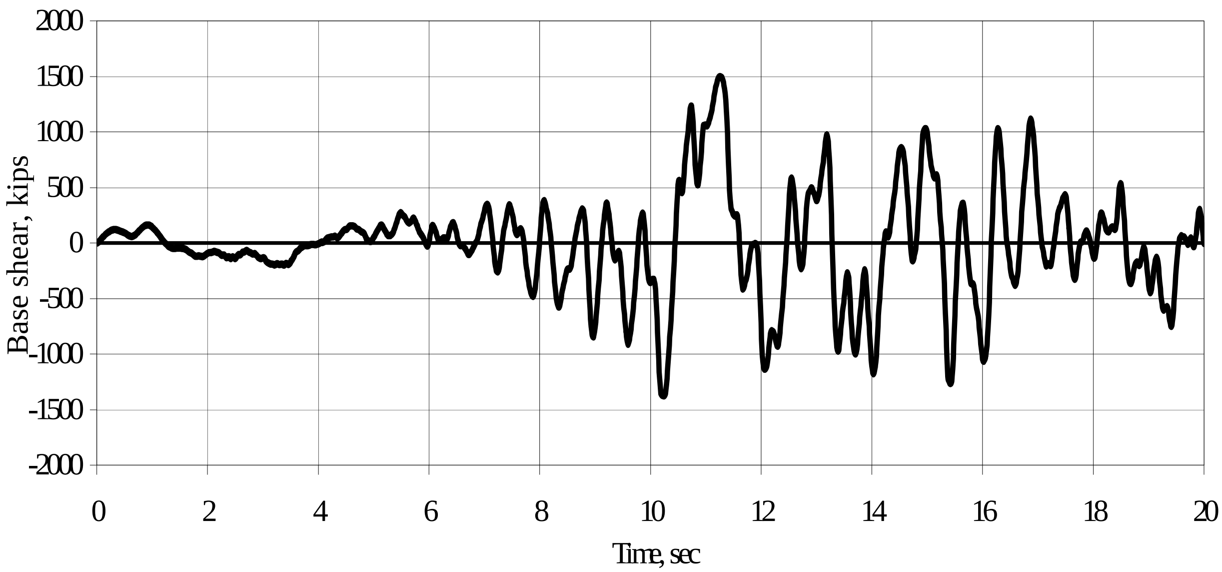

Figure 3.2-48 Time history of total base shear, Ground Motion A00, excluding P-delta effects.

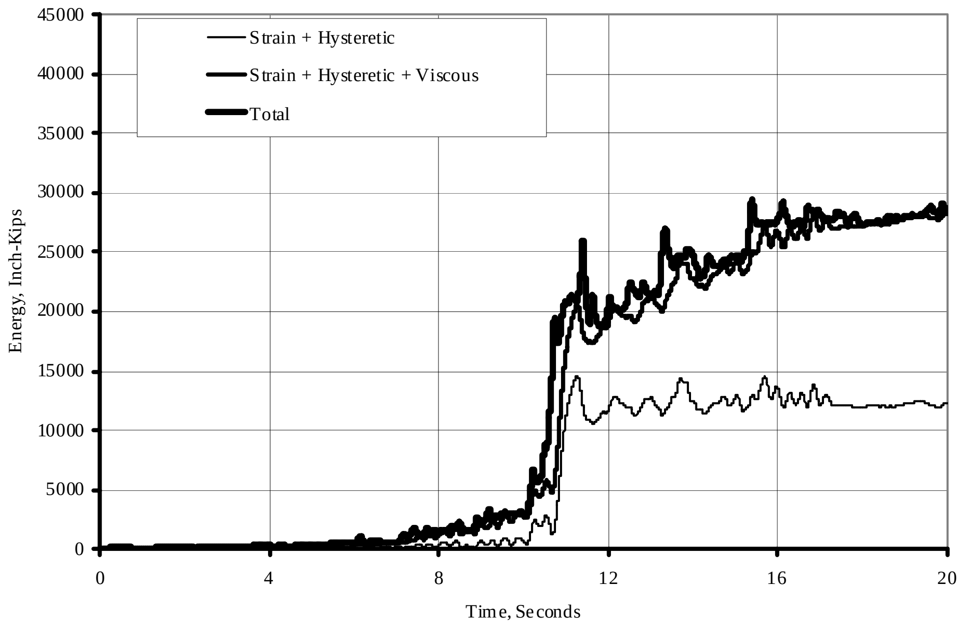

Figure 3.2-49 Energy time history, Ground MotionA00, excluding P-delta effects.

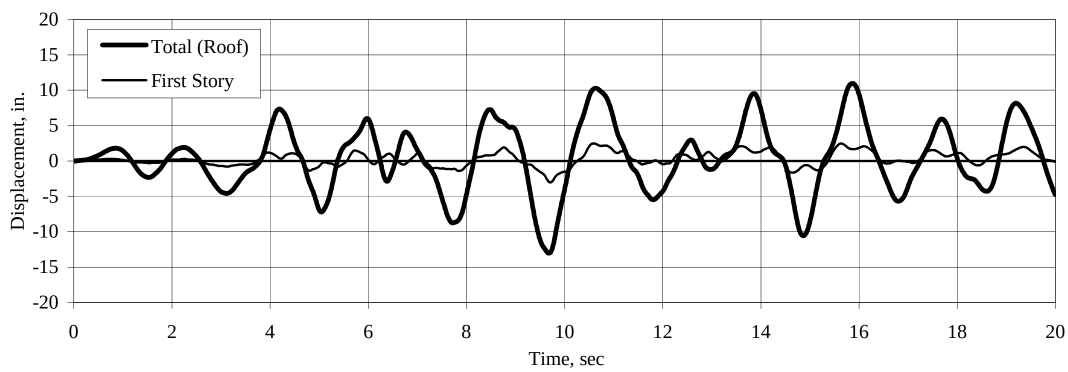

Figure 3.2-50 Time history of roof and first-story displacement. Ground Motion B00, excluding P-delta effects.

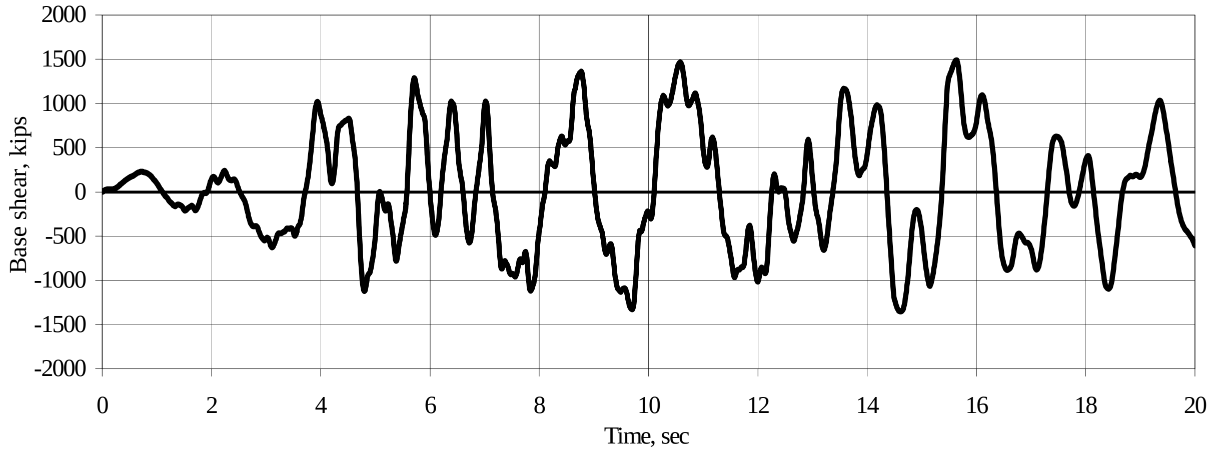

Figure 3.2-51 Time history of total base shear, Ground Motion B00, excluding P-delta effects.

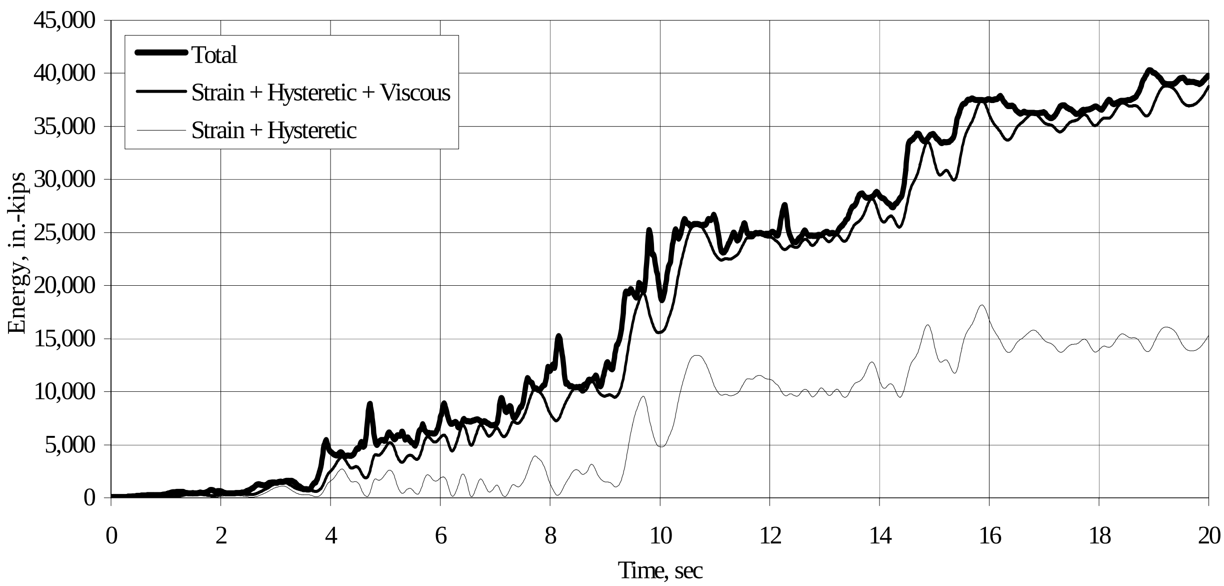

Figure 3.2-52 Energy time history, Ground Motion B00, excluding P-delta effects.

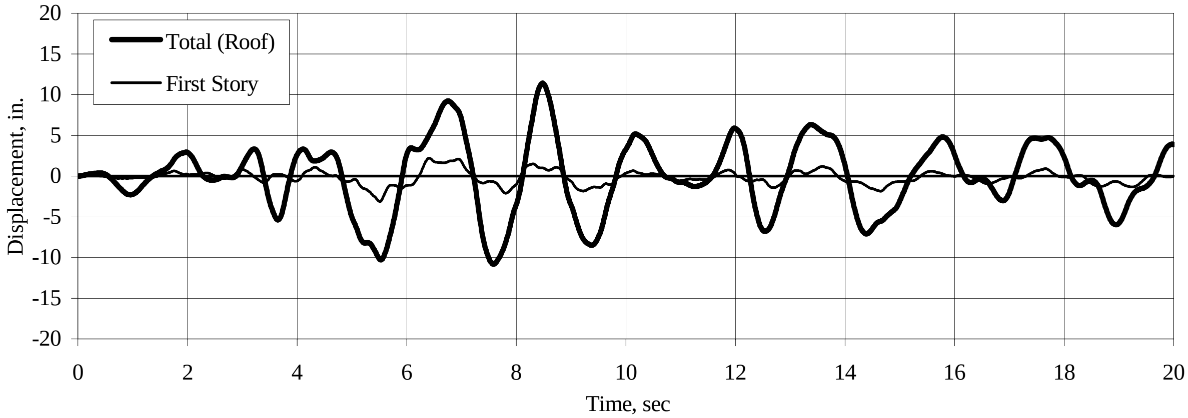

Figure 3.2-53 Time history of roof and first-story displacement, Ground Motion C00, excluding P-delta effects.

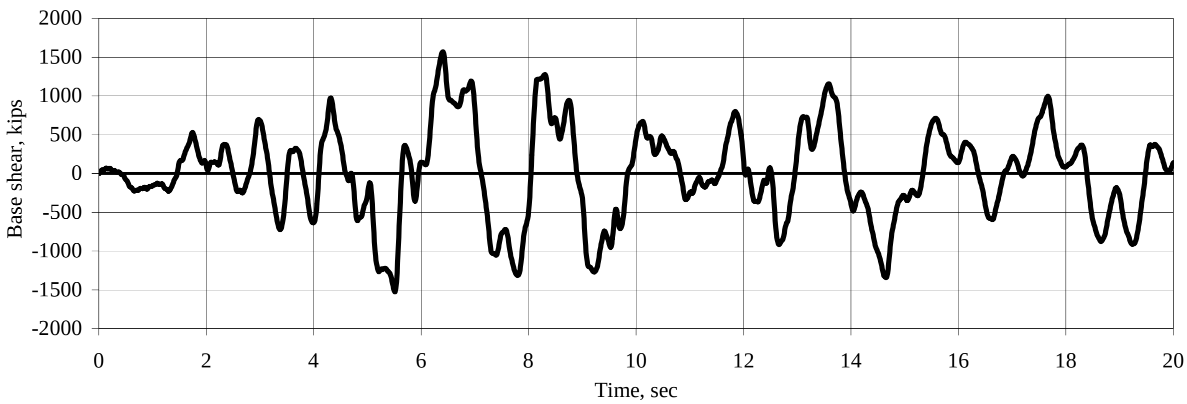

Figure 3.2-54 Time history of total base shear, Ground Motion C00, excluding P-delta effects.

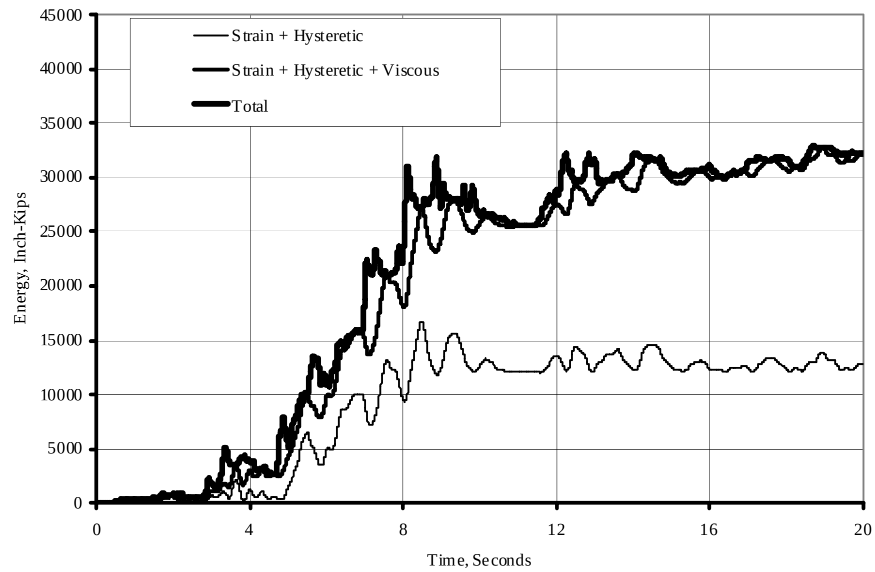

Figure 3.2-55 Energy time history, Ground Motion C00, excluding P-delta effects.

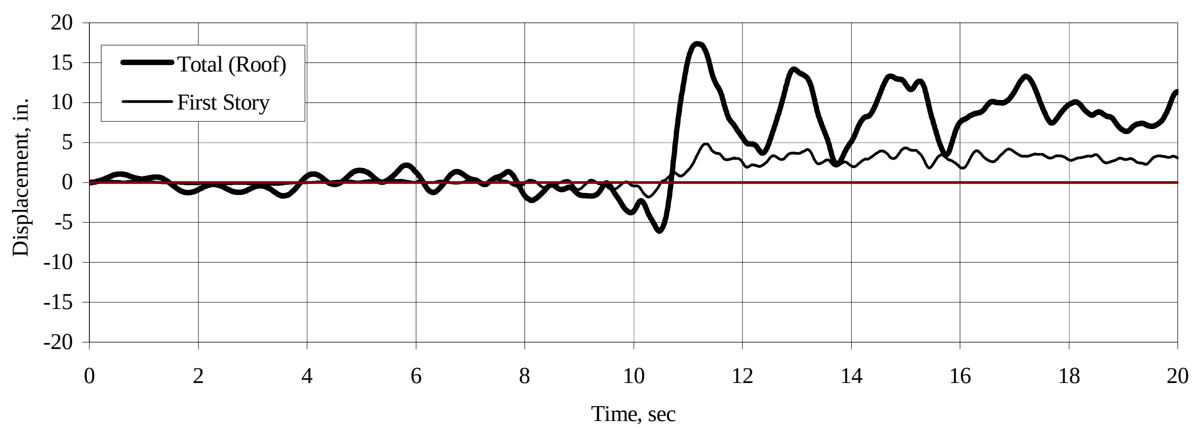

Figure 3.2-56 Time history of roof and first-story displacement, Ground Motion A00, including P-delta effects.

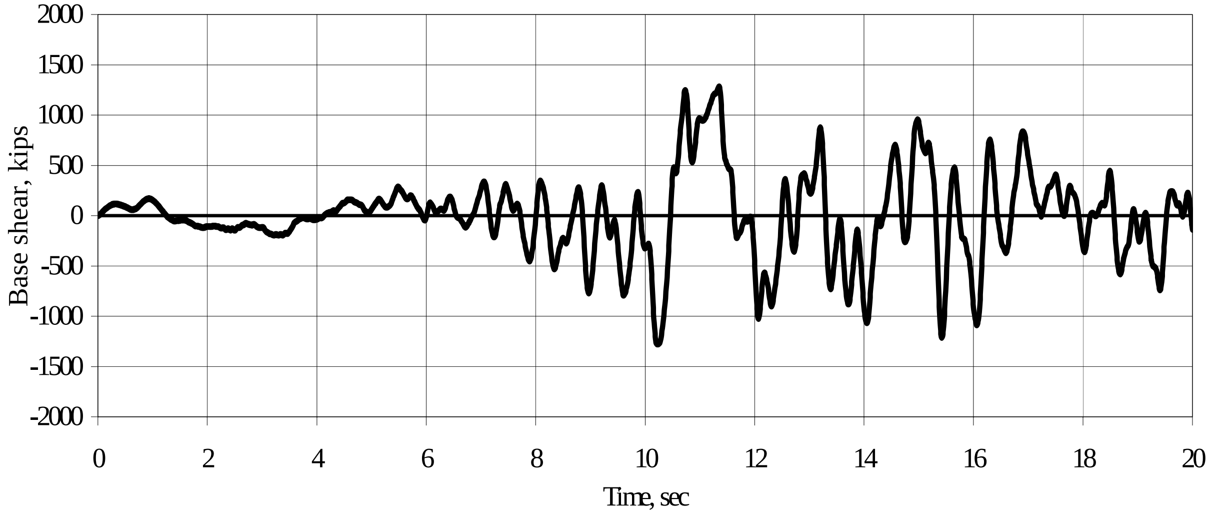

Figure 3.2-57 Time history of total base shear, Ground Motion A00, including P-delta effects.

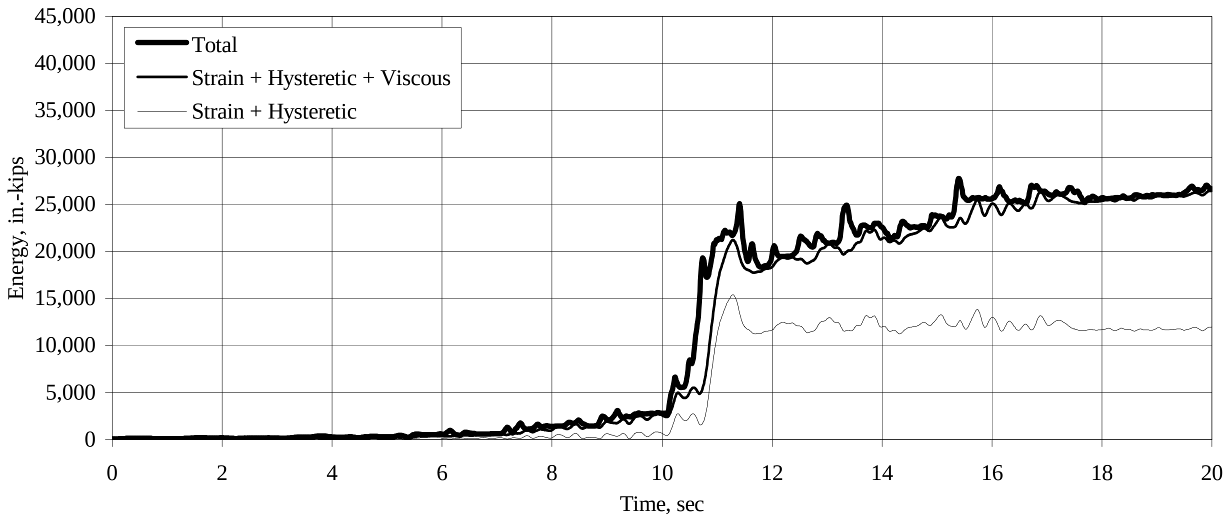

Figure 3.2-58 Energy time history, Ground Motion A00, including P-delta effects.

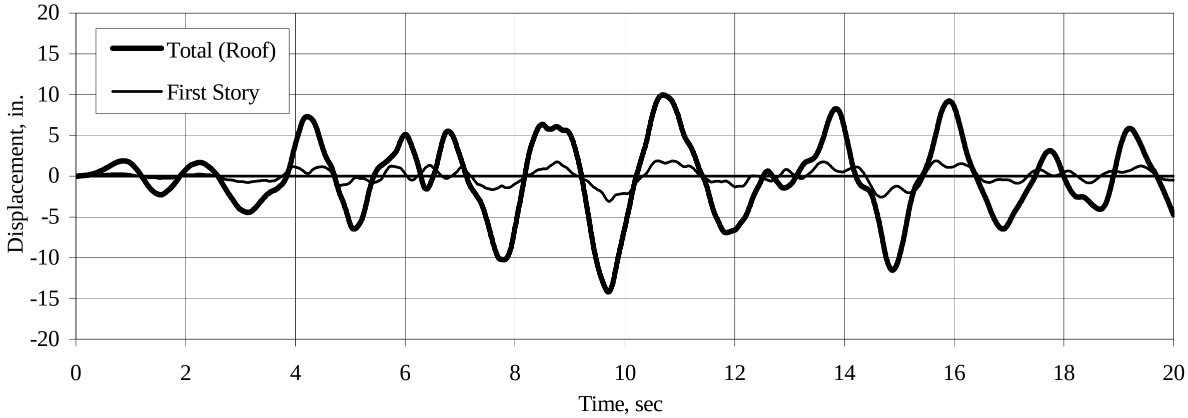

Figure 3.2-59 Time history of roof and first-story displacement, Ground Motion B00, including P-delta effects.

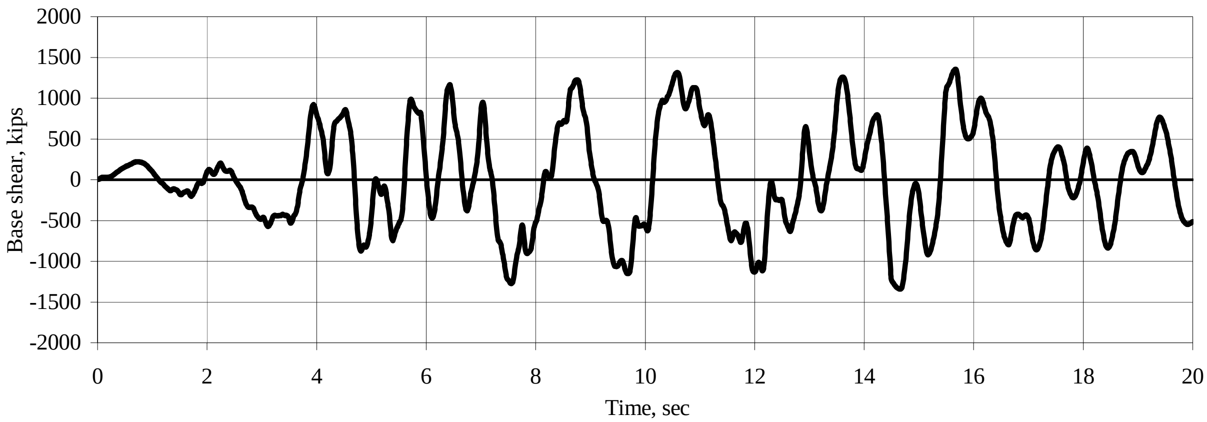

Figure 3.2-60 Time history of total base shear, Ground Motion B00, including P-delta effects.

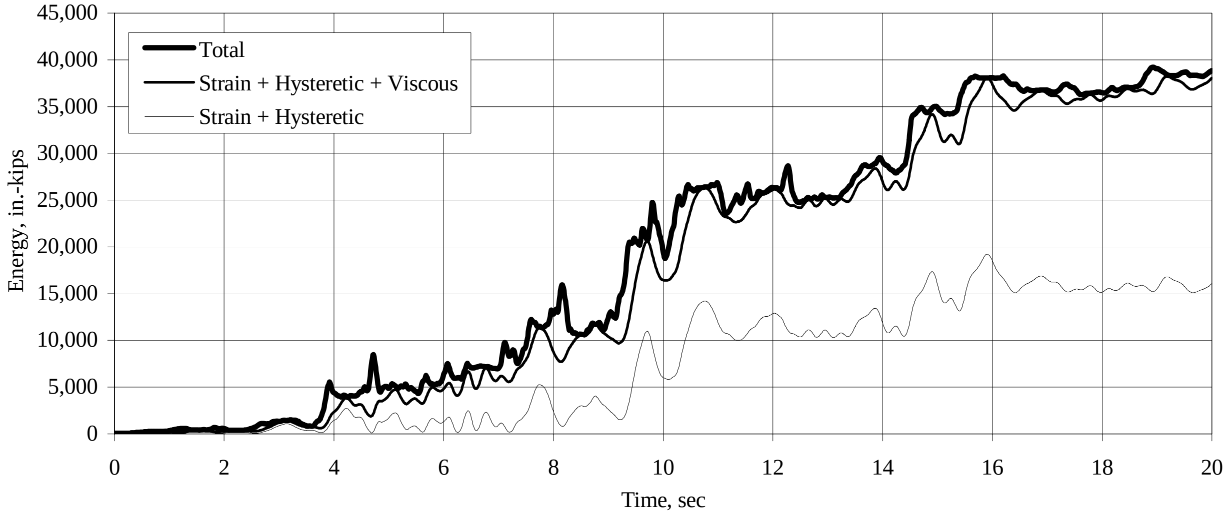

Figure 3.2-61 Energy time history, Ground Motion B00, including P-delta effects.

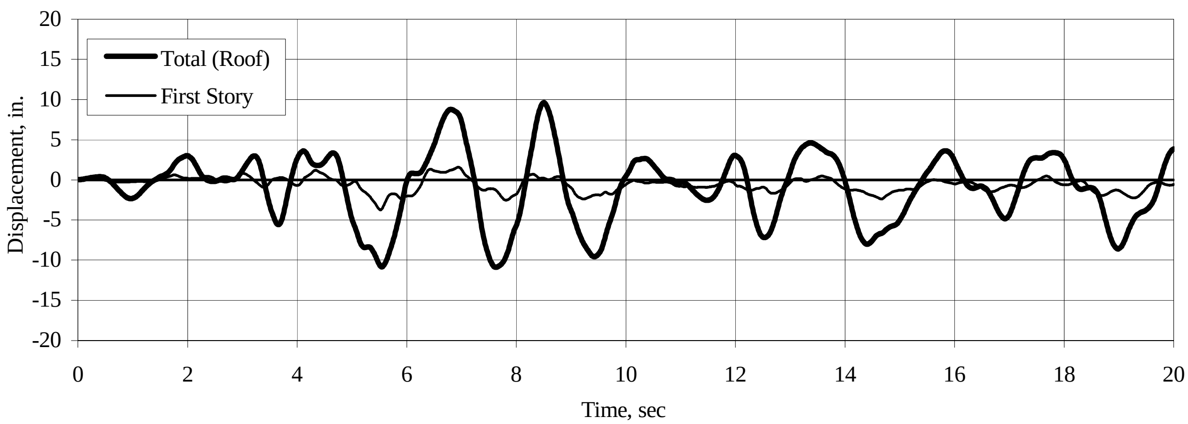

Figure 3.2-62 Time history of roof and first-story displacement, Ground Motion C00, including P-delta effects.

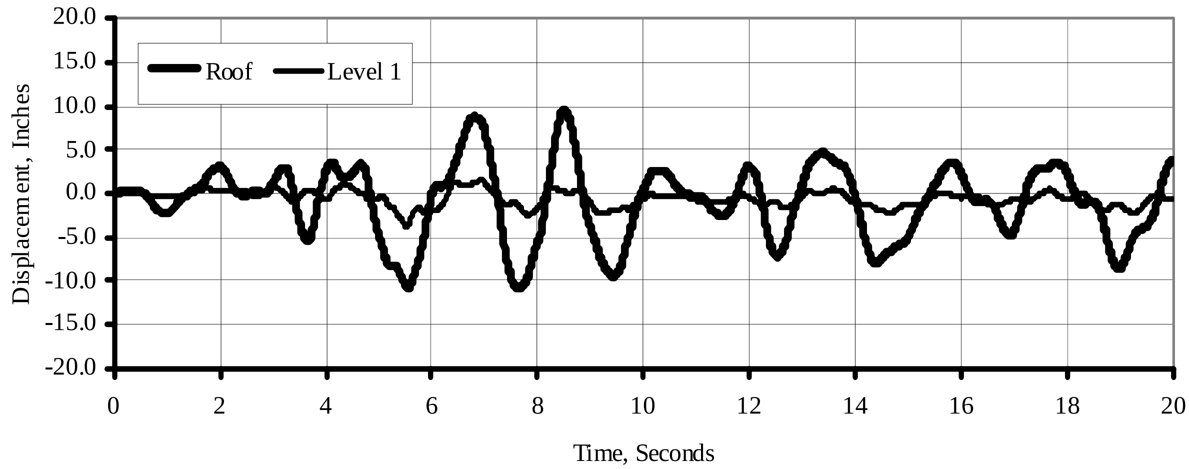

Figure 3.2-63 Time history of total base shear, Ground Motion C00, including P-delta effects.

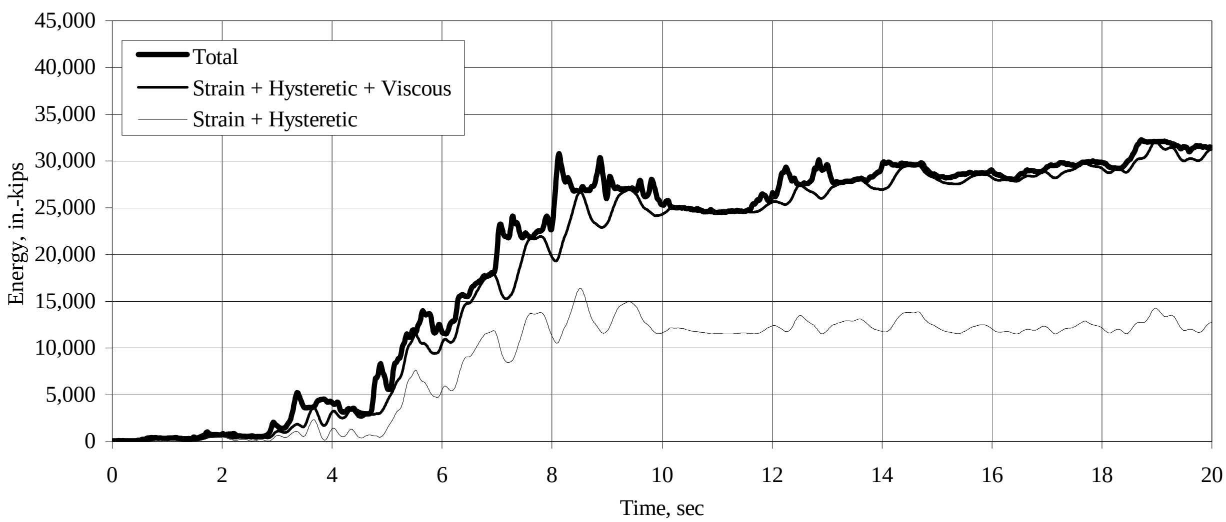

Figure 3.2-64 Energy time history, Ground Motion C00, including P-delta effects.

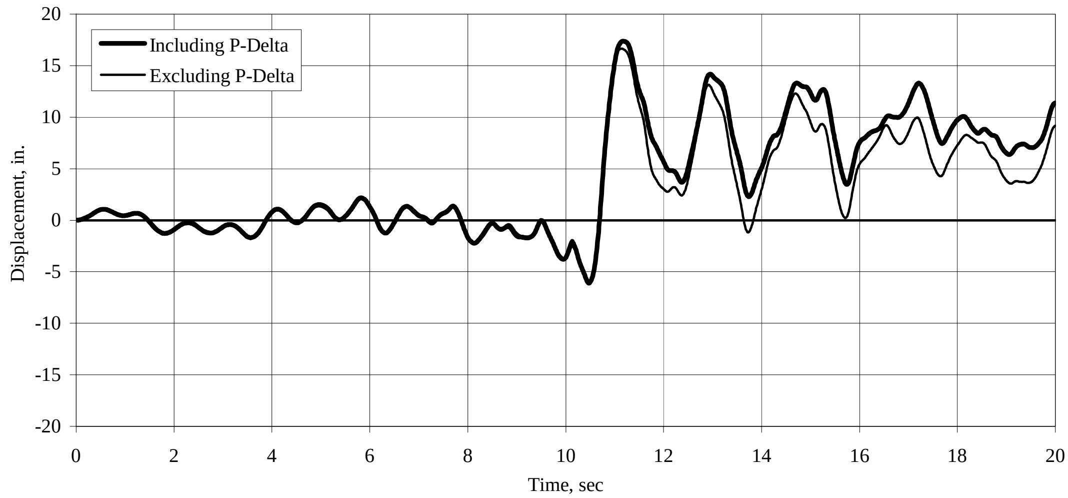

Figure 3.2-65 Time-history of roof displacement, Ground Motion A00, with and without P-delta effect.

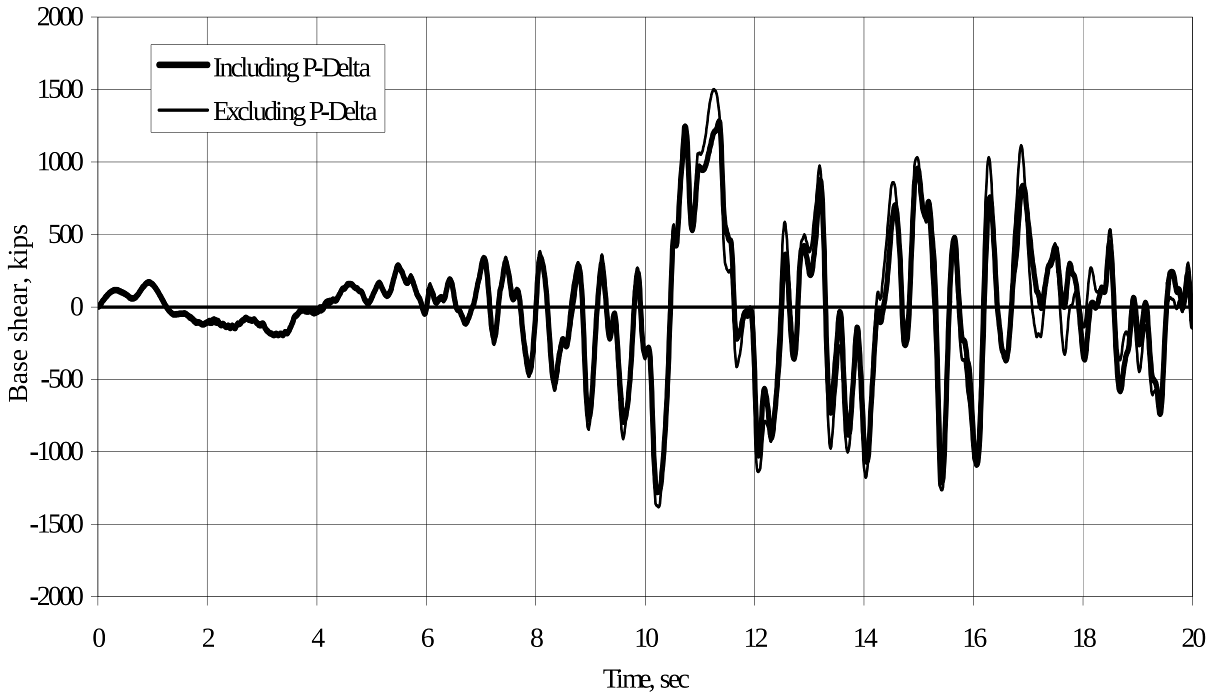

Figure 3.2-66 Time history of base shear, Ground Motion A00, with and without P-delta effects.

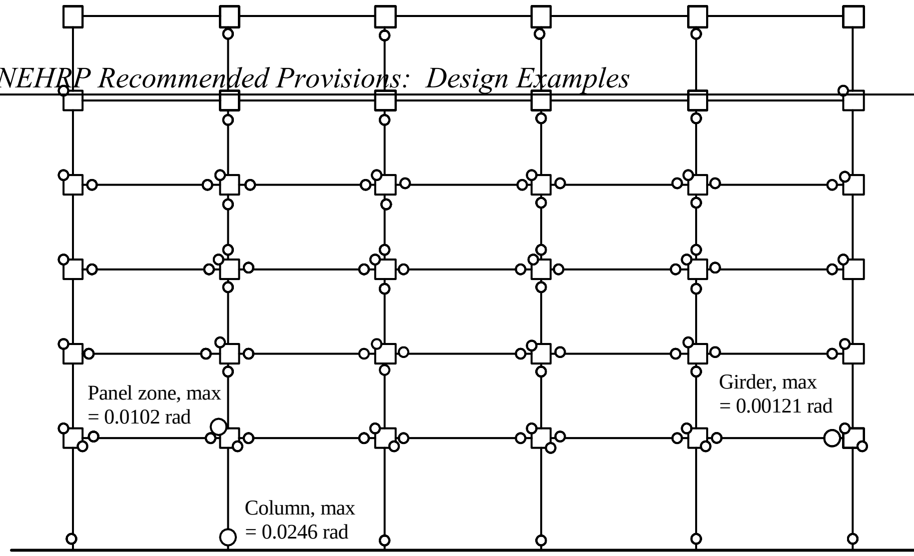

Figure 3.2-67 Yielding locations for structure with strong panels subjected to Ground Motion A00, including P-delta effects.

Figure 3.2-67 shows the pattern of yielding in the structure subjected to Gound Motion A00 including P-delta effects. Recall that the model analyzed incorporated panel zone reinforcement at the interior beam-column joints. Yielding patterns for the other ground motions and for analyses run with and without P-delta effects were similar but are not shown here. The circles on the figure represent yielding at any time during the response; consequently, yielding does not necessarily occur at all locations simultaneously. Circles shown at the upper left corner of the beam-column joint region indicate yielding in the rotational spring that represents the web component of panel zone behavior. Circles at the lower right corner of the panel zone represent yielding of the flange component.

Figure 3.2-67 shows that yielding occurred at both ends of each of the girders at Levels 2, 3, 4, 5, and 6, and in the columns at Stories 1 and 5. The panels zones at the exterior joints of Levels 2 and 6 also yielded. The maximum plastic hinge rotations are shown at the locations they occur for the columns, girders, and panel zones. Tabulated values are shown in Table 3.2-23. The maximum plastic shear strain in the web of the panel zone is identical to the computed hinge rotation in the panel zone spring.

3.2.6.3.2 Comparison with Results from Other Analyses

Table 3.2-23 compares the results obtained from the time-history analysis with those obtained from the ELF and the nonlinear static pushover analyses. Recall that the base shears in the table represent half of the total shear in the building. The differences shown in the results are quite striking:

1. The base shear from nonlinear dynamic analysis is more than four times the value computed from the ELF analysis, but the predicted displacements and story drifts are similar. Due to the highly empirical nature of the ELF approach, it is difficult to explain these differences. The ELF method also has no mechanism to include the overstrength that will occur in the structure although it is represented explicitly in the static and dynamic nonlinear analyses.

2. The nonlinear static pushover analysis predicts base shears and story displacements that are significantly less than those obtained from time-history analysis. It is also very interesting to note that

the pushover analysis indicates no yielding in the panel zones, even at an applied roof displacement of 42 in.

While part of the difference in the pushover and time-history response is due to the scale factor of 1.51 that was required for the time-history analysis, the most significant reason for the difference is the use of the first-mode lateral loading pattern in the nonlinear static pushover response. Figure 3.2-68 illustrates this by plotting the inertial forces that occur in the structure at the time of peak base shear and comparing this pattern to the force system applied for nonlinear static analysis. The differences are quite remarkable. The higher mode effects shown in the Figure 3.2-68 are the likely cause of the different hinging patterns and are certainly the reason for the very high base shear developed in the time-history analysis. (If the inertial forces were constrained to follow the first mode response, the maximum base shear that could be developed in the system would be in the range of 1100 kips. See, for example, Figure 3.2-24.)

Table 3.2-23 Summary of All Analyses for Strong Panel Structure, Including P-Delta Effects

Response Quantity	Analysis Method			
	Equivalent Lateral Forces	Static Pushover *Provisions* Method	Static Pushover Capacity-Spectrum	Nonlinear Dynamic
Base Shear (kips)	373	1051	1031	1474
Roof Disp. (in.)	18.4	12.7	10.3	17.4
Drift R-6 (in.)	1.87	1.02	0.78	1.90
Drift 6-5 (in.)	2.91	1.77	1.31	3.31
Drift 5-4 (in.)	3.15	2.34	1.81	3.48
Drift 4-3 (in.)	3.63	2.73	2.23	3.60
Drift 3-2 (in.)	3.74	2.73	2.27	4.08
Drift 2-1 (in.)	3.14	2.23	1.90	4.84
Girder Hinge Rot. (rad)	NA	0.0065	0.00732	0.0140
Column Hinge Rot. (rad)	NA	0.00130	0.00131	0.0192
Panel Hinge Rot. (rad)	NA	No Yielding	No Yielding	0.00624
Panel Plastic Shear Strain	NA	No Yielding	No Yielding	0.00624

Note: Shears are for half of total structure.

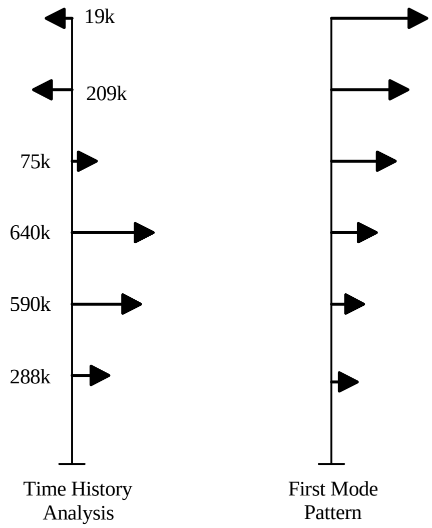

Figure 3.2-68 Comparison of inertial force patterns.

3.2.6.3.3 Effect of Increased Damping on Response

The time-history analysis of the structure with panel zone reinforcement indicates that excessive drift may occur in the first story. The most cost effective measure to enhance the performance of the structure would probably be to provide additional strength and/or stiffness at this story. However, added damping is also a viable approach.

To determine the effect of added damping on the behavior of the structure, preliminary analysis was performed by simply increasing the damping ratio from 5 percent to 20 percent of critical in 5-percent increments. For comparison purposes, an additional analysis was performed for a system with only 2.5 percent damping. In each case, the structure was subjected to Ground Motion A00, the panel zones were reinforced, and P-delta effects were included. A summary of the results is shown in Tables 3.2-24 and 3.2-25. As may be seen, an increase in damping from 5 to 10 percent of critical eliminates the drift problem. Even greater improvement is obtained by increasing damping to 20 percent of critical. In is interesting to note, however, that an increase in damping had little effect on the inertial base shear, which is the true shear in the system.

Table 3.2-24 Maximum Base Shear (kips) in Frame Analyzed Ground Motion A00, Strong Panels, Including P-Delta Effects

Item	Damping Ratio				
	2.5%	5%	10%	20%	28%
Column Forces	1354	1284	1250	1150	1132
Inertial Forces	1440	1426	1520	1421	1872

Table 3.2-25 Maximum Story Drifts (in.) from Time-History Analysis Ground Motion A00, Strong Panels, Including P-Delta Effects

Level	Damping Ratio				
	2.5%	5%	10%	20%	28%
Total Roof	18.1	17.4	15.8	12.9	11.4
R-6	1.81	1.90	1.74	1.43	1.21
6-5	3.72	3.31	2.71	2.08	1.79
5-4	3.87	3.48	3.00	2.42	2.13
4-3	3.70	3.60	3.33	2.77	2.40
3-2	4.11	4.08	3.69	2.86	2.37
2-G	4.93	4.84	4.21	2.90	2.18

If added damping were a viable option, additional analysis that treats the individual dampers explicitly would be required. This is easily accomplished in DRAIN by use of the stiffness proportional component of Rayleigh damping; however, only linear damping is possible in DRAIN. In practice, added damping systems usually employ devices with a "softening" nonlinear relationship between the deformational velocity in the device and the force in the device.

If a linear viscous fluid damping device (Figure 3.2-69) were to be used in a particular story, it could be modeled through the use of a Type-1 (truss bar) element. If a damping constant C_{device} were required, it would be obtained as follows:

Let the length of the Type-1 damper element be L_{device}, the cross sectional area A_{device}, and modulus of elasticity E_{device}.

The elastic stiffness of the damper element is simply:

$$k_{device} = \frac{A_{device} E_{device}}{L_{device}}$$

As stiffness proportional damping is used, the damping constant for the element is:

$$C_{device} = \beta_{device} k_{device}$$

The damper elastic stiffness should be negligible so set k_D = 0.001 kips/in. Thus:

$$\beta_{device} = \frac{C_{device}}{0.001} = 1000\ C_{device}$$

When modeling added dampers in this manner, the author typically sets E_{device} = 0.001 and A_{device} = the damper length L_{device}.

This value of β_{device} is for the added damper element *only*. Different dampers may require different values. Also, a different (global) value of β will be required to model the stiffness proportional component of damping in the remaining nondamper elements.

Modeling the dynamic response using Type-1 elements is *exact* within the typical limitations of finite element analysis. Using the modal strain energy approach, DRAIN will report a damping value in each mode. These modal damping values are approximate and may be poor estimates of actual modal damping, particularly when there is excessive flexibility in the mechanism that connects the damper to the structure.

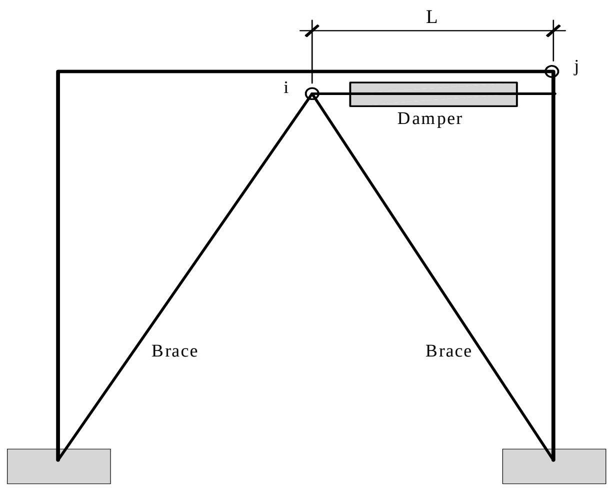

Figure 3.2-69 Modeling a simple damper.

In order to compare the response of the structure with fictitiously high Rayleigh damping to the response with actual discrete dampers, dampers were added in a chevron configuration along column lines C and D, between Bays 3 and 4 (see Figure 3.2-1). As before, the structure is subjected to Ground Motion A00, has strong panels, and has P-delta effects included.

Devices with a damping constant (C) of 80 kip-sec/in. were added in Stories 1 and 2, devices with C = 70 kip-sec/in. were added in Stories 3 and 4, and dampers with C = 60 kip-sec/in. were added at Stories 5 and 6. The chevron braces used to connect the devices to the main structure had sufficient stiffness to eliminate any loss of efficiency of the devices. Using these devices, an equivalent viscous damping of approximately 28 percent of critical was obtained in the first mode, 55 percent of critical damping was obtained in the second mode, and in excess of 70 percent of critical damping was obtained in modes three through six..

The analysis was repeated using Rayleigh damping wherein the above stated modal damping ratios were approximately obtained. The peak shears and displacements obtained from the analysis with Rayleigh damping are shown at the extreme right of Tables 3.2-24 and 3.2-25. As may be observed, the trend of decreased displacements and increased inertial shears with higher damping is continued.

Figure 3.2-70 shows the time history of roof displacements for the structure without added damping, with true viscous dampers, and with equivalent Rayleigh damping. As may be seen, there is a dramatic decrease in roof displacement. It is also clear that the discrete dampers and the equivalent Rayleigh damping produce very similar results.

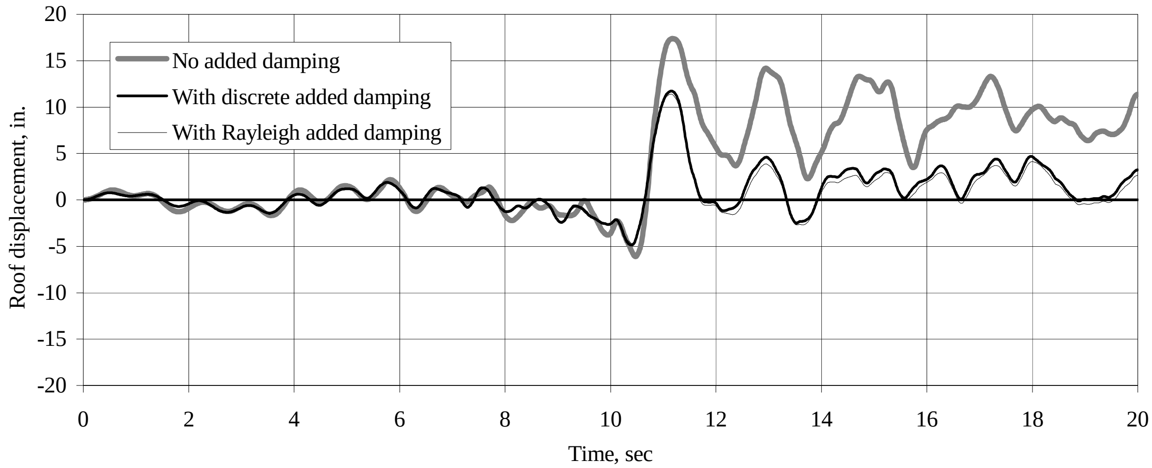

Figure 3.2-70 Response of structure with discrete dampers and with equivalent viscous damping (1.0 in. = 25.4 mm).

Figure 3.2-71 shows the time history of base shears for the structure without added damping, with discrete dampers, and with equivalent viscous damping. These base shears were obtained from the summation of column forces, including P-delta effects. For the discrete damper case, the base shears include the horizontal component of the forces in the chevron braces. The base shears for the discretely damped system are greater than the shears for the system without added damping. The peak base shear for the system with equivalent viscous damping is less than the shear in the system without added damping.

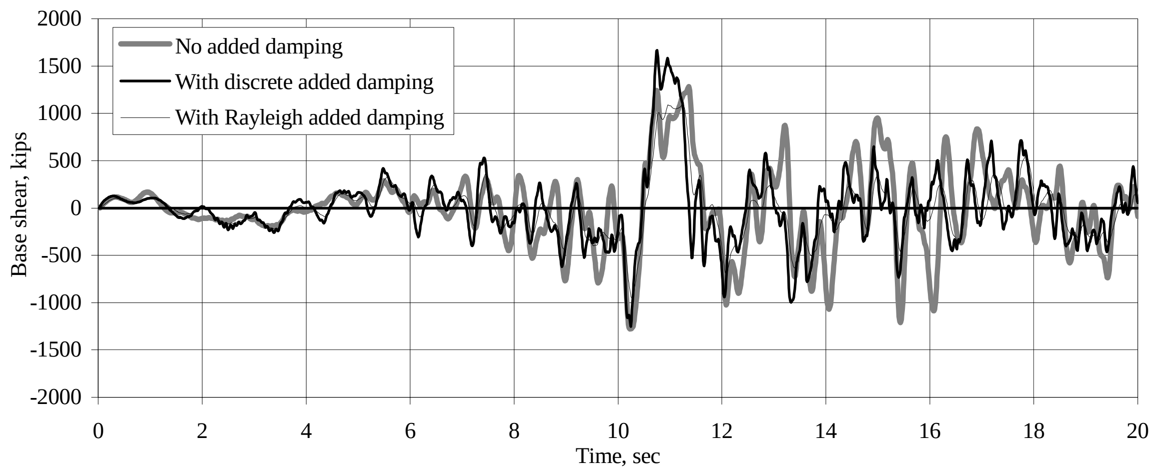

Figure 1Figure 3.2-71 Base shear time histories obtained from column forces (1.0 kip = 4.45 kN).

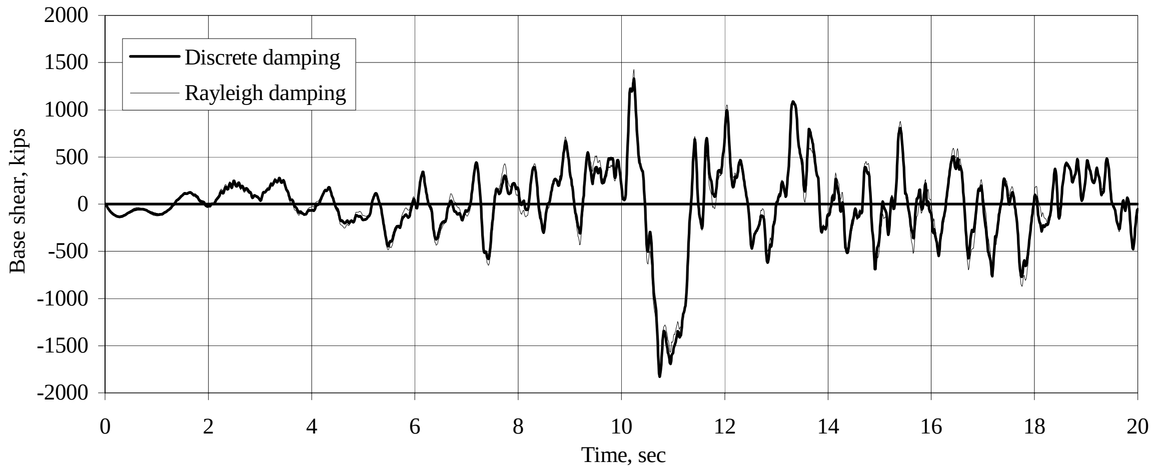

Figure 3.2-72 Base shear time histories as obtained from inertial forces (1.0 kip = 4.45 kN).

The inertial base shears in the system with discrete damping and with equivalent viscous damping are shown in Figure 3.2-72. As may be observed, the responses are almost identical. The inertial forces represent the true base shear in the structure, and should always be used in lieu of the sum of column forces.

As might be expected, the use of added discrete damping reduces the hysteretic energy demand on the structure. This effect is shown in Figure 3.2-73, which is an energy time history for the structure with added discrete damping (which yields equivalent viscous damping of 28 percent of critical). This figure should be compared to Figure 3.2-58, which is the energy history for the structure without added damping. The reduction in hysteretic energy demand for the system with added damping will reduce the damage in the structure.

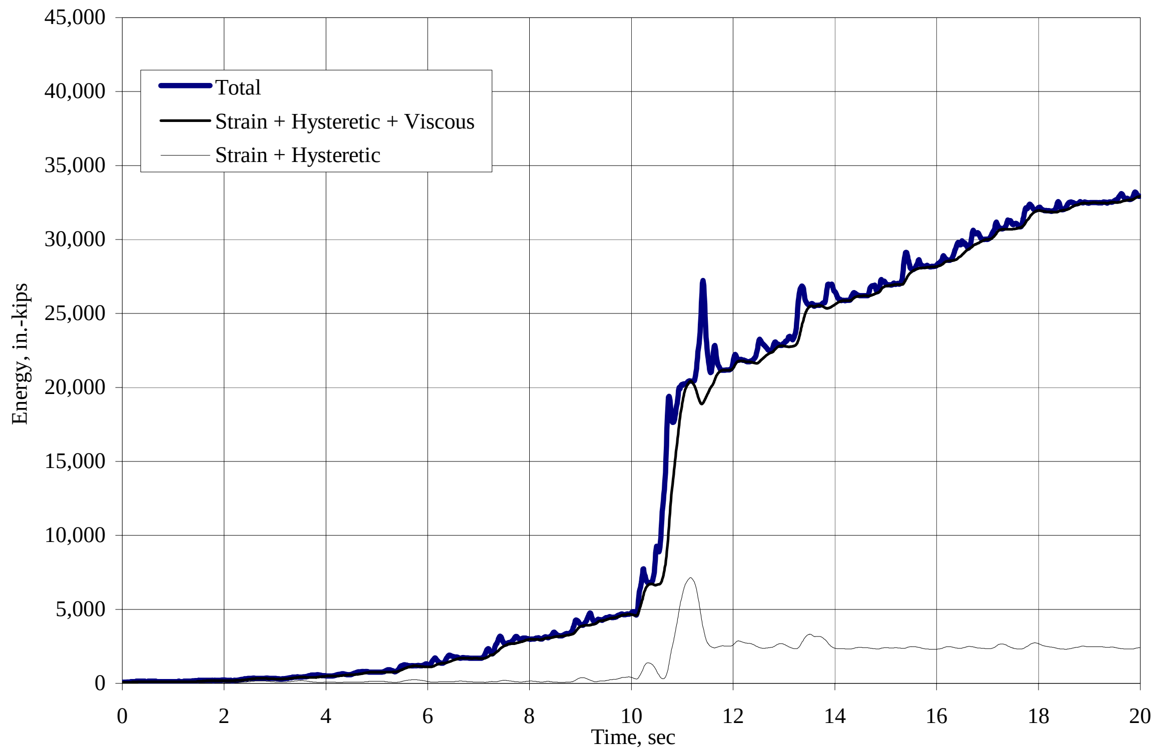

Figure 3.2-73 Energy time-history for structure with discrete added damping (1.0 in.-kip = 0.113 kN-m).

3.2.7 Summary and Conclusions

In this example, five different analytical approaches were used to estimate the deformation demands in a simple unbraced steel frame structure:

1. Linear static analysis (the equivalent lateral force method)
2. Plastic strength analysis (using virtual work)
3. Nonlinear static pushover analysis
4. Linear dynamic analysis
5. Nonlinear dynamic time-history analysis

Approaches 1, 3, and 5 were carried to a point that allowed comparison of results. In modeling the structure, particular attention was paid to representing possible inelastic behavior in the panel-zone regions of the beam-column joints.

The results obtained from the three different analytical approaches were quite dissimilar. Because of the influence of the higher mode effects on the response, pushover analysis, when used alone, is inadequate.[11] [In the 2003 *Provisions*, a number of substantive technical changes have been made to the appendix,

[11]Improved methods are becoming available for pushover analysis (see, for example, Chopra and Goel 2001).

largely as a result of work performed in the development of ATC 55. That report outlines numerous other technical modifications that could be considered in application of nonlinear static analysis methods.] Except for preliminary design, the ELF approach should not be used in explicit performance evaluation as it has no mechanism for determining location and extent of yielding in the structure.

This leaves time-history analysis as the most viable approach. Given the speed and memory capacity of personal computers, it is expected that time-history analysis will eventually play a more dominant role in the seismic analysis of buildings. However, significant shortcomings, limitations, and uncertainties in time-history analysis still exist.

Among the most pressing problems is the need for a suitable suite of ground motions. All ground motions must adequately reflect site conditions and, where applicable, the suite must include near-field effects. Through future research and the efforts of code writing bodies, it may be possible to develop standard suites of ground motions that could be published together with tools and scaling methodologies to make the motions represent the site. The scaling techniques that are currently recommended in the *Provisions* are a start but need improving.

Systematic methods need to be developed for identifying uncertainties in the modeling of the structure and for quantifying the effect of such uncertainties on the response. While probabilistic methods for dealing with such uncertainties seem like a natural extension of the analytical approach, the author believes that deterministic methods should not be abandoned entirely.

In the context of performance-based design, improved methods for assessing the effect of inelastic response and acceptance criteria based on such measures need to be developed. Methods based on explicit quantification of damage should be seriously considered.

The ideas presented above are certainly not original. They have been presented by many academics and practicing engineers. What is still lacking is a comprehensive approach for seismic-resistant design based on these principles. Bertero and Bertero (2002) have presented valuable discussions in these regards.